ML-TDR-64-3

INVESTIGATION OF THE EFFECTS OF STRESS CORROSION ON HIGH-STRENGTH STEEL ALLOYS

TECHNICAL DOCUMENTARY REPORT NO. ML-TDR-64-3

February 1964

AF Materials Laboratory
Research and Technology Division
Air Force Systems Command
Wright-Patterson Air Force Base, Ohio

Project No. 7381, Task No. 738103

(Prepared under Contract No. AF 33(657)-8705 by The Boeing Company, Airplane Division, Renton, Washington: Gary A. Dreyer and Wesley C. Gallaugher, authors)

NOTICES

When Government drawings, specifications, or other data are used for any purpose other than in connection with a definitely related Government procurement operation, the United States Government thereby incurs no responsibility nor any obligation whatsoever; and the fact that the Government may have formulated, furnished, or in any way supplied the said drawings, specifications, or other data, is not to be regarded by implication or otherwise as in any manner licensing the holder or any other person or corporation, or conveying any rights or permission to manufacture, use, or sell any patented invention that may in any way be related thereto.

Qualified requesters may obtain copies of this report from the Defense Documentation Center (DDC), (formerly ASTIA), Cameron Station, Bldg. 5, 5010 Duke Street, Alexandria 4, Virginia.

This report has been released to the Office of Technical Services, U.S. Department of Commerce, Washington 25, D. C., in stock quantities for sale to the general public.

Copies of this report should not be returned to the Aeronautical Systems Division unless return is required by security considerations, contractual obligations, or notice on a specific document.

ML-TDR-64-3

INVESTIGATION OF THE EFFECTS OF STRESS CORROSION ON HIGH-STRENGTH STEEL ALLOYS

TECHNICAL DOCUMENTARY REPORT NO. ML-TDR-64-3

February 1964

AF Materials Laboratory
Research and Technology Division
Air Force Systems Command
Wright-Patterson Air Force Base, Ohio

Project No. 7381, Task No. 738103

(Prepared under Contract No. AF 33(657)-8705 by The Boeing Company, Airplane Division, Renton, Washington; Gary A. Dreyer and Wesley C. Gallaugher, authors.)

FOREWORD

The program described in this report was conducted by the Metals Group, Materials and Process Unit, Structures Staff, Airplane Division, The Boeing Company, Renton, Washington. The work was administered by the Structural Materials Section, Materials Applications Division, Air Force Materials Laboratory, Research and Technology Division. This work was conducted under Project No. 7381, "Materials Application," Task No. 738103, "Data Collection and Correlation." Project Engineer was Lt. R. M. Dunco of the Structural Materials Section.

The investigation was initiated in June 1962 and concluded in December 1963. R. A. Davis of the Metals Group directed the technical aspects of the program under the supervision of M. A. Disotell, supervisor of the Metals Group, F. N. Markey, Chief of the Materials and Process Unit, and A. C. Larsen, Staff Engineer — Structures. Test work was carried out by G. A. Dreyer and W. C. Gallaugher, assisted by F. E. Machula. All laboratory testing and evaluation was done in the Metals Laboratory, Airplane Division. J. C. McMillan of the Airplane Division and Dr. R. M. N. Pelloux of the Boeing Scientific Research Laboratories aided in the preparation and interpretation of the electron micrograph studies.

ABSTRACT

The stress corrosion susceptibility of several high strength steels has been evaluated by alternate-immersion laboratory testing in a 3.5-percent sodium chloride solution. The steels evaluated were the stainless steels AFC 77, AM 350, AM 355, and 17-4PH: the low alloy steels D6AC, 4335M, 4340, H-11, 4330M, and HY-Tuf; and the high nickel steels 18Ni-9Co-5Mo, 18Ni-7Co-5Mo, and 9Ni-4Co. The variables investigated were product form, grain direction, tensile strength level, stress level, cold working, ausforming, welding, and protective coatings. Detailed results relating stress corrosion susceptibility to the variables and alloys studied are included. Notch tensile and fatigue cracked fracture toughness testing was carried out for correlation with stress corrosion susceptibility. Optical microscopy, electron microscopy, and X-ray diffraction studies were made to supplement the mechanical property and stress corrosion testing. A literature survey of related stress corrosion test data is included.

This technical documentary report has been reviewed and is approved.

W. P. Conrardy, Chief
Materials Engineering Branch
Materials Applications Division
AF Materials Laboratory

CONTENTS

ILLUSTRATIONS

TABLES

SYMBOLS

F_{tu}	Ultimate tensile strength
F_{ty}	0.2-percent tensile yield strength
F_{ntu}	Notched ultimate tensile strength
N/UN	Notched-to-unnotched tensile strength ratio
G_c	Fracture toughness index (lb-in)
K_c	Critical stress intensity factor, plane stress (ksi $\sqrt{in}$) (Appendix II)
K_{Ic}	Critical stress intensity factor, plane strain (ksi $\sqrt{in}$) = 0.233 $\sigma_N \sqrt{\pi D}$
psi	Pounds per square inch
RA	Percent reduction in area
K or k	Stress intensity factor
ksi	Kips per square inch
σ	Stress (psi or ksi)
E	Young's modulus (psi)
P	Plate
S	Sheet
B	Billet
RHR	Roughness height reading
HT	Heat treatment
°F	Degree Fahrenheit
NF	No failure in 1000 hours
ASTM	American Society for Testing Materials
DADF	Double age, double freeze heat treatment process
SCT	Subzero cool and temper heat treatment process
SCT'	Altered subzero cool and temper heat treatment process
BMS	Boeing Material Specification
BAC	Boeing Process Specification

I. INTRODUCTION

Stress-corrosion cracking of high-strength steel alloys has been of concern with the increased usage of these materials in the aerospace industry. The occurrence of stress-corrosion cracking is related in a complex manner to the amount of time a component has been exposed to both tensile stress and a corrosive environment. Because of the extreme complexity of this phenomenon in commercial steel alloys, there is generally considerable scatter in data obtained from laboratory tests, which further increases the difficulty in evaluating stress-corrosion results. Although laboratory test data have serious limitations for direct comparison with service performance, this type of data is the primary means of material evaluation and selection with respect to stress-corrosion susceptibility. The primary concern of the present investigation has been an engineering evaluation of the factors affecting stress-corrosion cracking in low-alloy, stainless, and high-nickel steels.

This program is a continuation and expansion of a previous evaluation (Reference 1), which was concerned with the effects of surface finish, grain direction, stress level, residual surface stress, and heat-treat strength on the stress-corrosion susceptibility of 4340, 4340M, 4330M, H-11, AM 350, and AM 355.

The selected steel alloys for this investigation were AFC 77, AM 350, AM 355, 17-4PH, Ladish D6AC, 18-7-5, 18-9-5, 4335M, 4340, 4330M, 9Ni-4Co, H-11, and HY-Tuf. The stress-corrosion testing involved alternate immersion of U-bend (billet and plate stock) and tensile-type (sheet) specimens in a 3.5 percent sodium chloride solution. The variables and alloys evaluated are summarized in Table 2 (Page 8) and briefly described below.

A. Product Shape

The materials were in three forms: billet (8 x 8 x 12 inches), plate (3/8 x 10 x 48 inches), and sheet (0.02 to 0.08 gage).

B. Environment

In addition to the alternate-immersion testing, one form of each alloy was tested in a semi-industrial atmosphere.

C. Grain Direction

Transverse and longitudinal grain directions were evaluated on all forms of each material.

Manuscript released by authors February 1964 for publication as a Materials Laboratory technical documentary report.

D. Processing Variables

1. Strength Levels

The high-strength alloys were tested in the 180- to 200-, 220- to 240-, and 260- to 280-ksi ultimate strength ranges.

2. Heat-Treat Variations

Alternate and additional heat treatments were performed on a selected number of alloys for the evaluation of delta ferrite content, carbide distribution, and stabilized structures on stress-corrosion susceptibility. Austempering and martempering were also evaluated on 4335M and 4340.

3. Ausforming

This method of strengthening was studied on 4340, 4335M, Ladish D6AC, and 9Ni-4Co.

4. Straightening

Various percentages of deformation were applied to heat-treated specimens of AFC 77, AM 355, 18-7-5, 4335M, 4340, and H-11 to simulate straightening operations.

5. Welding

Manual and automatic fusion welding were evaluated on all the alloys obtained in plate form. Except for D6AC plate, no attempt was made to check the effect of weld wire on stress-corrosion susceptibility.

6. Coatings

Five different coating techniques — epoxy paint, cadmium plating, cadmium-titanium plating, cadmium plating plus epoxy paint, and flame-sprayed aluminum coatings — were evaluated on all the alloys obtained in plate form.

E. Design Data

Design data were generated by evaluating two heats from eight of the 13 alloys. The specimens were stressed to 40, 60, and 80 percent of their yield strengths.

The stress-corrosion susceptibility of the alloys was related to notch sensitivity and fracture toughness. Metallography and microfractography were used to study the stress-corrosion fracture modes. Supplementary studies concerning anodic-cathodic charging experiments with 4340 and 18-9-5 steels and impact-energy/stress-corrosion-susceptibility relationships with the low-alloy steels used in the previous program have been included in this report.

II. SUMMARY

The stress-corrosion cracking susceptibility of several stainless, low-alloy, and high-nickel steels was evaluated by alternate-immersion testing in a 3.5-percent sodium chloride solution. These steels were: AFC 77, AM 350, AM 355, 17-4PH, Ladish D6AC, 4335M, 4340, H-11, 4330M, HY-Tuf, 18Ni-9Co-5Mo, 18Ni-7Co-5Mo, and 9Ni-4Co. Several variables were considered: alloy form, environment, grain direction, strength level, heat treatment, ausforming, straightening, welding, coatings, and stress level. Billet and plate stress-corrosion specimens were stressed to the desired levels by bending: sheet specimens were loaded in tension. In addition to the alternate-immersion testing, comparisons were made after semi-industrial environmental exposure. The longitudinal and transverse grain directions of all alloy forms were compared. All materials were heat treated to their maximum ultimate strengths and the AFC 77, 18-7-5, D6AC, 4335M, 4340, and H-11 alloys, which have maximum ultimate strengths in the 260- to 280-ksi range, were also heat treated in the 220- to 240- and 180- to 200-ksi ultimate strength ranges. The heat treatment variable involved mill processing, martempering, and austempering of 4335M and 4340: heat treating AM 350 and AM 355 to give DADF and altered SCT 850 conditions: and expanding the tempering temperature range of AFC 77. The 4340, 4335M, D6AC, and 9Ni-4Co were ausformed and heat treated to their maximum strengths. AFC 77, AM 355, 18-7-5, 4335M, 4340, and H-11 were plastically deformed after heat treating. Manual- and fusion-welding procedures were compared using 17-4PH, 18-7-5, D6AC, 4335M, 4340, 9Ni-4Co, H-11, AM 355, and AM 350. Cadmium, cadmium-titanium, epoxy paint, cadmium plus epoxy paint, and flame-sprayed aluminum coatings were evaluated on 18-7-5, D6AC, 4335M, 4340, H-11, and 9Ni-4Co. Duplicate heats of AM 350, AM 355, 17-4PH, D6AC, 4335M, 4340, H-11, and 4330M were evaluated at stress levels of 80, 60, and 40 percent of the 0.2-percent yield. All of the previously mentioned variables were evaluated at the 80-percent stress level. To complement the stress-corrosion testing, x-ray residual surface stress measurements were made. Metallographic and fractographic studies were carried out using the optical and electron microscopes. Fracture toughness panels were prepared for the plate and sheet materials and the 18-7-5, 4335M, and 4340 billet materials. Notch tensile specimens were prepared for all billet and sheet materials.

The areas covered in this program have shown the following results:

1) Plate material was usually less susceptible to stress corrosion than billet material. The longitudinal grain directions were usually less susceptible than the transverse grain directions.

2) Alternate-immersion testing provides a laboratory means of evaluating materials and processes. Final evaluation of alternate-immersion data would depend on judgment and experience with a material having a known service performance.

3) Lowering the tensile strengths of AFC 77, D6AC, and 4335M billet materials increases the notched-to-unnotched ultimate strength ratio and decreases the stress-corrosion susceptibility. The 4340 at the 260- to 280-ksi strength level was less susceptible than 4340 at the 220- to 440-ksi strength. There was no difference in the N/UN ratios of 4340 at these two strengths. Fracture toughness was not evaluated at the 180- to 200- and 220- to 240-ksi ultimate strength ranges for the low-alloy and high-nickel steels.

4) AM 355 in the DADF and altered SCT 850 conditions was less susceptible than after the SCT 850 heat treatment. Martempering, compared to oil quenching, decreased the susceptibility of 4340 and 4335M. Changes in susceptibility of D6AC, 4340, and 4335M after ausforming indicated a dependence on material chemistry.

5) Laboratory duplication of mill annealing processes on 4335M and 4340, and results obtained from testing AM 355 thin sheet and high-nickel steels, indicate that mill processing may have an influential effect on stress-corrosion susceptibility.

6) The least susceptible alloys as rated by alternate-immersion testing are shown in Table 1.

Table 1 SUMMARY OF LEAST-SUSCEPTIBLE ALLOYS

Yield Strength (ksi)	Alloy	Alloy Form
270	18-7-5	Billet
210 to 230	18-7-5, martempered 4335M, and D6AC	Billet
170 to 190	H-11, 4335M, and 4340	Billet
255	18-7-5	Plate
210 to 220	9Ni-4Co, 4335M	Plate
180 to 200	17-4PH	Plate

7) Evaluation of plastically deformed 4340 and H-11 indicated a decrease in susceptibility after 0.5-percent strain and an increase in susceptibility after 1.0-percent strain. AM 355, after 1.0-percent strain, was less susceptible than before straining or after 3.0-percent strain.

8) Manual and fusion welds were more susceptible than the base materials. No separation could be made between the two welding methods.

9) All coatings decreased the failure tendencies of the test alloys. Of the five coatings, cadmium and cadmium-titanium plating appeared to offer the least protection.

10) Tests to determine a threshold stress below which stress-corrosion failures would not occur showed duplicate 4330M billets to be failure resistant at

60 and 40 percent of yield and duplicate 4335M and 4340 billets to be resistant at 40 percent of yield during 1000 hours of alternate-immersion testing.

11) Final surface stresses could be determined by adding residual surface stresses determined by x-ray measurements and applied stresses. No correlation was noted between the magnitude of the final stresses and stress-corrosion susceptibility.

12) The optical and electron microscope studies show the primary fracture origin to be intergranular. Electron microscope studies indicated that hydrogen embrittlement and stress-corrosion fractures are similar.

13) Increased fracture toughness generally corresponded to a decrease in stress-corrosion susceptibility. One exception to this general rule is the low fracture toughness and high resistance to stress-corrosion cracking of the 17-4PH alloy.

III. PROCEDURE

A. MATERIAL EVALUATION

The alloys selected for evaluation in this program were the stainless steels AFC 77, AM 350, AM 355, and 17-4PH; the low-alloy steels Ladish D6AC, 4335M, 4340, H-11, 4330M, and HY-Tuf; and the high-nickel steels 18Ni-9Co-5Mo, 18Ni-7Co-5Mo, and 9Ni-4Co. Three material forms were evaluated: billet, plate, and sheet. These alloys and their respective forms are listed in Table 2. All billets and plates were ultrasonically inspected and all billets macroexamined prior to testing. Preliminary tensile tests were used to determine the billet transverse grain direction having the lowest ductility. This grain direction was used in the majority of testing, since previous data (Reference 1) showed that the direction having the lowest reduction in area was the most susceptible to stress corrosion. Chemical compositions of all billets, plates, and sheets were determined.

B. SPECIMEN PREPARATION

Stress-corrosion specimens were removed from all materials. Smooth tensile, notch tensile, and fracture toughness specimens were cut from selected alloys and alloy forms. A breakdown of the mechanical property specimens used for each alloy condition is given in Table 2. Typical billet, plate, and sheet specimen locations in as-received material and detail drawings of all specimen configurations are given in Appendix I.

All billet and plate specimens were heat treated to the desired conditions and final machined. The stress-corrosion specimens were ground to final dimensions with a nominal 32 RHR finish since this had been shown to be the most stress-corrosion susceptible of several machining processes (Reference 1). Aircraft process specifications require tempering of the low-alloy steels after grinding. This postgrind temper produced an oxide that was removed by vapor blasting. To be consistent, the surface-ground stainless and maraging steels were also vapor blasted. Vapor-blasted specimens used in the deformation studies were deformed by bending in four-point loading. All fusion-welded stress-corrosion specimens were radiographically inspected after grinding to final dimensions. Vapor-blasted plate specimens were used to evaluate various surface coatings.

Sheet specimens were precoated to prevent decarburization, heat treated, grit blasted to remove the precoat, and machined to final width dimensions. Sheet deformation specimens were deformed in tension. The amounts of deformation in both the U-bend and sheet specimens were determined from strain-gage measurements. Fusion-welded sheet stress-corrosion specimens were radiographically inspected after welding.

Table 2 ALLOYS AND TEST PROGRAM

TESTING VARIABLES	AFC 77	AM 350					AM 355		17-4PH	18-9-5	18-7-5		Ladish D6AC		4335M		4340			4330M		9Ni-4Co			H-11		HY-Tuf
	Billet A	Sheet A 0.042"	Sheet A 0.062"	Sheet B 0.079"	Sheet F 0.020"	Sheet C 0.060"	Sheet D 0.020"	Plate Q	Plate R	Plate M	Billet B	Plate S	Billet C	Billet D	Plate T	Billet E	Billet J	Plate U	Billet F	Billet G	Plate V	Sheet E 0.080"	Billet N	Billet O	Plate W	Plate X	Plate Y	Billet H	Billet I	Plate Z	Billet K
	S.C. N.T. S.T.	S.C. N.T. S.T.	S.C. N.T. S.T.	S.C. N.T. S.T.	S.C. N.T. S.T.	S.C. N.T. S.T.	S.C. N.T. S.T.	S.C. N.T. S.T.	S.C.	S.C. N.T. S.T.	S.C. N.T. S.T.	S.C. N.T. S.T.	S.C. N.T. S.T.	S.C.	S.C. N.T. S.T.	S.C. N.T. S.T.	S.C.	S.C. N.T. S.T.	S.C. N.T. S.T.	S.C.	S.C. N.T. S.T.	S.C. N.T. S.T.	S.C. N.T. S.T.	S.C. N.T. S.T.	S.C. N.T. S.T.	S.C. N.T. S.T.	S.C. N.T. S.T.	S.C. N.T. S.T.	S.C.	S.C. N.T. S.T.	S.C. N.T. S.T.
Product Form		XXX	X	XXX	X	X	X			X	X	X			X	X		X	X		X	X							X		X	
Environment	X		X			X			X		X		X			X			X						X				X			
Grain Direction	XXX		XXX		XX	XXX	XX	XXX		XXX	XXX	XXX	XXX		XXX	XXX		XXX	XXX		XXX	XXX			XXX	XXX	XX	XXX		XXX	XXX	
Strength Level	XXX										XXX		XX			XXX			XXX									XXX				
Heat Treatment	XXX		XXX			XXX										XXX			XXX													
Ausform													X			X			X								XXX					
Straightening	X					X						X						X			X									X		
Coatings												X			X			X			X				X					X		
Welding						X		X				X			X			X			X	X			X					X		
Design Data			X		X	X	X	X	X				X	X		X	X		X	X			XXX	XXX				X	X			
	1	1							3	2	2									3			3					3	4			

1 ASD Supplied
2 Vacuum Melted
3 Vacuum Degassed
4 Designated as Billet V in Previous Program (Reference 1)

KEY
S.C. - Stress-Corrosion Specimen
N.T. - Notch Tensile Specimen or Fracture Toughness Specimen
S.T. - Smooth Tensile Specimen
(See Appendix I for Specimen Drawings)

C. X-RAY RESIDUAL SURFACE STRESS MEASUREMENTS

The residual surface stresses in selected specimens from various billet, plate, and sheet heat-treat groups were measured using an X-ray diffractometer (Reference 2). Previously, residual surface stresses were determined using an X-ray back-reflection technique (Reference 1), but use of the X-ray diffractometer was found to provide quicker and more accurate results with these small stress-corrosion specimens. (The back-reflection technique has a minimum accuracy of ±10,000 psi; the diffractometer has an accuracy of ±5000 psi.) To obtain some idea as to the depth to which the residual stresses produced by grinding and vapor blasting extend, and also to determine if there is a linear relationship between residual and applied stresses, successive layers of material on a ground and vapor-honed 4330M billet specimen were removed by electropolishing. This specimen was stressed to various levels, as measured with strain gages, and the resultant surface stresses at a given point were determined using X-ray diffraction.

D. STRESS-CORROSION TESTING

Billet and plate stress-corrosion specimens were stressed to the desired level by bending. A special jig had been designed for this purpose and the jig and specimen combination is known as the Boeing U-bend configuration (Reference 1). A stressed U-bend specimen is shown in Figure 1. The stress level was determined by leg deflection measurements and checked with selected strain-gaged specimens. A graph showing the relationship between stress level and leg deflection is given in Figure 2.

Sheet stress-corrosion specimens were loaded in tension, with strain-gage measurements determining stress levels. A stressed sheet specimen is shown in Figure 3.

All strain gages on stressed billet, plate, and sheet specimens were removed with acetone. The possibility of picking up hydrogen from the acetone was checked using a hydrogen-detection gage (Reference 3) in which no free hydrogen ions were detected. All exposed surfaces were painted with red glyptal* enamel except for the center section test area. The test area measured 2 inches by 1 inch on all billet and plate specimens and 2 by 0.3 inches on all sheet specimens.

The stressed stress-corrosion specimens were placed on a ferris wheel 4 feet in diameter and 1.5 feet wide and alternately immersed in the 3.5-percent sodium chloride solution. The test solution was prepared using chemically pure salt and distilled water and was changed approximately every 5 days. The specimens were immersed in the test solution for 8 minutes of every hour by means of the testing apparatus shown in Figure 4.

---

*General Electric lacquer cement.

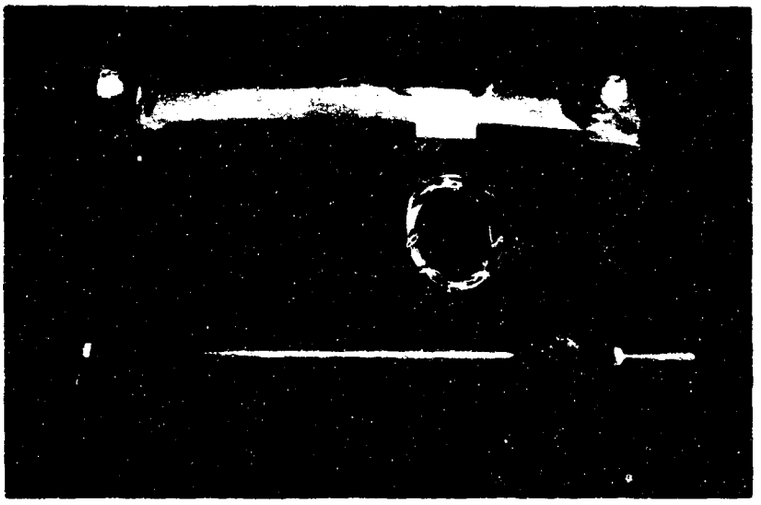

Figure 1 BOEING U-BEND CONFIGURATION

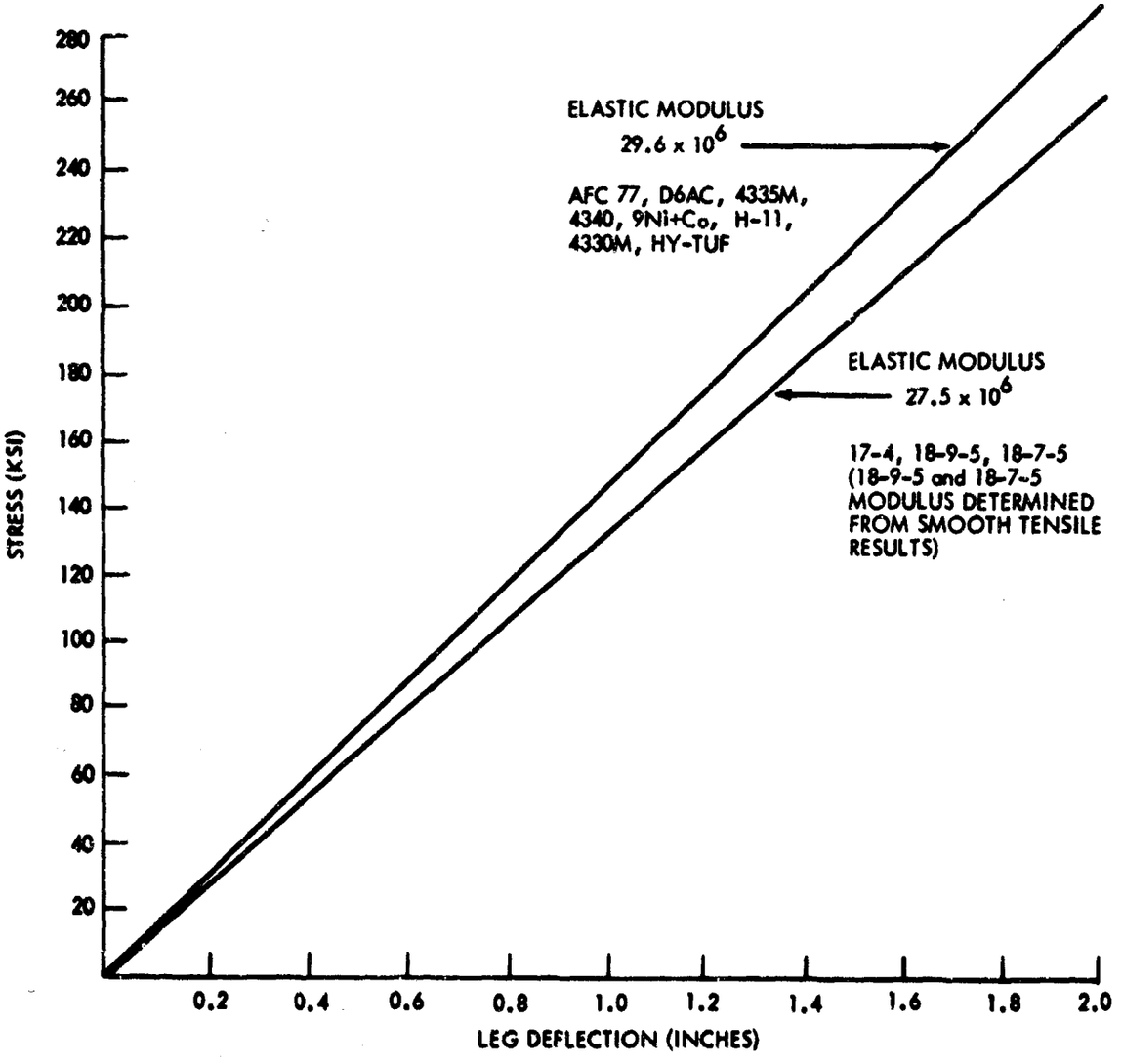

Figure 2 STRESS LEVEL AS A FUNCTION OF U-BEND CONFIGURATION LEG DEFLECTION

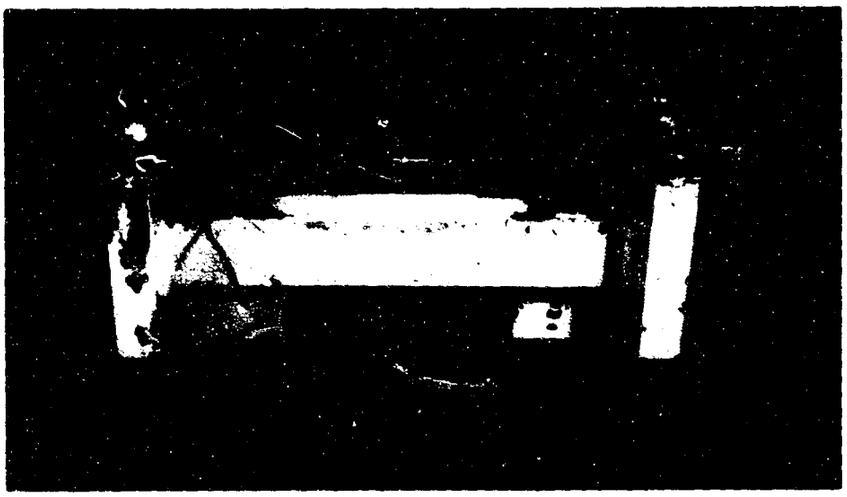

Figure 3 SHEET STRESS-CORROSION CONFIGURATION

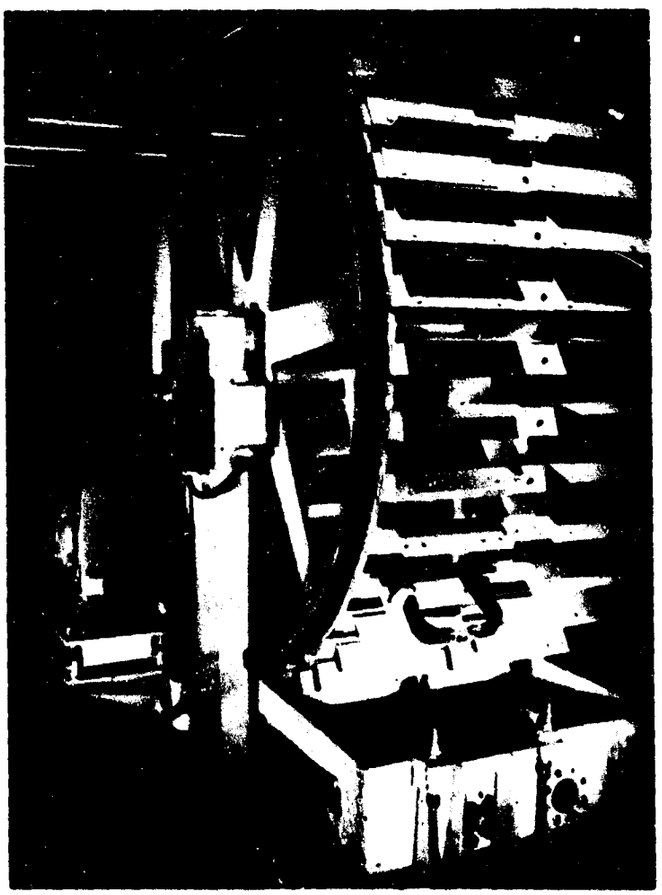

Figure 4 ALTERNATE-IMMERSION TEST APPARATUS

Alternate-immersion stress-corrosion testing continued until failure occurred or a 1000-hour test period had elapsed. The 1000-hour test limit was selected on the basis of previous data that indicated the majority of failures of susceptible alloys or conditions would occur within this time. A specimen was considered to have failed when complete fracture had occurred or when the fractured test specimens were held together by only a small section of metal. Actual growth of cracks could not be detected on any specimens.

In addition to the alternate-immersion testing, comparative data was obtained from specimens exposed to the Seattle Boeing Field atmosphere, which may be considered a semi-industrial environment. Specimens were left exposed until failure or contract time limitations curtailed further testing.

E. TEST VARIABLES

The standardization of specimen preparation methods permitted an evaluation of the effects of several variables on stress-corrosion susceptibility. These variables were selected so that a representative range of material forms, processing procedures, and environmental conditions would be considered. Five groupings were evaluated: product shape, environment, grain direction, processing variables, and design data. Processing variables were further divided to include heat-treat variations, strength level, ausforming, straightening, welding, and coatings. Design variables included comparative evaluations of different material heats and the effects of altering the stress level. These groupings are described in Table 3. A breakdown of the alloys tested in each phase is given in Table 2. The majority of testing was accomplished using the transverse grain directions. The only exception to this occurred when evaluating the stress-corrosion susceptibilities of the different grain directions. All materials, unless otherwise noted, were heat treated to their highest strength levels and stressed to 80 percent of the 0.2-percent yield strength.

Each alloy test phase was carried out using three stress-corrosion specimens. Mechanical properties of the billets, plates, and sheets were determined from two smooth tensile and two notched tensile (or two fracture toughness) specimens representing the various heat-treatment conditions.

F. FRACTOGRAPHY AND METALLOGRAPHY

Standard metallographic techniques were used to evaluate the microstructures and determine the modes of cracking in fractured specimens. In addition to these standard techniques, a recently devised etchant permitted determination of the low-alloy-steel grain sizes.

Fracture faces were studied using three methods: examination of etched and unetched surfaces, extraction replicas, and profile studies. The fracture replicas studied in the electron microscope were prepared from faxfilm imprints of the fracture faces. The faxfilm was placed in a vacuum chamber, shadowed

with germanium, and then with carbon. Dissolving the faxfilm in acetone produced replicas suitable for examination. Carbide-extraction replicas were produced by vacuum deposition of carbon on a polished specimen surface and then removing the carbon (plus carbides) in a methanol bromine solution. Fracture profiles were obtained by cutting specimens transverse to the fracture face, coating with electroless nickel, and polishing until the origin was exposed. Direct carbon extraction replicas were also taken of these profile specimens.

G. SUPPLEMENTAL INFORMATION — PREVIOUS STRESS-CORROSION STUDY

1. Environmental Testing

During the previous study (Reference 1) of stress-corrosion cracking, a similar study was underway at Aerojet-General Corporation. To obtain comparative information on the relative effects of the Boeing alternate-immersion and Aerojet-General constant-immersion aqueous NaCl test solutions, stressed 4340 specimens were sent to Aerojet. The test results were then compared to those obtained from duplicate specimens at Boeing.

2. Impact Testing

The previous work showed that a decrease in the 4340, 4340M, 4330M, and H-11 notched-to-unnotched strength ratios corresponds to an increase in stress-corrosion susceptibility. Comparison of these low-alloy-steel impact values reported in the literature with the stress-corrosion results indicated that a decrease in impact strengths also corresponds to an increase in stress-corrosion susceptibility. To check this latter relationship, impact specimens were cut from the same billet transverse grain direction and heat treated to the same strengths as the previous 4340, 4340M, 4330M, and H-11 stress-corrosion specimens.

H. LITERATURE SURVEY

A continuing literature survey has been maintained during this program. Particular attention has been directed to those articles dealing with stress-corrosion cracking and dislocation distributions.

Table 3 DESCRIPTION OF TEST VARIABLES

Phase	Description
Product Shape	Three alloy forms were considered: billet, plate, and sheet. All billets were 8 by 8 by 12 inches except for one 8-inch-diameter by 12-inch billet of 4340 (Billet G). Plates were 3/8 by 10 by 48 inches and sheet gages were between 0.02 and 0.08 inch.
Environment	The majority of testing consisted of alternate immersion in a 3.5-percent NaCl solution for 8 minutes per hour. Supplemental testing involved exposure to a semi-industrial environment at Boeing Field, Seattle, Washington.
Grain Direction	The longitudinal and transverse grain directions of all alloy forms were compared.
Processing Variables	
Heat Treatment Variations	AM 350 and AM 355 were studied using two approaches. The first approach consisted of studying the relationship between percent delta ferrite and stress-corrosion susceptibility. Boeing-procured and ASD-provided sheets were compared after heat treating using the SCT process and an alteration of this process introduced by raising the H annealing temperature by 50°F. The second approach was an evaluation of the precipitated carbide distribution in these materials after the DADF heat treatments. A trip by Boeing metallurgists to several steel and forging companies revealed two processes used in the mill annealing of several steels. Comparisons between these heat-treat processes were necessary to determine the effect of this early heat treatment on stress-corrosion susceptibility. One process consisted of holding 4335M and 4340 at 1600°F for 72 hours; the other process involved thermal cycling these same steels between 600 and 1200°F. The latter process required 16 hours for each of three cycles. Although oil quenching is used extensively during the heat treatment of low-alloy steels, there are a number of instances where austempering and martempering are used. To compare these latter two processes with oil quenching (which was used extensively in this program) 4335M and 4340 were chosen. The AFC 77 tensile properties (reduction in area) were approximately the same between tempering temperatures of 800 and 1000°F. To determine if a similar relationship existed between stress-corrosion susceptibility, comparisons were made after tempering at 800, 900, and 1000°F. Heat treatment procedures are given in Tables 4 and 5.
Strength Level	The AFC 77, 18-7-5, D6AC, 4335M, 4340, and H-11 steels were heat treated to the 260- to 280-, 220- to 240-, and 180- to 200-ksi strength levels. Heat-treatment procedures are given in Table 4.

Table 3 DESCRIPTION OF TEST VARIABLES

Phase	Description
Product Shape	Three alloy forms were considered: billet, plate, and sheet. All billets were 8 by 8 by 12 inches except for one 8-inch-diameter by 12-inch billet of 4340 (Billet G). Plates were 3/8 by 10 by 48 inches and sheet gages were between 0.02 and 0.08 inch.
Environment	The majority of testing consisted of alternate immersion in a 3.5-percent NaCl solution for 8 minutes per hour. Supplemental testing involved exposure to a semi-industrial environment at Boeing Field, Seattle, Washington.
Grain Direction	The longitudinal and transverse grain directions of all alloy forms were compared.
Processing Variables	
Heat Treatment Variations	AM 350 and AM 355 were studied using two approaches. The first approach consisted of studying the relationship between percent delta ferrite and stress-corrosion susceptibility. Boeing-procured and ASD-provided sheets were compared after heat treating using the SCT process and an alteration of this process introduced by raising the H annealing temperature by 50°F. The second approach was an evaluation of the precipitated carbide distribution in these materials after the DADF heat treatments. A trip by Boeing metallurgists to several steel and forging companies revealed two processes used in the mill annealing of several steels. Comparisons between these heat-treat processes were necessary to determine the effect of this early heat treatment on stress-corrosion susceptibility. One process consisted of holding 4335M and 4340 at 1600°F for 72 hours; the other process involved thermal cycling these same steels between 600 and 1200°F. The latter process required 16 hours for each of three cycles. Although oil quenching is used extensively during the heat treatment of low-alloy steels, there are a number of instances where austempering and martempering are used. To compare these latter two processes with oil quenching (which was used extensively in this program) 4335M and 4340 were chosen. The AFC 77 tensile properties (reduction in area) were approximately the same between tempering temperatures of 800 and 1000°F. To determine if a similar relationship existed between stress-corrosion susceptibility, comparisons were made after tempering at 800, 900, and 1000°F. Heat treatment procedures are given in Tables 4 and 5.
Strength Level	The AFC 77, 18-7-5, D6AC, 4335M, 4340, and H-11 steels were heat treated to the 260- to 280-, 220- to 240-, and 180- to 200-ksi strength levels. Heat-treatment procedures are given in Table 4.

Table 4 STANDARD STEEL HEAT TREATMENT PROCEDURES

Alloy	Nominal Ultimate Strength (ksi)	Austenitizing Temperature (°F)	Austenitizing Time (hr)	Quenching Medium	Tempering Temperature (°F)	Tempering Time (hr)
AFC 77*	260 to 280	1900	0.5	Oil	900	2 + 2
	220 to 240	1900	0.5	Oil	1200	2 + 2
	180 to 200	1900	0.5	Oil	1300	2 + 2
18-7-5	260 to 280	1500	0.5	Air	900	3
	220 to 240	1500	0.5	Air	1075	3
	180 to 200	1500	0.5	Air	1150	3
D6AC	260 to 280	1550	0.5	Oil	500	3 + 3
	220 to 240	1550	0.5	Oil	800	2.5 + 2.5
	180 to 200	1550	0.5	Oil	1100	1.5 + 1.5
4335M	260 to 280	1550	0.5	Oil	500	3 + 3
	220 to 240	1550	0.5	Oil	700	2.5 + 2.5
	180 to 200	1550	0.5	Oil	950	1.5 + 1.5
4340	260 to 280	1525	0.5	Oil	400	3 + 3
	220 to 240	1525	0.5	Oil	600	2.5 + 2.5
	180 to 200	1525	0.5	Oil	800	1.5 + 1.5
H-11	270 to 300	1850	0.5	Oil	1000	3 + 3 + 3
	220 to 240	1850	0.5	Oil	1100	3 + 3 + 3
	180 to 200	1850	0.5	Oil	1150	3 + 3 + 3
HY-Tuf	240 to 260	1600	0.5	Oil	550	1 + 1
9Ni-4Co*	260 to 280	1475	0.5	Oil	400	2 + 2
18-9-5	280 to 310	1500	0.5	Air	900	3
17-4PH	180 to 200	1900	0.5	Air	900	1
AM 350*	180 to 200**	1925	0.5	Air	850	3
AM 355*	180 to 200**	1925	0.5	Air	850	3

* These steels required a subzero cool at -100°F prior to tempering
** SCT 850 condition

Table 5 SPECIAL STEEL HEAT TREATMENT PROCEDURES

Alloy	Description of Heat Treatment
AM 350 and AM 355	**Double Age, Double Freeze** Procedure was identical to that used for SCT 850 condition (Table 4), except a subzero freeze (-100°F for 3 hours) was introduced after solution anneal. **Altered SCT 850 Condition** The solution annealing temperature was increased to 1975°F (see Table 4 for procedure for SCT 850 condition).
AFC 77	**800 and 1000°F Tempers** Identical procedures were used in the 800 to 1000°F tempers as in the 900, 1200, and 1300°F tempers described in Table 4.
4340 and 4335M	**Milling Annealing** Cycling — Specimens were thermally cycled between 600 and 1200°F, allowing 6 hours at each temperature, the total elapsed time for three complete cycles was 50 hours. Specimens were then heat treated to maximum strength according to Table 4. Holding — Specimens were held at 1600°F for 72 hours, and then air cooled followed by heat treating to maximum strength according to Table 4. **Austempering** Specimens were austenitized at 1525°F for 0.5 hour, quenched in 600°F salt and held for 24 hours, and air cooled. **Martempering** Specimens were austenitized at 1525°F for 0.5 hour, quenched in 375°F salt and held for 30 seconds, followed by air cooling. Specimens were then tempered at 450°F for 4 hours.

Table 6 COATING PROCESSES

Type of Coating	Coating Process
Epoxy Paint*	The specimens were prepared by degreasing and vapor blasting. The coating material consisted of a Type 1 primer and a Type 2 enamel. The primer base material plus converter and thinner were mixed to give a spray viscosity of 32 to 40 seconds, determined by a No. 1 Zahn cup. The primer film thickness was 0.9 to 1.1 mils. The finish coating consisted of an enamel base mixed with a catalyst and thinner to give a spray viscosity of 17 to 19 seconds determined by a No. 2 Zahn cup. The enamel film thickness was 2.5 to 2.9 mils. The epoxy paint was air dried for 10 hours — 4 hours for the primer and 6 hours for the enamel.
Cadmium Plating**	The specimens were prepared by vapor degreasing in trichloroethylene and cleaned by abrasive blasting with novaculite silica spherical glass beads (180 to 625 grit). The specimens were then cold rinsed and maintained in a cyanide bath at 70 to 85°F until plated. The cyanide holding solution was: 1) Sodium Cyanide — Original Preparation: 31 lb/100 gal. — Control Concentration: 4 to 5 oz/gal. 2) Sodium Hydroxide — Original Preparation: 10 lb/100 gal. — Control Concentration: 1 to 2 oz/gal. The specimens were placed directly from the cyanide bath to the cadmium plating solution, which was maintained at a current density of approximately 40 amps/ft^2. The cadmium plating solution was operated at 70 to 85°F and had the following composition: 1) Sodium Cyanide — Original Preparation: 146 lb 100 gal. 2) Cadmium Oxide — Original Preparation: 47 lb 100 gal. 3) Cadmium (metal) — Control Concentration: 6.5 to 7.5 oz/gal. 4) Sodium Carbonate — Control Concentration: 8.0 oz/gal. (max.) 5) Sodium Hydroxide — Control Concentration: 3.5 to 5.0 oz/gal. 6) Free Sodium Cyanide (Total NaCn - 1.75 x Cd) — Control Concentration: 9 to 15 oz/gal. 7) Water, deionized — Original Preparation: Maintain Volume The specimens were then rinsed in cold water, air dried, and baked for 24 hours at 375°F.
Cadmium-Titanium Plating***	The specimens were prepared the same as for the cadmium plating. The hold bath also was similar, except it was operated at a maximum iron concentration of 50 ppm. The specimens were rinsed in cold water and then immersed in a 2- to 4-percent HCl solution for 30 seconds to activate the surfaces. Another cold water rinse was given prior to the cadmium-titanium plating step. The plating solution was maintained at 70 to 85°F and had the following composition:

* BMS 10-11
** BAC 5718
*** BAC 5604

Table 6 (continued)

Type of Coating	Coating Process
	Control Concentration 1) Cadmium (metal) — 2.5 to 3.5 oz/gallon 2) Total Cyanide (as NaCn) — 13 to 17 oz/gallon 3) Sodium Hydroxide — 2.5 to 3.6 oz/gallon 4) Total Iron Concentration — 50 ppm 5) Other Foreign Metal Impurities (Zn, Sn, Ni, Cu, Pb) — 30 ppm 6) Titanium — 60 to 100 ppm 7) Total Cyanide to Cadmium Ratio (NaCn/Cd) — 4/1 to 5/1 The specimens were then immersion rinsed in a 3- to 5-percent chromic acid in water solution (room temperature) for 0.5 to 2 minutes, cold water rinsed for a maximum of 5 minutes, and then air dried. The specimens were baked at 375°F for 12 hours.
Cadmium Plating plus Epoxy Paint	First, the specimens were cadmium plated according to the previously described procedure. Immediately following the plating operation, the specimens were painted (also previously described).
Flame-Sprayed Aluminum	Specimens were lightly sand blasted and flash coated with Metco Sprabond, and then finished to desired thickness using high-purity aluminum.

IV. RESULTS

A. MATERIAL EVALUATION

The billets and plates used in this program were free from flaws larger than 3/64 of an inch (minimum detectable flaw size), except for one billet of 4340 and one plate of 9Ni-4Co. Ultrasonic inspection showed a number of indications ranging from 3/64 to 5/64 inch at the center of the 4340 billet. Ultrasonic inspection also revealed a large number of indications in the 9Ni-4Co plate approximately 3/64 of an inch in length. Macroetching of all billets revealed no gross segregation. All billets, plates, and sheets were within chemistry allowables. Chemical compositions are given in Table 7.

The selection of the primary transverse grain direction (i.e., grain direction used in the majority of testing) was based on the reduction-in-area properties. Since the reduction-in-area values of each billet's two transverse grain directions were the same, except for the 4340 billet having the flaws, the primary grain direction was arbitrarily selected. The transverse grain direction in the above 4340 billet with the lowest reduction-in-area value was the grain direction tested.

B. SPECIMEN PREPARATION

Microscopic examination showed that all decarburized areas on the billet and plate stress corrosion specimens were eliminated by grinding 0.050 inch from each specimen side. No difficulty was encountered in obtaining a 32 RHR surface finish. Precoating prevented any decarburization of sheet material during heat treatment, as shown by microscopic examination. Grit blasting removed the precoat, leaving a blue or gray discoloration on the surface.

Radiography revealed several instances of porosity in the fusion-welded specimens. This is discussed in detail in the welding subsection.

C. X-RAY RESIDUAL SURFACE STRESS MEASUREMENTS

All measured billet and plate residual surface stresses were compressive after grinding. Vapor blasting considerably increased the surface compressive stresses. This was revealed by X-ray residual stress measurements of 17-4PH and 18-9-5 before and after vapor blasting, and agrees with the results reported previously (Reference 1). The surface stresses after vapor blasting were usually greater than 100 ksi, though exceptions were noted in AFC 77, Ladish D6AC, 4340, and 18-9-5. No correlation was noted between residual surface stresses and heat-treat strength or chemical composition. Residual surface stresses of the billet and plate alloys are shown in Table 8.

Sheet residual surface stress measurements were very erratic, ranging from high compression to low tension. Apparently, the discoloration on the sheet surface was

Table 7 CHEMISTRIES OF TEST MATERIALS

Material	C	Mn	Ni	Si	Cr	Mo	S	P	V	Cu	Al	Co	Ti
AFC 77 Billet A	0.14	0.20	0.17	0.31	14.75	4.24	0.006	0.018	0.031	--	--	--	--
AM 350 Sheet A_1	0.10	0.88	4.23	0.67	16.38	3.14	0.013	0.011	--	--	--	--	--
AM 350 Sheet A_2	0.12	0.75	4.25	0.47	16.38	2.84	0.009	0.004	--	--	--	--	--
AM 350 Sheet B	0.09	0.76	4.34	0.43	16.15	3.23	0.015	0.005	--	--	--	--	--
AM 350 Sheet F	0.12	0.79	4.18	0.35	15.92	2.98	0.007	0.012	--	--	--	--	--
AM 355 Sheet C	0.15	0.77	4.29	0.41	15.40	2.95	0.020	0.012	--	--	--	--	--
AM 355 Sheet D	0.16	0.69	4.26	0.37	15.35	2.70	0.011	0.011	--	--	--	--	--
17-4PH Plate Q	0.06	0.25	4.99	0.46	16.10	0.15	0.016	--	--	4.20	--	--	--
17-4PH Plate R	0.05	0.34	4.55	0.57	15.90	--	0.015	0.007	--	3.20	--	--	0.26
18-9-5 Plate M	0.009	0.018	18.32	0.05	--	4.88	0.004	0.002	--	9.06	0.11	--	0.73
18-7-5 Billet B	0.030	0.052	17.25	0.054	--	5.86	0.003	0.003	--	--	0.22	8.15	0.49
18-7-5 Plate S	0.014	0.058	17.02	0.030	--	5.42	0.004	0.009	--	--	0.09	8.10	0.43
D6AC Billet C	0.47	0.68	0.06	0.22	1.05	0.82	--	--	0.067	0.10	--	--	--
D6AC Billet D	0.43	0.69	--	0.22	1.05	1.11	0.008	0.002	0.070	--	--	--	--
D6AC Plate T	0.40	0.69	--	0.57	1.01	0.99	0.007	0.006	0.08	0.06	--	--	--
4335M Billet E	0.37	0.72	1.70	0.32	0.82	0.37	0.011	0.011	0.18	--	--	0.17	--
4335M Billet J	0.35	0.77	1.82	0.32	0.81	0.35	0.010	0.012	0.20	0.13	--	--	--
4335M Plate U	0.35	0.82	1.96	0.29	0.74	0.35	0.015	0.019	0.19	0.11	0.015	--	--
4340 Billet F	0.40	0.69	1.80	0.21	0.88	0.27	0.020	0.012	--	--	--	--	--
4340 Billet G	0.39	0.79	1.70	0.28	0.89	0.25	0.012	0.020	--	0.092	--	--	0.013
4340 Plate V	0.40	0.78	1.85	0.28	0.76	0.28	0.003	0.015	--	0.094	0.04	--	--
4340 Sheet E	0.39	0.80	1.89	0.29	0.78	0.27	0.012	0.017	--	0.10	--	--	--
9Ni-4Co Plate W	0.26	0.17	8.86	0.042	0.35	0.35	0.012	0.002	--	--	--	3.82	--
9Ni-4Co Plate X	0.38	0.12	8.19	0.033	0.17	0.10	0.006	0.041	--	--	--	3.88	--
9Ni-4Co Plate Y	0.33	0.12	8.89	0.01	0.35	0.31	0.007	0.006	0.08	--	--	3.83	--
H-11 Billet H	0.40	0.27	0.16	0.82	4.90	0.99	0.012	0.023	0.42	--	--	--	--
H-11 Billet I	0.43	0.34	0.15	1.01	4.50	0.92	0.018	0.013	0.43	--	--	--	--
H-11 Plate Z	0.37	0.38	0.15	0.71	4.54	1.05	0.012	0.014	0.45	0.095	0.070	--	--
HY-Tuf Billet K	0.26	1.33	1.76	1.55	0.40	0.41	0.006	0.007	--	--	--	--	--

Table 8 RESIDUAL SURFACE STRESSES IN BILLETS AND PLATES

32 RHR SURFACE FINISH

Material	Identification	Heat Treatment	Ultimate Strength (ksi)	Yield Strength (ksi)	Residual Surface Stresses (ksi) (Negative Sign Indicates Compression)
AFC 77	Billet A	Standard	255	208	-200
		Standard	220	168	- 90
		Standard	195	140	-100
		Special 800°F	241	197	-140
		Special 1000°F	257	200	-172
Ladish D6AC	Billet C	Standard	284	233	- 85
		Standard	242	216	- 55
		Standard	222	204	-130
		Ausform at 1500°F	284	233	- 90
	Plate T	Standard	278	252	-172
4335M	Billet E	Standard	257	221	-115
		Standard	234	205	-135
		Standard	199	187	- 60
		Ausform at 1500°F	257	221	-135
4335M	Plate U	Standard	252	214	-125
		Standard	252	216	-130*
4340	Billet F	Standard	273	215	-140
		Standard	242	205	- 85
		Standard	186	170	-120
		Mill Anneal at 1600°F	270	206	-175
		Mill Anneal at 600 to 1200°F	271	210	-190
		Ausform at 1000°F	273	215	-200
		Ausform at 1200°F	273	215	-145
	Plate V	Standard	266	211	-165
H-11	Billet H	Standard	279	224	-190
		Standard	187	150	-150
	Plate Z	Standard	280	225	-180
9Ni-4Co	Plate X	Standard	220	205	-180
17-4PH	Plate R	Standard	210	186	- 30**
		Standard	210	186	-160
13-9-5	Plate M	Standard	310	300	- 14**
		Standard	310	300	- 90
18-7-5	Billet B	Standard	280	272	-125
	Plate S	Standard	266	255	-100

* Longitudinal Grain Direction

**Surface Not Vapor Blasted

the cause of these variations because sandpapering produced surfaces that provided reproducible results. However, this latter condition did not represent the actual testing surface conditions; consequently, detailed sheet residual surface stress measurements were not made.

Measurements of residual surface stresses in plate and billet with the X-ray diffractometer revealed a linear relationship between residual surface stresses produced by grinding and applied stresses produced during loading. The magnitude of the final surface stresses after loading could be determined by adding residual and applied stresses. X-ray stress analysis of a 4330M U-bend specimen before and after electropolishing showed a change in the residual surface stresses from compressive to tension at approximately 0.002 inch below the surface. This relationship between residual and applied stresses with depth is shown in Figure 5.

D. STRESS-CORROSION TESTING

The stress level in loaded billet and plate specimens was checked for 1 month. The relaxation in stress level was found to occur within 24 hours after loading. The stress level of the sheet specimens was also found to be constant after the initial 24 hours. All test specimens were rechecked after the relaxation period and restressed when required.

The use of the U-bend configuration for evaluating billet and plate material provided an excellent means of determining relative stress-corrosion susceptibilities. In addition, examination of these fracture faces allowed the study of rapid-cracking and slow-cracking modes of fracture. Often these fracture modes could be directly compared to those observed on fracture toughness specimens. Although the sheet specimens were smaller, the electron microscope permitted observation of the fracture origin and associated areas. However, the geometrical limitations of these specimens did not provide the large rapid crack areas produced on the U-bend specimens.

E. TEST VARIABLES

The stress-corrosion test results are described in the following subsections. Mechanical properties of the alloys after the several heat treatments are listed in Tables 9, 10, and 11. Appendix II describes the method of fracture toughness testing.

1. Product Shape

There were no 18-7-5 billet or plate failures. Comparison of the 4335M and 4340 billets and plates showed that the billet material was more stress-corrosion susceptible. Determination of the relative susceptibilities of D6AC billet and plate depended on the grain direction under consideration. The D6AC comparisons based on the transverse grain direction showed billet to be the more susceptible, while

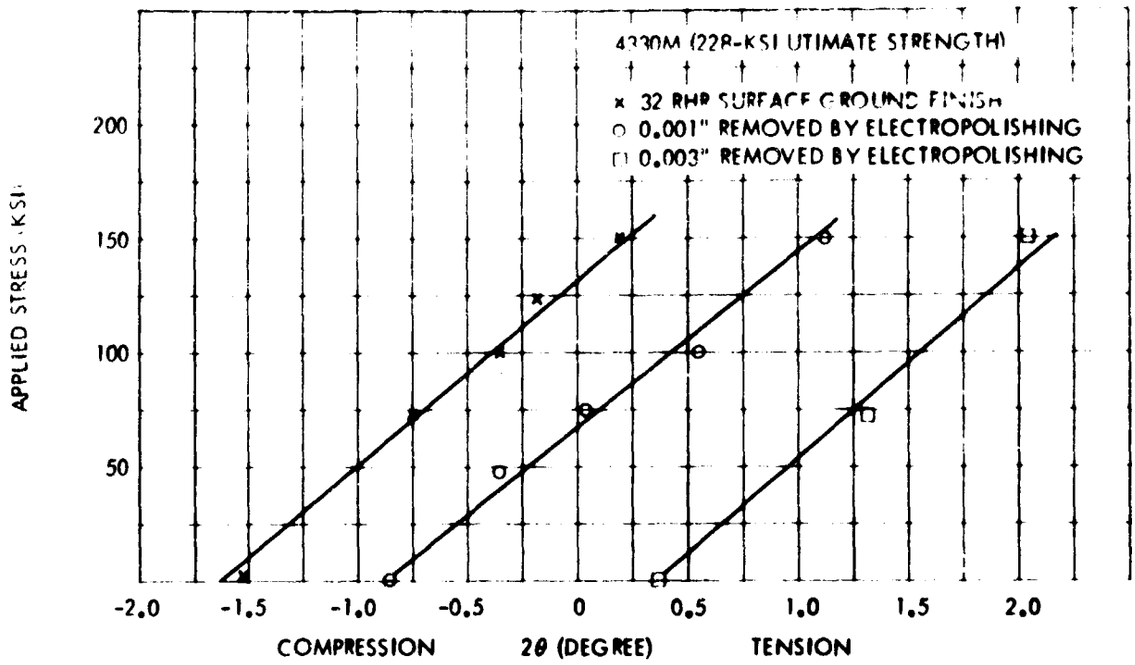

Figure 5 RELATIONSHIP BETWEEN RESIDUAL AND APPLIED STRESSES

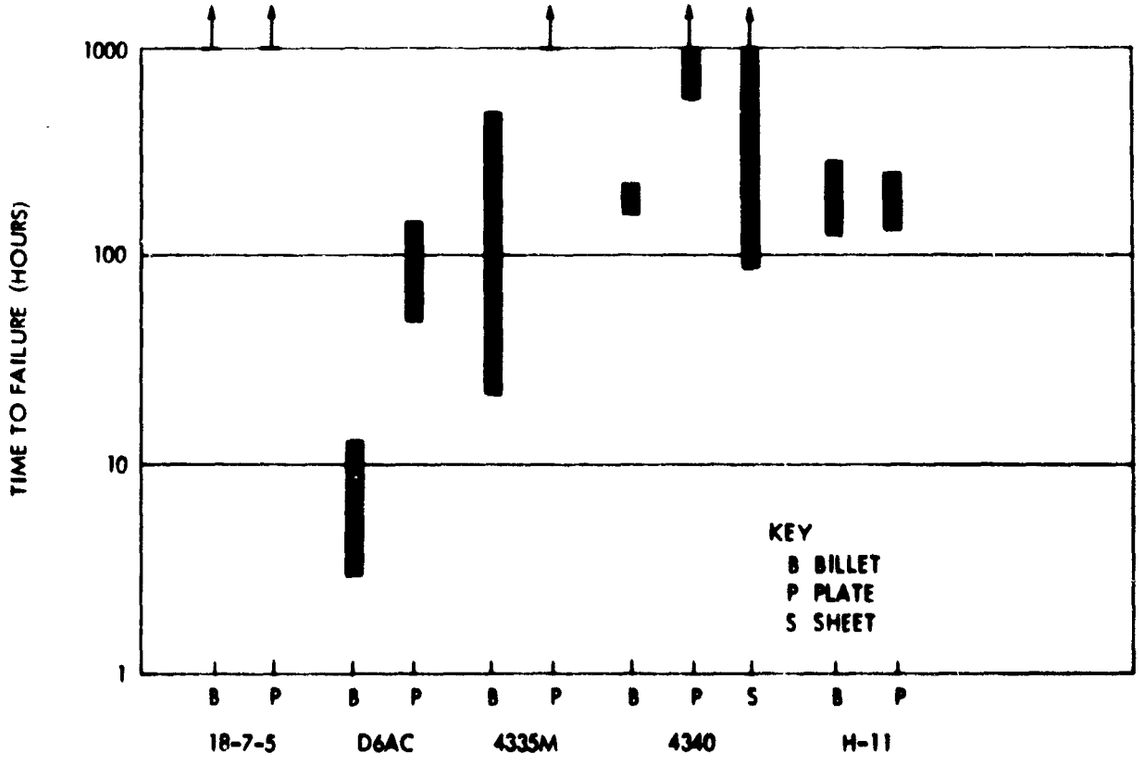

Figure 6 RELATIVE STRESS-CORROSION SUSCEPTIBILITY OF COMPARATIVE ALLOY FORMS

Table 9 TENSILE PROPERTIES OF STEEL ALLOYS — STANDARD HEAT TREATMENT

VALUES AVERAGED FROM TWO SPECIMENS PER CONDITION

Material	Grain Direction	Ultimate Strength (ksi)	Yield Strength (ksi)	Elongation (% in 1 in.)	Reduction in Area (%)	Notched Ultimate Strength (ksi)	N/UN Ratio
AFC 77	T	255	208	~5.0	3.0	161	0.63
Billet A	T	220	168	3.5	2.5	113	0.51
	T	195	140	7.5	11.0	143	0.73
	T_2*	259	210	4.5	4.0	153	0.59
	L	269	211	16.0	34.5	168	0.62
18-7-5	T	280	272	7.0	28.7	261	0.93
Billet B	T	231	213	12.0	30.6	280	1.21
	T	203	177	17.0	44.6	282	1.39
	T_2	278	270	7.0	25.6	247	0.89
	L	283	269	11.5	52.3	361	1.34
Ladish D6AC	T	285	233	7.5	16.5	205	0.72
Billet C	T	242	216	8.0	26.0	266	1.23
	T	222	204	11.5	35.0	287	1.29
	T_2	278	219	6.0	16.0	223	0.80
	L	286	241	11.0	44.0	260	0.91
4335M	T	257	221	9.0	24.8	252	0.98
Billet E	T	234	~205	8.0	24.3	256	1.09
	T	199	~187	12.5	32.5	251	1.26
	T_2	256	218	10.0	28.5	252	0.98
	L	257	218	13.0	33.7	274	1.06
4340	T	273	215	8.3	20.1	195	0.71, 0.34*
Billet F	T	242	205	7.3	15.7	172	0.71
	T	186	170	10.5	25.2	239	1.28, 0.78*
	T_2	267	208	6.5	14.6	186	0.70
	L	274	209	14.0	47.7	250	0.91
4330M Billet N	T	228	198	8.0	37.0	302	1.32
4330M Billet O	T	230	196	8.0	25.0	257	1.11
H-11	T	279	224	10.0	34.5	221	0.79
Billet H	T	224	190	10.5	33.5	277	1.23
	T	186	150	--	--	251	1.36
	T_2	279	225	8.0	16.5	178	0.69
	L	274	221	10.5	41.5	221	0.80
HY-Tuf Billet K	T	249	215	12.0	36.1	296	1.19
17-4PH	T	210	186	15.0	48.7	--	0.27
Plate Q	L	209	187	16.0	50.0	--	0.30
18-9-5	T	304	299	6.5	--	--	0.58
Plate M	L	305	297	7.1	--	--	0.65

*Notched ultimate strength from large notched tensile specimens

Table 9 (continued)

Material	Grain Direction	Ultimate Strength (ksi)	Yield Strength (ksi)	Elongation (% in 1 in.)	Reduction in Area (%)	Notched Ultimate Strength (ksi)	N'/UN Ratio
18-7-5	T	266	255	10.5	55.7	--	0.68
Plate S	L	263	257	10.0	53.3	--	0.64
D6AC	T	278	252	11.0	41.7	--	0.30
Plate T	L	275	252	10.0	39.7	--	0.35
4335M	T	252	214	11.0	42.5	--	0.60
Plate U	L	252	216	12.0	53.5	--	0.66
4340	T	266	211	10.0	35.0	--	0.31
Plate V	L	267	214	12.5	48.0	--	0.43
9Ni-4Co 0.26C	T	244	212	11.5	62.1	--	0.70
Plate W	L	225	208	12.0	64.6	--	0.79
9Ni-4Co 0.38C	T	~220	~205	8.0	34.0	--	0.56
Plate X	L	238	227	7.0	28.0	--	0.41
H-11	T	280	225	13.5	50.0	--	0.16
Plate Z	L	281	225	14.0	47.0	--	--
AM 350 Sheet A_1	T	194	161	11.0	--	163	0.84
AM 350	T	201	164	11.0	--	173	0.86
Sheet A_2	L	203	167	12.7	--	183	0.90
AM 350 Sheet B	T	203	167	10.7	--	137	0.68
AM 350 Sheet F	T	230	198	9.0	--	188	0.82
AM 355	T	229	195	10.8	--	170	0.74
Sheet C	L	229	195	10.0	--	150	0.66
AM 355 Sheet D	T	216	187	7.7	--	133	0.62
4340	T	261	210	9.8	--	177	0.68
Sheet E	L	261	200	10.3	--	169	0.65

Table 10 TENSILE PROPERTIES OF STEEL ALLOYS — SPECIAL HEAT TREATMENT

VALUES AVERAGED FROM TWO SPECIMENS TAKEN FROM THE PRIMARY TRANSVERSE GRAIN DIRECTION

Material	Heat Treatment	Ultimate Strength (ksi)	Yield Strength (ksi)	Elongation (% in 1 in.)	Reduction in Area (%)	Notched Ultimate Strength (ksi)	N/UN Ratio
AFC 77 Billet A	a	241	197	2.5	2.5	151	0.63
	b	257	200	3.5	2.5	154	0.60
AM 350 Sheet A_2	c	203	161	18.0	--	167	0.82
	d	204	171	14.0	--	174	0.85
AM 355 Sheet C	c	220	184	16.5	--	164	0.75
	d	197	143	13.5	--	109	0.55
D6AC Billet C	e_1	301	261	7.8	18.1	--	--
4335M Billet E	e_1	286	230	9.3	26.2	--	--
	f	270*	--	1.0	4.0	128	0.47
	g	260	220	7.5	20.0	219	0.84
	h	265	225	7.0	16.0	219	0.83
	i	199	173	10.0	33.5	239	1.20
4340 Billet F	e_1	308	259	8.0	19.9	--	--
	e_2	298	251	8.5	24.0	--	--
	e_3	287	242	8.0	20.8	--	--
	f	--*	--	--	--	91.9	--
	g	277	210	9.0	16.5	190	0.69
	h	255	221	6.0	17.5	187	0.73
	i	197	166	8.0	24.5	221	1.12
9Ni-4Co Plate Y	e	290	248	9.0	54.8	--	0.44

Heat-Treatment Code

a — Tempered at 800°F for 2 + 2 hours

b — Tempered at 1000°F for 2 + 2 hours

c — DADF condition (double aged, double freeze)

d — SCT 850 condition with the annealing temperature increased by 50°F

e — Ausformed
- 1 — 25 percent reduction at 1500°F
- 2 — 25 percent reduction at 1200°F
- 3 — 25 percent reduction at 1000°F

f — Mill annealed by holding at 1600°F for 72 hours

g — Mill annealed by cycling between 600 and 1200°F

h — Martempered at 450°F

i — Austempered at 600°F

*Specimens broke outside the gage section

Table 11 FRACTURE TOUGHNESS PROPERTIES

ALL MATERIALS HEAT TREATED TO MAXIMUM STRENGTH LEVEL

Material	Grain Direction	F_{ty} (ksi)	Stress Rate $\dot{\sigma}_G$(ksi/sec)	Net Stress (ksi)	Max σ_G (ksi)	K_c or K_{Ic} (ksi $\sqrt{in.}$)	k_c or k_{Ic} (ksi $\sqrt{in.}$)	Shear (%)
17-4PH	T	186	535	56.8	36.1	36.5	20.6	1
Plate Q	L	187	506	61.9	36.8	38.5	21.7	1
18-9-5	T	299	270	21.3	12.3	14.0	7.9	0
Plate M	L	297	349	31.8	20.5	20.2	11.4	1
18-7-5	T	255	500	181.0	120.8	122.2	68.9	67
Plate S	L	257	500	168.0	115.3	115.7	65.3	64
18-7-5 Billet B	T	270	737	137.0	79.6	80.6	45.5	30
D6AC	T	252	500	83.0	55.0	60.2	34.0	13
Plate T	L	252	500	96.7	63.5	62.9	35.5	15
4335M	T	214	701	150.0	91.7	96.8	54.6	53
Plate U	L	216	707	167.0	103.5	107.2	60.5	60
4335M Billet E	T	221	738	102.0	66.3	61.3	34.6	17
4340	T	211	623	82.8	51.0	54.0	30.5	17
Plate V	L	214	712	116.0	74.6	74.4	42.0	20
4340 Billet F	T	215	725	96.8	58.7	57.5	32.5	13
9Ni-4Co	T	212	500	170.0	112.4	115.5	65.2	60
Plate W	L	208	500	177.0	115.9	120.8	68.2	63
9Ni-4Co	T	205	500	124.0	82.9	83.4	47.0	18
Plate X	L	227	500	98.0	65.9	67.2	37.9	13
9Ni-4Co	T	248	500	127.0	83.0	85.2	48.1	33
Plate Y	L	—	500	100.0	66.2	76.5	43.2	30
H-11	T	225	506	45.6	28.0	28.9	16.3	1
Plate Z	L	225	506	48.7	29.9	30.7	17.3	2
AM 355	T	187	762	79.6	53.2	129.4	73.1	100
Sheet D	L	—	845	58.0	38.1	94.1	53.1	100
AM 350	T	198	927	88.8	60.5	143.7	81.0	100
Sheet F	L	—	983	107.6	73.3	173.0	97.6	100
4340 Sheet E	T	210	473	114.6	76.7	187.0	105.5	100
4340*	T	170	2.5	145.0	—	70.9	—	—
Billet F	T	215	2.5	94.2	—	46.3	—	—

T — Transverse

L — Longitudinal

*Large Notched Tensile Specimens

comparison of the longitudinal grain direction revealed plate to be the more susceptible. No differences were evident between H-11 billet and plate. The 4340 sheet data was somewhat confusing because two failures occured within 90 hours, and the remaining specimen did not fracture during test. Additional testing would be necessary before any estimates can be made concerning the susceptibility of 4340 sheet. Figure 6 (Page 25) shows the relative susceptibilities of the billets and plates. Actual testing times are given in Table 12.

Table 12 TESTING TIMES OF COMPARATIVE ALLOY FORMS

TRANSVERSE GRAIN DIRECTION; ALL MATERIAL HEAT TREATED TO MAXIMUM STRENGTHS AND STRESSED TO 80 PERCENT OF YIELD

Material	Form*	Fty (ksi)	Stress (ksi)	Time-to-Failure (hr)
18-7-5	B	272	215	No Failures (NF)
	P	255	205	NF
D6AC	B	223	185	3, 5, 13
	P	252	200	-, 50, 148
4335M	B	221	175	22, 162, 500
	P	214	170	NF
4340	B	215	170	166, 172, 238
	P	211	170	612, 720, NF
	S	210	170	90, 90, NF
H-11	B	224	180	134, 134, 295
	P	225	180	143, 174, 260

* B, Billet
P, Plate
S, Sheet

2, Environment

Alternate-immersion testing of D6AC, 4340, 4335M, H-11, AFC 77, and AM 355 proved to be more severe than exposure to the Seattle semi-industrial environment. Failure times of these materials, with the exception of 4335M, were much shorter with alternate-immersion testing than with natural environment testing. The 4335M with relatively short alternate-immersion failure times did not fail in the semi-industrial atmosphere. Comparison of these steels revealed one unexpected abnormality. Those materials first to fail during alternate immersion were not necessarily the first to fail in the atmosphere. Ladish D6AC had failed within 13 hours on the ferris wheel but required over 3000 hours in the atmosphere, whereas AFC 77 failure times were 25 to 238 hours, respectively. Moreover, although 4340 and H-11 had approximately the same failure times with alternate-immersion testing, the 4340 was much more stress-corrosion susceptible in the semi-industrial atmosphere.

One partial explanation for these differences in relative stress corrosion susceptibilities revealed by the two testing methods may be related to the variation in rainfall. A plot showing the rainfall per month and the time periods during which these steels were tested is shown in Figure 7, which indicates that the majority of testing, and most of the failures, took place during the relatively dry months of May through September 1963. Similar results were obtained from the testing of alloy steels at Kure Beach. In these tests, Avery (Reference 4) observed that a majority of the failures occurred between April and November. Since both D6AC and AFC 77 were tested during this period, the reversal in relative susceptibilities from that noted during alternate-immersion testing could not be due to testing during different periods. However, the H-11 testing was initiated in March and failures occurred in June, September, and early October; the 4340 testing, starting in June, was completed in September. This indicates that testing H-11 and 4340 during the same periods may have revealed failure times more nearly the same.

There were no 18-7-5 alternate-immersion fractures, but one failure did occur during atmospheric exposure. Neither test method produced 17-4PH, 9Ni-4Co (low carbon heat), or AM 350 failures. Comparative results for all steels are plotted in Figure 8 and tabulated in Table 13.

3. Grain Direction

The transverse grain directions in 4340 billet and plate, D6AC billet, 4335M and H-11 plates, and AM 355 sheet were more stress-corrosion susceptible than the longitudinal grain directions. The only exception to this trend was shown by the H-11 billet, in which all grain directions had approximately the same failure times. The failure times of the two billet transverse grain directions in 4340, D6AC, and H-11 were approximately the same. This was expected because all billets had square cross sections and their mechanical properties proved to be nearly the same. One 4335M transverse grain direction appeared to be slightly more susceptible than the other transverse grain direction. The reason for this latter disparity is not known. The 4340 sheet results were inconclusive since there were specimens from both the transverse and longitudinal directions that were intact after testing. There were no 18-7-5, 17-4PH, 9Ni-4Co, and AM 350 failures. Test results are plotted in Figure 9 and tabulated in Table 14.

4. Processing Variables

a. Strength Level

The tensile properties listed in Table 9 show that the ultimate strengths were, with one exception, within or near to the desired 260- to 280-, 220- to 240-, or 180- to 220-ksi strength levels. The D6AC heat treated to obtain an ultimate strength between 180 and 200 ksi provided a strength of 222 ksi. Stress-corrosion susceptibility versus strength level for the AFC 77, 18-7-5, D6AC, 4335M, 4340, and H-11 alloys is given in Table 15 and plotted in Figures 10 through 16. A general trend of greater susceptibility with increased strength was evident for the AFC 77,

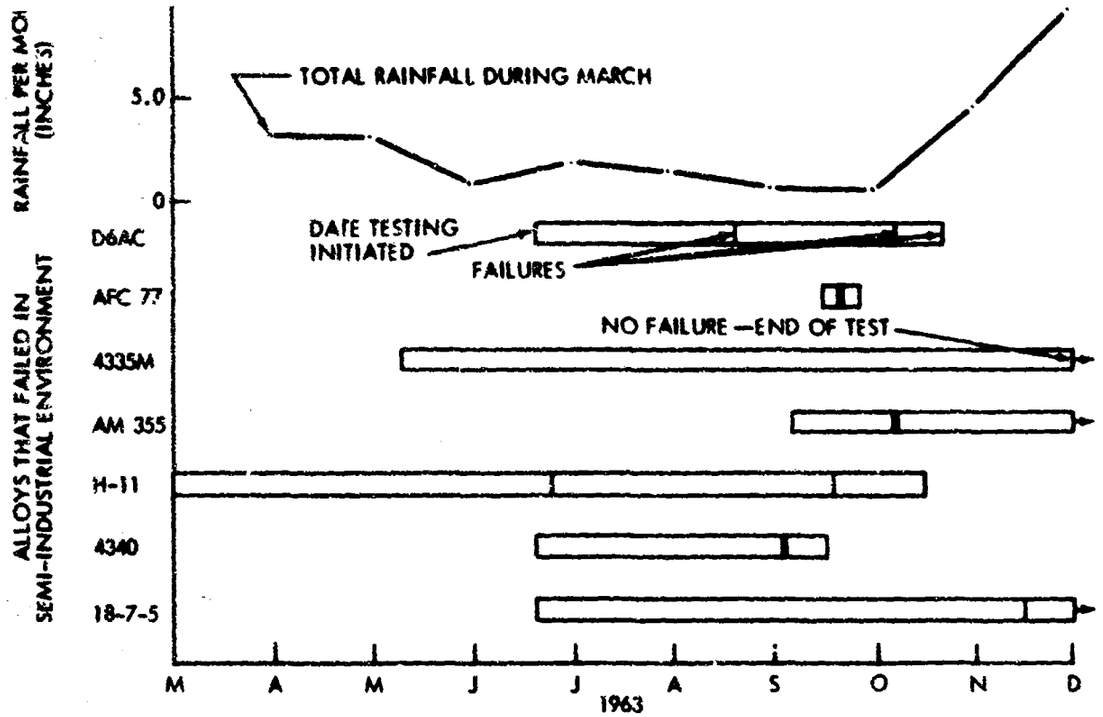

Figure 7 RAINFALL DURING SEMI-INDUSTRIAL ENVIRONMENT TESTING

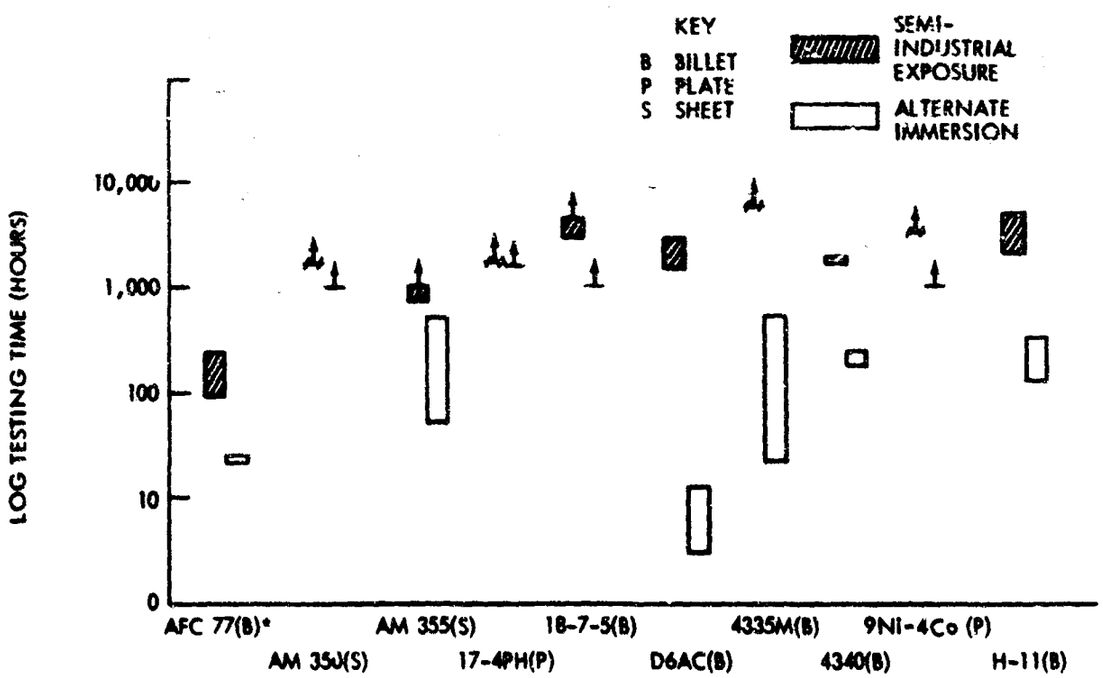

Figure 8 COMPARISON BETWEEN ALTERNATE-IMMERSION AND SEMI-INDUSTRIAL EXPOSURE

Table 13 ENVIRONMENTAL TESTING TIMES

TRANSVERSE GRAIN DIRECTION; ALL MATERIAL HEAT TREATED TO MAXIMUM STRENGTHS AND STRESSED TO 80 PERCENT OF YIELD

Material	Environment*	F_{ty} (ksi)	Stress (ksi)	Time to Failure (hr)
AFC 77	a	208	165	94, 94, 238
Billet A	b	208	165	**c, 23, 25
AM 350	a	164	130	NF 1700
Sheet A_2	b	164	130	NF 1000
AM 355	a	195	155	720, 720, NF 2048
Sheet C	b	195	155	55, 185, 478
17-4PH	a	185	150	NF 1700
Plate R	b	185	150	NF 1000
18-7-5	a	272	215	3456, NF 3730
Billet B	b	272	215	NF 1000
D6AC	a	233	185	1500, 2688, 2856
Billet C	b	233	185	3, 5, 13
4335M	a	221	175	NF 4780
Billet E	b	221	175	22, 162, 500
4340	a	215	170	1946, 1946, 2091
Billet F	b	215	170	166, 172, 238
9Ni-4Co	a	212	170	NF 2630
Plate W	b	212	170	NF 1000
H-11	a	224	180	2016, 4105, 4694
Billet H	b	224	180	134, 134, 295

* a — Semi-industrial atmosphere in Seattle, Washington
b — Alternate immersion in a 3.5-percent NaCl solution
**c — Specimen failed while stressed but before testing

Table 14 EFFECT OF GRAIN DIRECTION ON STRESS-CORROSION SUSCEPTIBILITY

MATERIALS HEAT TREATED TO MAXIMUM STRENGTHS AND STRESSED TO 80 PERCENT OF YIELD

Material	Grain Direction*	F_{ty} (ksi)	Stress (ksi)	Time to Failure (hr)
AFC 77	T	208	165	**a. 23, 25
Billet A	T_2	210	170	17, 17, 18
	L	211	170	17, 56, 56
18-7-5	T	272	215	No Failures
Billet B	T_2	270	215	No Failures
	L	269	215	No Failures
D6AC	T	233	185	3, 5, 13
Billet C	T_2	219	175	6, 7, 13
	L	241	190	271, 458, 458
4335M	T	221	175	22, 262, 500
Billet E	T_2	218	175	262, 647, NF
	L	218	175	604, 651, NF
4340	T	215	170	166, 172, 238
Billet F	T_2	208	165	166, 238, 238
	L	209	165	507, 533, 862
H-11	T	224	180	134, 134, 295
Billet H	T_2	225	180	134, 296, 296
	L	221	175	187, 217, 292
17-4PH	T	186	150	No Failures
Plate Q	L	187	150	No Failures
18-9-5	T	299	240	**a, 1, 1
Plate M	L	297	240	1, 1, 2
18-7-5	T	255	205	No Failures
Plate S	L	257	205	No Failures
D6AC	T	252	200	50, ---, 148
Plate T	L	252	200	94, 96, 168
4335M	T	214	170	No Failures
Plate U	L	216	170	No Failures
4340	T	211	170	612, 720, NF
Plate V	L	214	170	No Failures
9Ni-4Co	T	212	170	No Failures
Plate W	L	208	165	No Failures

Table 14 (continued)

Material	Grain Direction*	F_{tv} (ksi)	Stress (ksi)	Time to Failure (hr)
9Ni-4Co	T	205	165	263, 263, 504
Plate X	L	227	180	641, 816, 816
H-11	T	225	180	143, 175, 260
Plate Z	L	225	180	159, 313, 473
AM 350	T	164	130	No Failures
Sheet A	L	167	130	No Failures
AM 355	T	195	155	55, 175, 478
Sheet C	L	195	155	175, 360, --
4340	T	210	170	90, 90, NF
Sheet E	L	200	160	330, NF, NF

* T — Primary transverse grain direction
T_2 — Second transverse grain direction from billet material only
L — Longitudinal grain direction
**a — Specimen failed while stressed but before testing

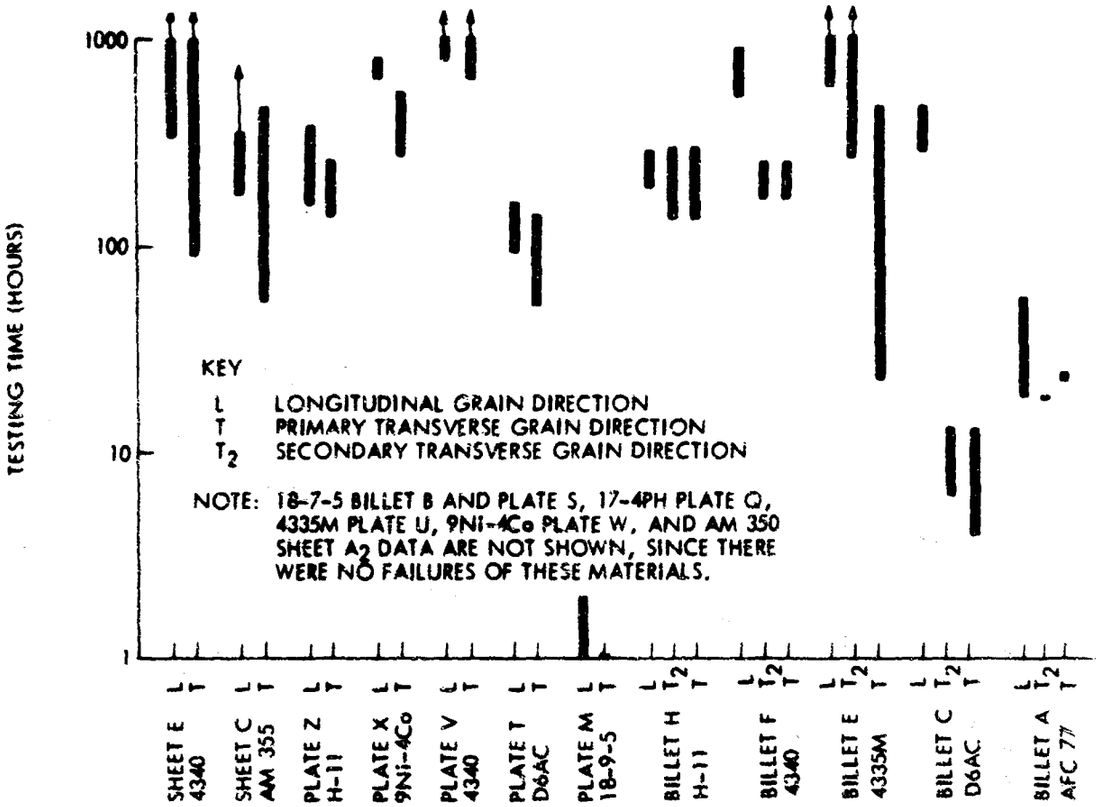

Figure 9 RELATIONSHIP BETWEEN GRAIN DIRECTION AND STRESS-CORROSION SUSCEPTIBILITY

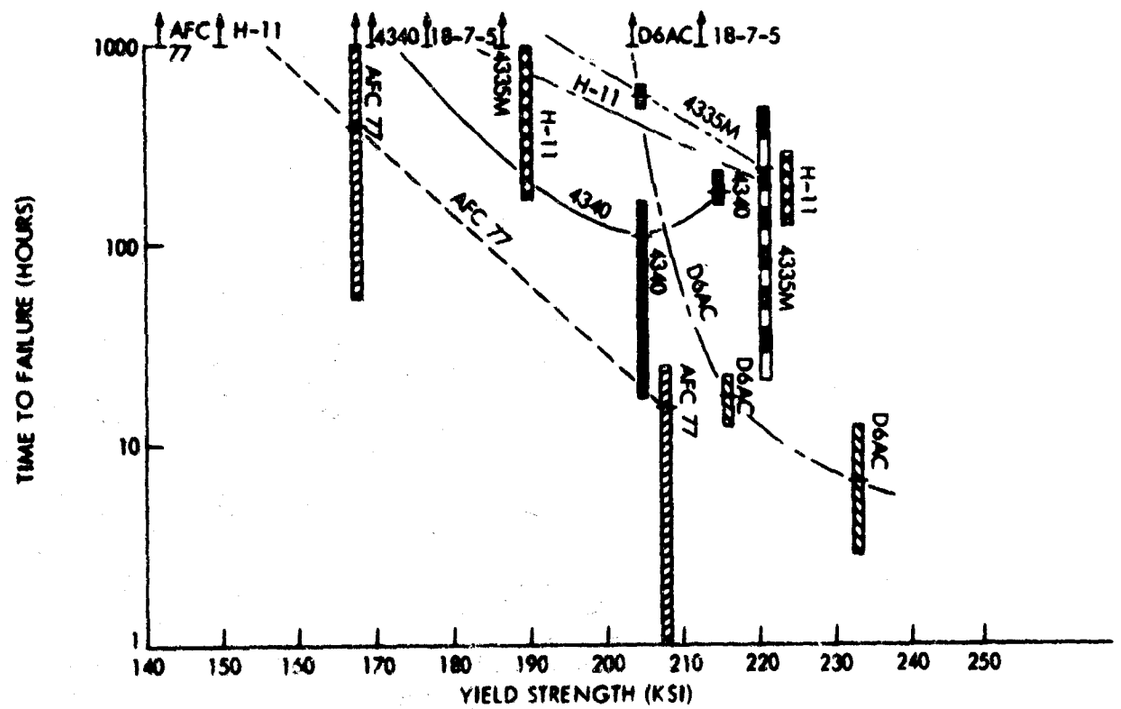

Figure 10 CHANGE IN STRESS-CORROSION SUSCEPTIBILITY WITH STRENGTH LEVEL

Table 15 EFFECT OF STRENGTH LEVEL ON STRESS-CORROSION SUSCEPTIBILITY

TRANSVERSE GRAIN DIRECTION; MATERIALS HEAT TREATED TO THE 180- TO 200-, 220- TO 240-, OR 260- TO 280-KSI ULTIMATE STRENGTH RANGES AND STRESSED TO 80 PERCENT OF YIELD

Material	Yield Strength (ksi)	Stress (ksi)	Time to Failure (hr)
AFC 77	208	165	*a, 23, 25
Billet A	168	135	56, 188, NF
	140	110	No Failures
18-7-5	272	220	No Failures
Billet B	213	170	No Failures
	177	140	No Failures
D6AC	233	185	3, 5, 13
Billet C	216	170	*b, 13, 23
	204	165	No Failures
4335M	221	175	22, 262, 500
Billet E	205	165	506, 566, 652
	187	150	No Failures
4340	215	170	166, 172, 238
Billet F	205	165	18, 161, 171
	170	135	No Failures
H-11	224	180	134, 134, 295
Billet H	190	150	180, NF, NF
	150	120	No Failures

* a — Specimen failed while stressed but before testing
b — Specimen ruined during machining

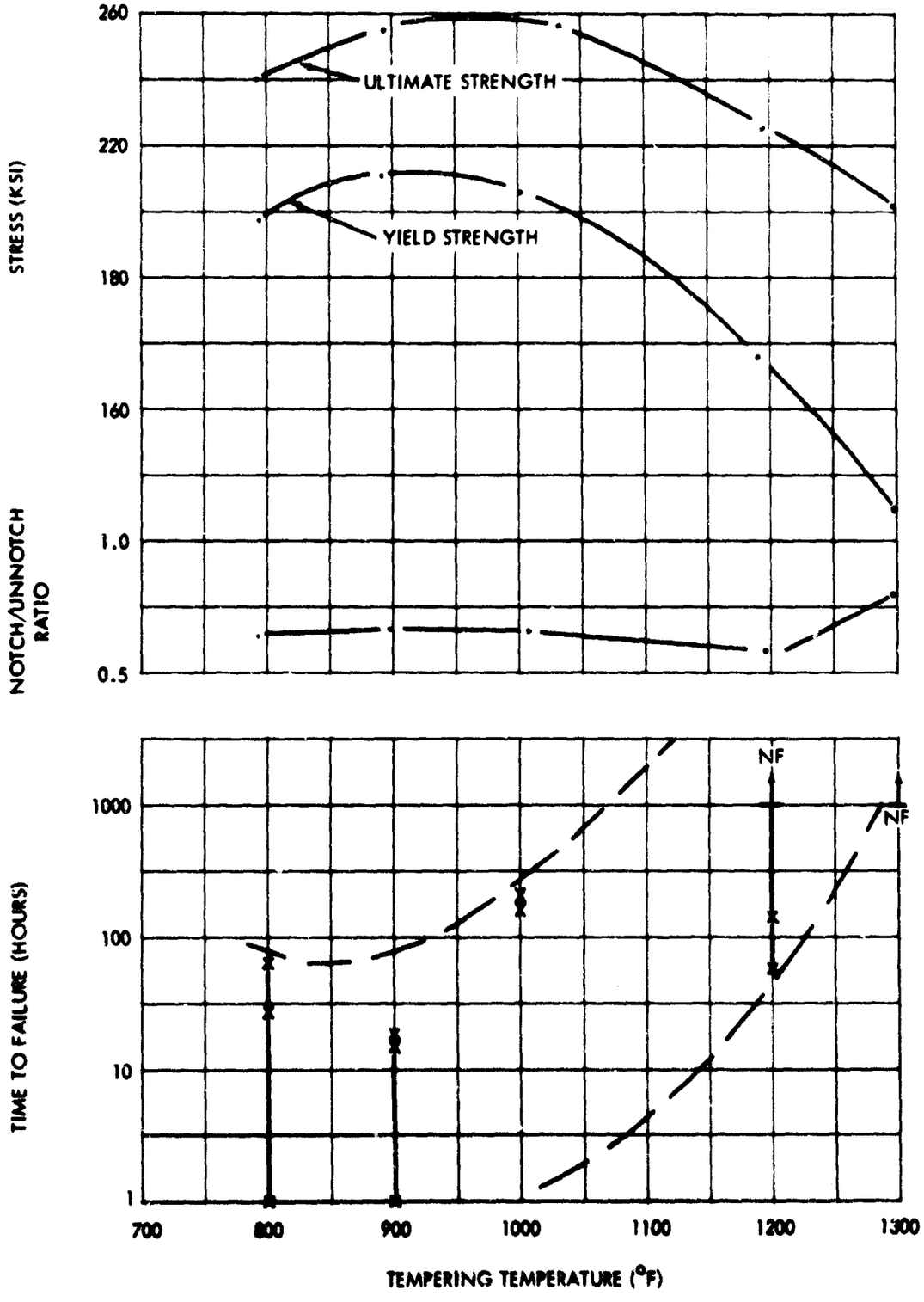

Figure 11 STRESS-CORROSION SUSCEPTIBILITY OF AFC 77 BILLET A

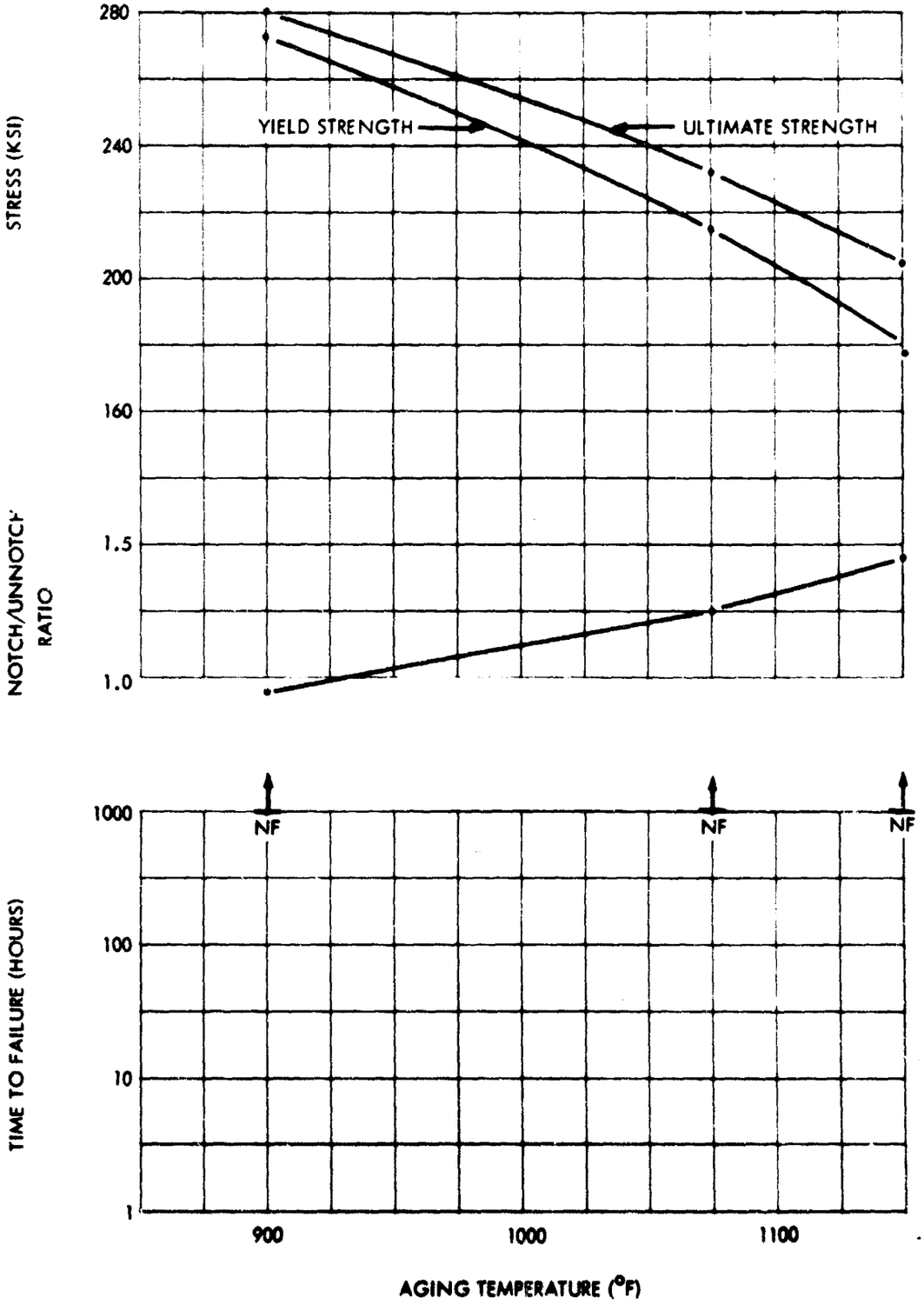

Figure 12 STRESS-CORROSION SUSCEPTIBILITY OF 18-7-5 BILLET B

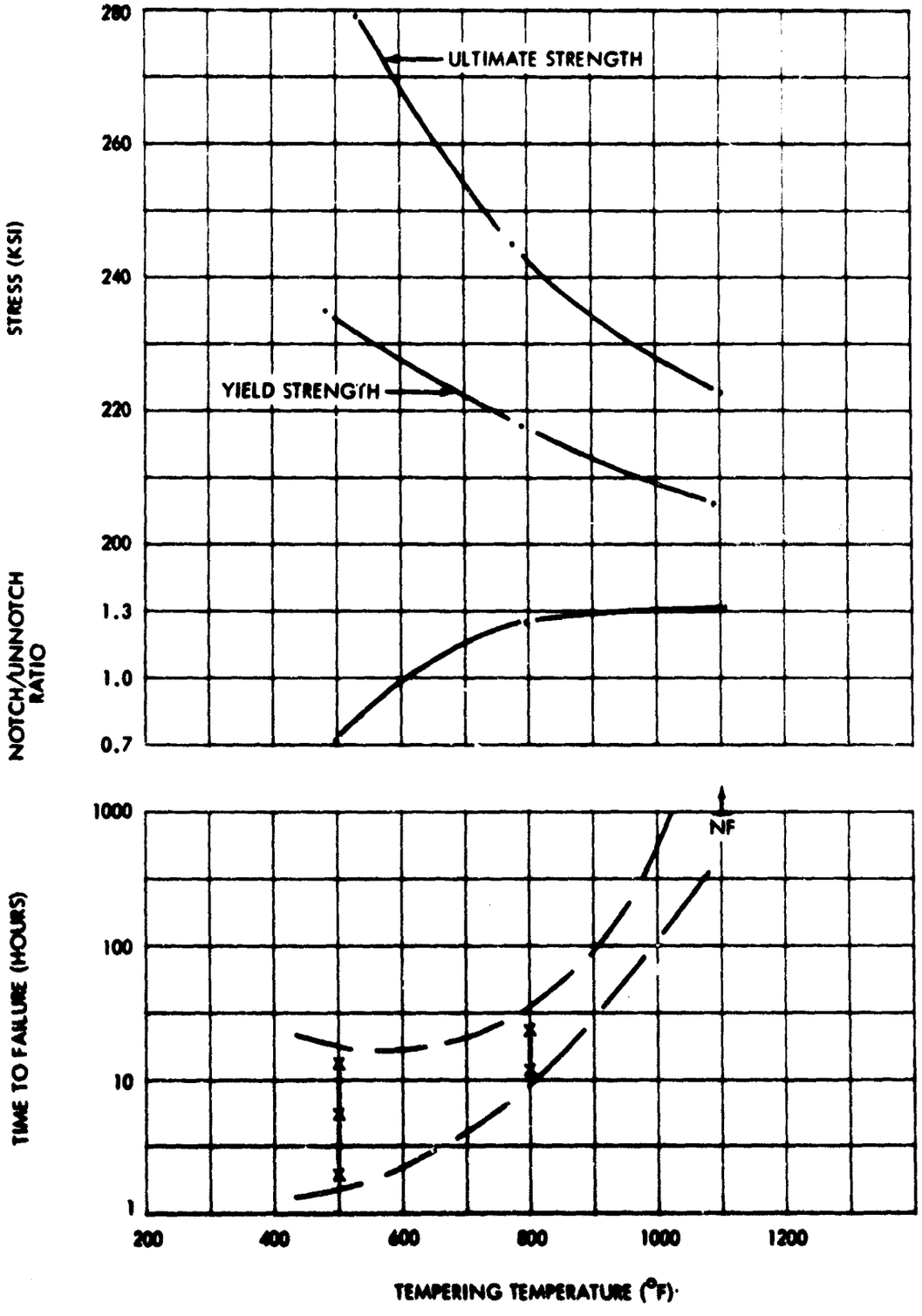

Figure 13 STRESS-CORROSION SUSCEPTIBILITY OF D6AC BILLET C

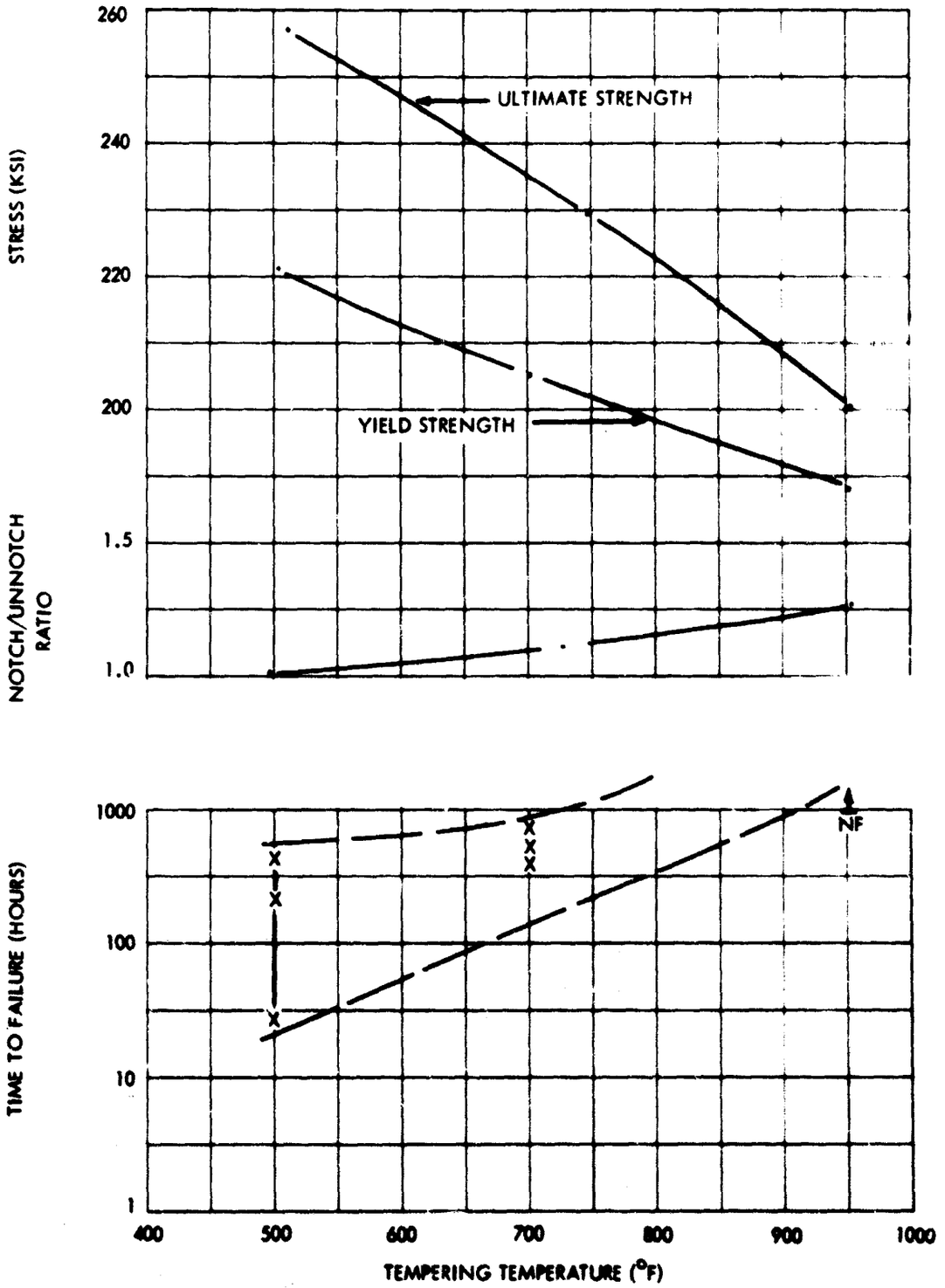

Figure 14 STRESS-CORROSION SUSCEPTIBILITY OF 4335M BILLET E

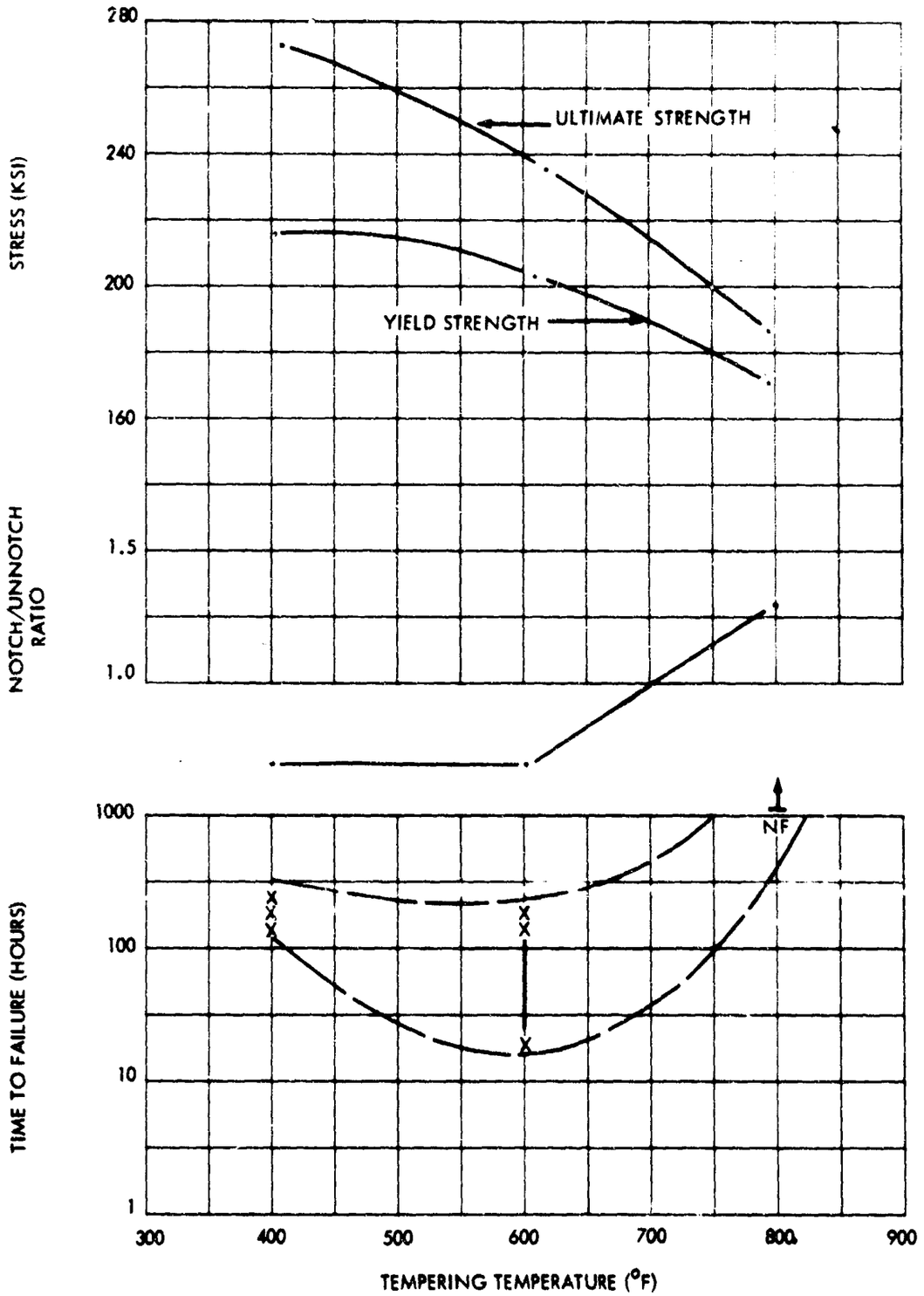

Figure 15 STRESS-CORROSION SUSCEPTIBILITY OF 4340 BILLET F

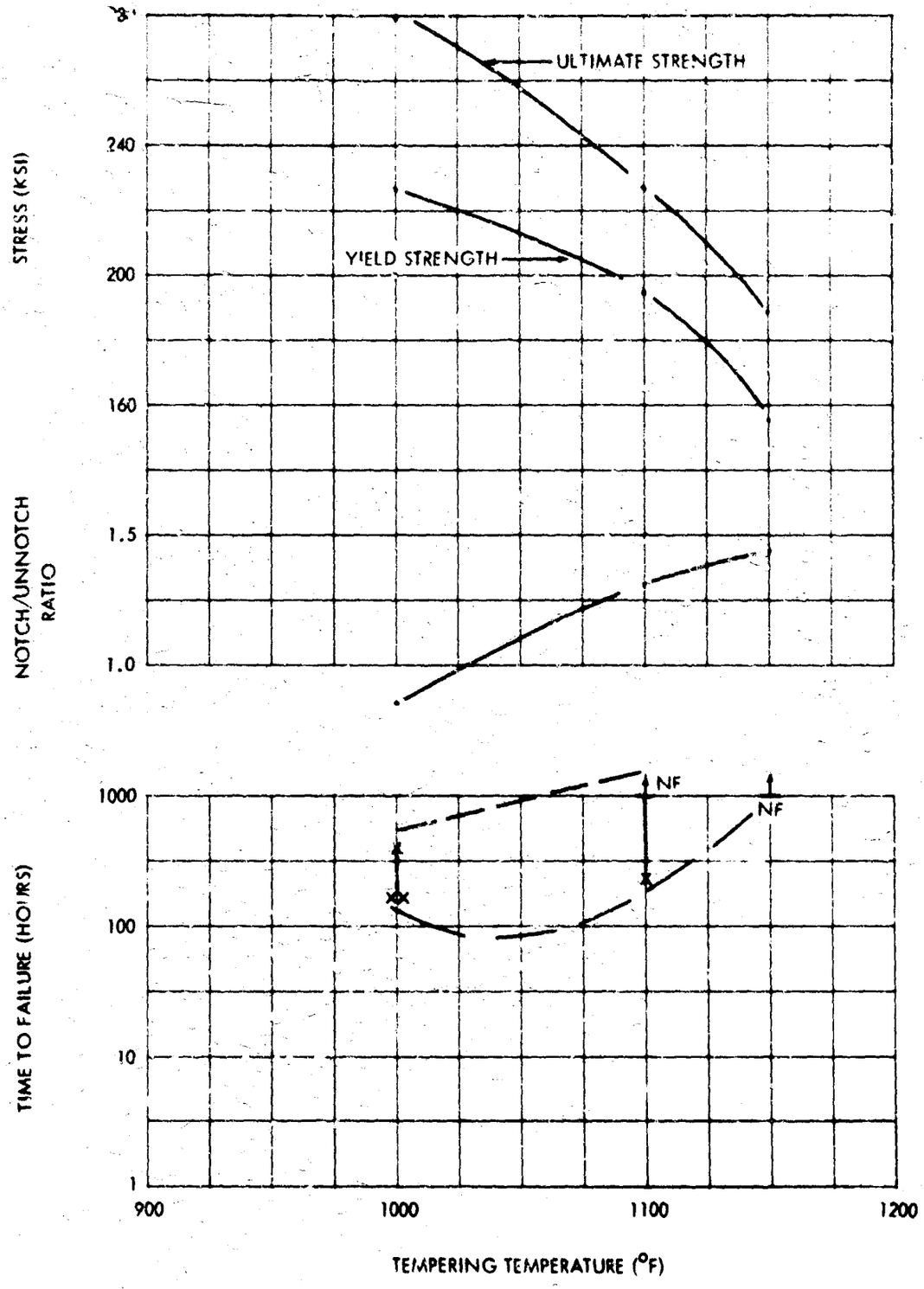

Figure 16 STRESS-CORROSION SUSCEPTIBILITY OF H-11 BILLET H

D6AC, 4335M, and H-11 alloys. The 18-7-5 alloy resisted stress corrosion at all strength levels. The 220- to 240-ksi strength level of 4340 was slightly more susceptible than the 260- to 280-strength level. All of these alloys were stress-corrosion resistant in the 180- to 200-ksi ultimate strength range.

The notch-to-unnotch ratios and the stress-corrosion resistance increased with tempering temperature for all the alloys except 18-7-5, which was not susceptible, and 4340, which revealed a minimum in the 220- to 240-ksi strength range.

b. Heat Treatment Variations

The stress-corrosion susceptibility results for the variation in heat treating and strengthening of AFC 77, AM 350, AM 355, 4340, 4335M, and 9Ni-4Co are given in Table 16.

The changes in susceptibility for the tempering of AFC 77 at 800 and 1000°F are plotted in Figure 11. The notch-to-unnotch ratios and the yield strengths were equal for the two treatments, but the specimens tempered at 800°F were more susceptible. In addition, the ultimate strength level was 15 to 20 ksi greater for the 1000°F temper. It appears that the notch-to-unnotch ratios for this alloy do not correlate well with the stress-corrosion susceptibilities. Also, the constant reduction-in-area values with tempering AFC 77 from 800 to 1000°F does not correlate with the stress-corrosion susceptibility.

The alternate heat-treating conditions applied to AM 350 could not be evaluated because of the lack of failures. The DADF and altered SCT 850 conditions of AM 355 decreased the susceptibility compared to the normal SCT 850 condition.

Martempering of 4340 and 4335M at 450°F significantly decreased the stress-corrosion susceptibility compared to the quench and tempered heat treatments. The martempered tensile strengths were comparable to the tensile strengths obtained by oil quenching and tempering as shown in Tables 14 and 15. The notch-to-unnotch ratios of the comparable strengths were increased in both alloys; martempering of 4340 was only slightly affected.

Austempering of 4340 and 4335M at 600°F produced a strength level of 200 ksi. It was not possible to compare the stress-corrosion susceptibilities of the austempered treatment with the quench and tempered treatment of comparable strengths because of the lack of failures in both cases.

The greatest effect on simulated mill annealing treatments (holding at 1600°F or cycling between 600 and 1200°F) on the stress-corrosion susceptibility of 4340 and 4335M was to increase the scatter of the failure times (see Table 16). One exception occurred for the holding treatment used for 4335M. In this treatment, a significant increase in the stress-corrosion susceptibility of this alloy was noted. The cycling treatment on 4335M and both treatments on 4340 produced a much larger scatter band of failure times than the specimens not given the simulated

Table 16 TESTING TIMES OF SEVERAL ALLOYS AFTER VARYING HEAT TREATMENT AND STRENGTHENING PROCESSES

TRANSVERSE GRAIN DIRECTION; ALL MATERIAL STRESSED TO 80 PERCENT OF YIELD AFTER HEAT TREATMENT

Material	Treatments*	F_{ty} (ksi)	Stress (ksi)	Time to Failure (hr)
AFC 77	a	197	160	(1), 29, 56
Billet A	b	200	160	113, 160, 213
AM 350	c	161	130	No Failures (NF)
Sheet A_2	d	171	135	No Failures
AM 355	c	184	145	952, NF, NF
Sheet C	d	143	115	598, NF, NF
D6AC Billet C	e_1	—	180	26, 44, 88
4335M	e_1	—	175	138, 666, 786
Billet E	f	—	175	22, 22, 67
	g	220	175	67, 652, NF
	h	173	140	No Failures
	i	225	180	1050, NF, NF
4340	e_1	—	170	(2), 62, 62
Billet F	e_2	251	170	19, 27, 142
	e_3	242	170	22, 26, 48
	f	—	170	23, 404, 540
	g	210	170	26, 238, 404
	h	166	135	No Failures
	i	221	175	186, 503, NF
9Ni-4Co Plate Y	,	248	200	No Failures

(1) Specimen failed while stressed, but before testing
(2) Specimen ruined during machining

*a — Tempered at 800°F for 2 + 2 hours
b — Tempered at 1000°F for 2 + 2 hours
c — DADF condition
d — Altered SCT 850 condition
e — Ausformed
1—Hot/cold worked at 1500°F, 25-percent reduction
2—Hot/cold worked at 1200°F, 25-percent reduction
3—Hot/cold worked at 1000°F, 25-percent reduction
f — Mill annealed by holding at 1600°F for 72 hours
g — Mill annealed by cycling between 600°F and 1200°F
h — Austempered at 600°F
i — Martempered at 450°F
j — Material received in ausformed condition, heat treated to 260- to 280-ksi tensile strength

mill annealing treatments. Therefore, this overlapping of failure times makes it difficult to determine the extent to which the mill annealing processes change the susceptibility of these two alloys. The annealing treatments did not alter the smooth tensile properties, except that the holding treatment caused the 4340 tensile specimens to break in the threads. The notched tensile ultimate strengths of 4340 and 4335M alloys were significantly decreased by the holding treatment, but were not affected by the cycling treatment.

c. Ausforming

Increasing the ausforming temperature from 1000 to 1500°F improved the strength and ductility of 4340. Ausforming also improved these properties in 4335M and D6AC over those obtained before this processing (see Tables 9 and 10). These ausformed materials were stressed to the nonausformed stress levels so that direct comparisons could be made between the two processing methods.

The stress-corrosion susceptibility of the ausformed specimens varied with each material, as shown in Table 16. The D6AC ausformed specimens were less susceptible than the conventionally heat-treated specimens. Ausforming of 4335M did not appreciably change its susceptibility. The 4340 specimens ausformed at different temperatures showed approximately the same amount of increased susceptibility. The as-received hot/cold-worked plate of 9Ni-4Co (0.35 carbon) was immune to failure within the 1000-hour time limit.

The fracture faces from the ausformed specimens were inclined 45 degrees to the tension surface. Fracture faces of the comparable nonausformed specimens were normal to the tension surface.

d. Straightening

The effect of cold deformation after heat treating on the stress-corrosion susceptibility of AFC 77, AM 355, 18-7-5, 4335M, 4340, and H-11 is given in Table 17 and plotted in Figure 17. Specimens without prior strain are also plotted for comparison.

There were no failures in 4335M and 18-7-5. The scatter in the failure times of the 4340 specimens was too great for a proper evaluation. It does appear, however, that the susceptibility first decreases at 0.5-percent strain and then increases at 1.0-percent strain. The susceptibility of H-11 decreases slightly at both percentages of strain. AM 355 revealed a decrease in susceptibility at 1.0-percent strain and an increase at 3.0-percent strain.

The AFC 77 specimens were so brittle that the percentages of strain did not exceed approximately 0.30 percent; consequently, the strained specimens could not be evaluated.

Table 17 TESTING TIMES OF DEFORMED ALLOYS

TRANSVERSE GRAIN DIRECTION; MATERIAL HEAT TREATED TO MAXIMUM STRENGTH, DEFORMED, AND STRESSED TO 80 PERCENT OF THE UNDEFORMED YIELD STRENGTH

Material	Strain (percent)	F'_{ty} (ksi)	Stress (ksi)	Time to Failure (hr)
AFC 77	0	208	165	*a, 23, 25
	1.0	208	165	*b
	5.0	208	165	*b
AM 355	0	195	155	55, 175, 478
Sheet C	1.0	195	155	*c, NF, NF
	3.0	195	155	167, 192, NF
18-7-5	0	272	220	No Failures
Plate S	1.0	272	220	*b, NF, NF
	5.0	272	220	No Failures
4335M	0	214	170	No Failures
Plate U	0.5	214	170	No Failures
	1.0	214	170	No Failures
4340	0	211	170	612, 720, NF
Plate V	0.5	211	170	781, 864, 1000
	1.0	211	170	313, 612, NF
H-11	0	224	180	143, 174, 260
Plate Z	0.5	224	180	128, 174, 612
	1.0	224	180	127, 154, 612

* a — Specimen failed while stressed, but before testing
b — Specimen(s) failed during deforming
c — Specimen overloaded during stressing and therefore was not tested

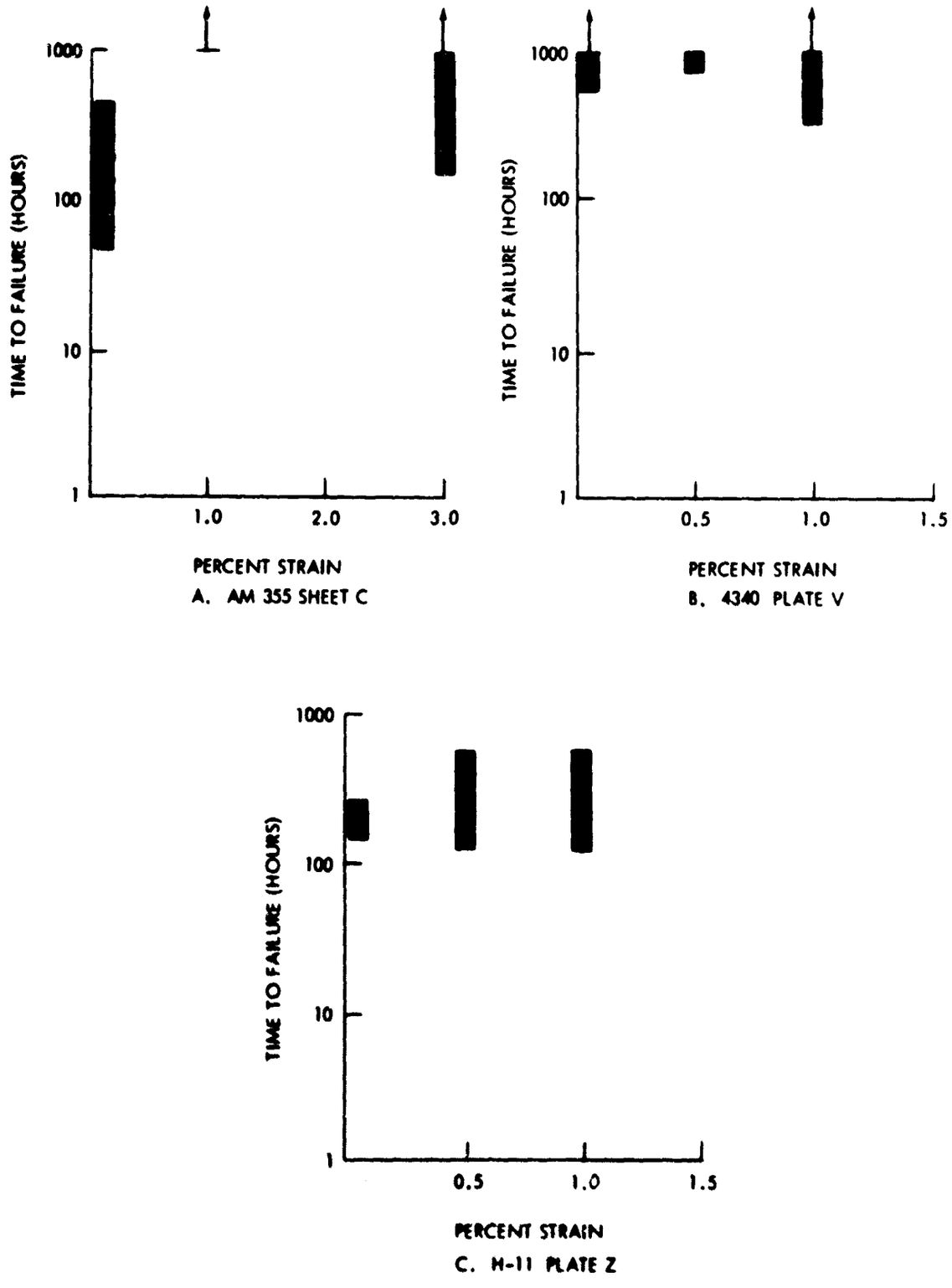

Figure 17 EFFECT OF DEFORMATION ON STRESS-CORROSION SUSCEPTIBILITY

e. Welding

Chemical compositions of the weld wires are given in Table 18.

The stress-corrosion test results for automatic and manual fusion welding of 17-4PH, 18-7-5, D6AC, 4335M, 4340, 9Ni-4Co, H-11, AM 355, and AM 350 are given in Table 19. A majority of the welded plate specimens failed in the welds while the welded sheet specimens failed both in the welds and in the heat-affected zones.

The test results from the D6AC, 4335M, 4340, H-11, and 9Ni-4Co plate materials are not typical because of the porosity detected in a number of the welded specimens. For all specimens with satisfactory welds, it appears that both welding methods have comparable stress-corrosion susceptibilities that are greater than the susceptibility of the base metals. There were no failures in the AM 350 and 17-4PH welded specimens.

f. Coatings

The stress-corrosion susceptibility for the five types of coatings on 18-7-5, D6AC, 4335M, 4340, H-11, and 9Ni-4Co is given in Table 20. In all cases where stress-corrosion failures occurred, the susceptibility of the coated specimens was less than that of the bare specimens. The only failures were the cadmium-titanium plated D6AC, and the epoxy paint, cadmium plate, and cadmium-titanium coated H-11. Because the epoxy paint failures occurred outside the test area, near the tie-down point on the U-bend specimen, these were not considered typical. There were no other coated-specimen failures.

5. Design Data

The failure times of both D6AC billets were nearly the same at the 80- and 60-percent stress levels. One D6AC billet successfully passed the 1000-hour test with no fractures at the 40-percent stress level, while the other billet had all failures within this test period. The billets of 4340 and those of 4335M had widely varying times at stresses of 80 percent of yield. These latter discrepancies disappeared at the 60- and 40-percent stress levels. The vacuum melt H-11 proved to be less prone to failure than the air melt. Comparison of air and vacuum melt 4330M billets was inconclusive, because at 80 percent of yield vacuum melt failures occurred between 47 hours and no failures at 1000 hours, while all air melt failures occurred in approximately 432 hours.

There were no 17-4PH failures at 80, 60, or 40 percent of yield. Since one sheet of AM 350 had no failures at the 80-, 60-, or 40-percent levels, the other AM 350 sheet was tested only at 80 percent of yield. There were no failures of the second group of AM 350 sheet specimens. AM 355 sheet results were complicated by the testing of two gages. The thinner gage material (0.020 inch) had failures at all stress levels, but individual specimens survived the 1000 hours of testing. The

Table 18 WELD WIRE CHEMICAL COMPOSITIONS

Alloy	C	Si	Mn	Cr	V	Mo	Co	Ni	S	P	W	Cu	Ti
4335M and 4340	0.32	-	0.62	0.97	-	0.08	-	0.02	-	-	-	-	-
18-7-5	0.03	-	-	-	-	4.37	9.36	16.36	-	-	-	-	0.47
9Ni-4Co	0.36	0.12	0.26	0.31	0.09	0.28	3.75	8.45	0.006	0.008	-	-	-
H-11	0.38	0.90	0.24	4.80	0.46	1.34	-	-	0.010	0.016	-	-	-
17-4PH	0.06	-	-	17.17	-	-	-	4.74	-	-	-	3.17	-
AM 350 and AM 355	0.13	-	0.97	15.20	-	3.40	-	4.31	-	-	-	-	-
D6AC	0.36	-	-	1.12	-	1.07	-	0.58	-	-	-	-	-
D6AC	0.47	0.26	0.52	1.12	0.09	1.06	-	0.62	0.005	0.010	-	-	-

Table 19 TESTING TIMES OF WELDED ALLOYS

TRANSVERSE GRAIN DIRECTION; MATERIAL WELDED, HEAT TREATED TO MAXIMUM STRENGTHS, AND STRESSED TO 80 PERCENT OF YIELD

Material	Welding Means*	F_{ty} (ksi)	Stress (ksi)	Time to Failure (hr)**
17-4PH	A	186	150	No Failures (NF)
Plate Q	M	186	150	No Failures
18-7-5	A	255	205	No Failures
Plate S	M	255	205	No Failures
D6AC (1)	A	252	200	a, b, 28
Plate T	M	252	200	a, 143, 143
D6AC (2)	A	252	200	g, 110, 212
Plate T	M	252	200	g, 80, 140
4335M	A	214	170	143c, 150c, 751
Plate U	M	214	170	143, 312, 503
4340	A	211	170	86, 121d, 225
Plate V	M	211	170	62, 134c, 225
9Ni-4Co	A	212	170	751, NF, NF
Plate W	M	212	170	150c, NF, NF
H-11	A	225	180	b, 71c, 71
Plate Z	M	225	180	71c, 71, NF
AM 355	A	195	155	95, 839e, NF
Sheet C	M	195	155	71, 532e, NF
AM 350	A	164	130	No Failures
Sheet A_2	M	164	130	No Failures
4340	A	210	170	696f, 936e, NF
Sheet E	M	210	170	360e, 696c, NF

(1) — Welded with 0.36-inch carbon wire
(2) — Welded with 0.47-inch carbon filler wire
* A — Automatic welding method
M — Manual welding method
** a — Specimen failed while stressed, but before testing
b — Specimen had internal crack and was not tested
c — X ray indicated internal porosity
d — X ray indicated tungsten inclusions
e — Specimen failed in heat-affected zone
f — Specimen failed in base metal
g — Specimen failed during machining

Table 20 TESTING TIMES OF COATED ALLOYS

TRANSVERSE GRAIN DIRECTION; MATERIAL HEAT TREATED FOR MAXIMUM STRENGTHS, COATED, AND STRESSED TO 80 PERCENT OF YIELD

Material	Coating Materials	F_{ty} (ksi)	Stress (ksi)	Time to Failure (hr)
18-7-5	a	255	205	No Failures
Plate S	b	255	205	No Failures
	c	255	205	No Failures
	d	255	205	No Failures
	e	255	205	No Failures
D6AC	a	252	200	No Failures
Plate T	b	252	200	No Failures
	c	252	200	696, NF, NF
	d	252	200	No Failures
	e	252	200	No Failures
4335M	a	214	170	No Failures
Plate U	b	214	170	No Failures
	c	214	170	No Failures
	d	214	170	No Failures
	e	214	170	No Failures
4340	a	211	170	No Failures
Plate V	b	211	170	No Failures
	c	211	170	No Failures
	d	211	170	No Failures
	e	211	170	No Failures
H-11	a	225	180	722*, 864*, NF
Plate Z	b	225	180	No Failures
	c	225	180	641, 720, NF
	d	225	180	641, NF, NF
	e	225	180	No Failures
9Ni-4Co	a	212	170	No Failures
Plate W	b	212	170	No Failures
	c	212	170	No Failures
	d	212	170	No Failures
	e	212	170	No Failures

*Failed outside test area

a — Epoxy paint

b — Cadmium plating

c — Cadmium-titanium plating

d — Cadmium plus epoxy paint

e — Flame-sprayed aluminum coating

thicker-material (0.060 inch) failures occurred as expected, with earliest failures occurring at the higher stresses. Data is given in Table 21 and plotted in Figures 18 and 19.

F. FRACTOGRAPHY AND METALLOGRAPHY

The optical microscopic examination of the low-alloy steels was greatly enhanced with the use of the new etching reagent. In the past, it has been quite difficult to determine the prior austenitic grain sizes of these steels in the quenched and tempered condition because of difficulty in showing prior austenite grain boundaries. This reagent, in addition to helping determine grain size, was also quite useful in determining the mode of cracking (whether transgranular or intergranular), and hence, supplementing much of the electron microscope work. This etchant, known as the ADS reagent, had the following nominal composition:

100-ml saturated aqueous picric acid;

1.5-gm sodium tridecyl benzene sulfonate.

Analysis of the fracture faces of 75 failed stress-corrosion and 25 fracture toughness specimens was accomplished using the electron microscope. The optical and electron microscope results are described in the "Discussion" section of this report.

G. SUPPLEMENTAL INFORMATION — PREVIOUS STRESS-CORROSION STUDY

Comparisons between Aerojet constant-immersion and Boeing alternate-immersion test methods indicate, although the test solutions were of slightly different concentrations, that alternate immersion causes much earlier failures.

The indicated correlation between impact strength and stress-corrosion susceptibility does exist for the 4330M, 4340, 4340M, and H-11 steels. Briefly, the lower the impact strength, the greater the stress-corrosion susceptibility. A discussion of the environmental and Izod test results and an analysis of the impact-specimen fracture faces is contained in Appendix III.

H. LITERATURE SURVEY

A survey of the current publications on stress-corrosion cracking is given in Appendix IV.

Table 21 COMPARATIVE TESTING TIMES OF DUPLICATE SHEETS, BILLETS, AND PLATES

TRANSVERSE GRAIN DIRECTION; MATERIAL HEAT TREATED TO MAXIMUM STRENGTHS AND STRESSED TO 40, 60, OR 80 PERCENT OF YIELD

Material	F_{ty} (ksi)	Stress (ksi)	Time to Failure (hr)
AM 350	164	130	No Failures
Sheet A_2	164	100	No Failures
(0.060 inch)	164	65	No Failures
Sheet F	198	160	No Failures
(0.020 inch)	198	120	Not tested
	198	80	Not tested
AM 355	195	155	55, 175, 478
Sheet C	195	115	No Failures
(0.060 inch)	195	80	No Failures
Sheet D	187	150	95, 191, NF
(0.020 inch)	187	110	71, 263, NF
	187	75	98, --, NF
17-4PH	186	150	No Failures
Plate Q	186	110	No Failures
	186	75	No Failures
Plate R	185	150	No Failures
	185	110	No Failures
	185	75	No Failures
D6AC	233	185	3, 5, 13
Billet C	233	140	35, 295, 333
	233	95	No Failures
Billet D	—	185	2, 6, 23
	—	140	23, 27, 126
	—	95	504, 720, 1000
4335M	221	175	22, 262, 500
Billet E	221	130	936, NF, NF
	221	90	No Failures
Billet J	—	175	720, NF, NF
	—	130	No Failures
	—	90	No Failures

Table 21 (continued)

Material	F_{ty} (ksi)	Stress (ksi)	Time to Failure (hr)
4340	215	170	166, 172, 238
Billet F	215	130	554, 768, NF
	215	86	No Failures
Billet G	—	170	3, 98, 166
(vacuum degased)	—	130	697, NF, NF
	—	85	No Failures
H-11	224	180	134, 134, 295
Billet H	224	135	500, NF
(vacuum melt)	224	90	No Failures
Billet I	248	200	14, 14, 47
(air melt)	248	160	61, 103, 183
	248	100	409, 580, 607
4330M	229	160	47, NF, NF
Billet N	229	120	No Failures
(vacuum melt)	229	80	No Failures
Billet O	232	160	431, 432, 432
(air melt)	232	120	No Failures
	232	80	No Failures

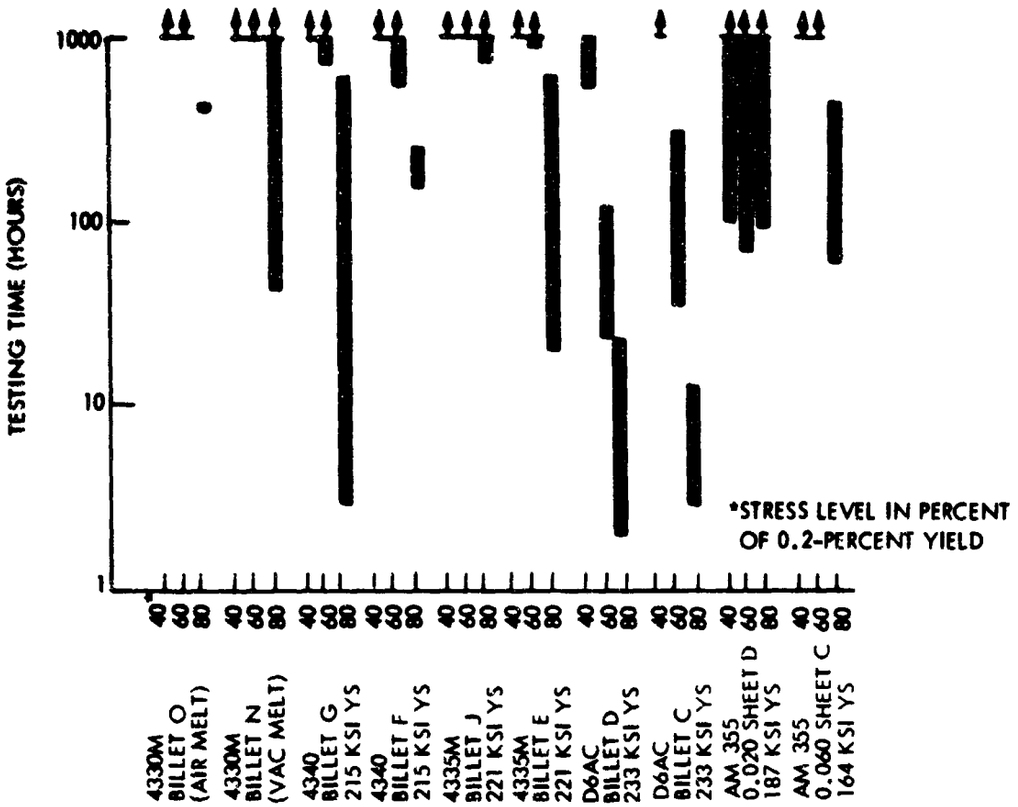

Figure 18 RELATIVE STRESS-CORROSION SUSCEPTIBILITIES OF DUPLICATE SHEETS, BILLETS, AND PLATES

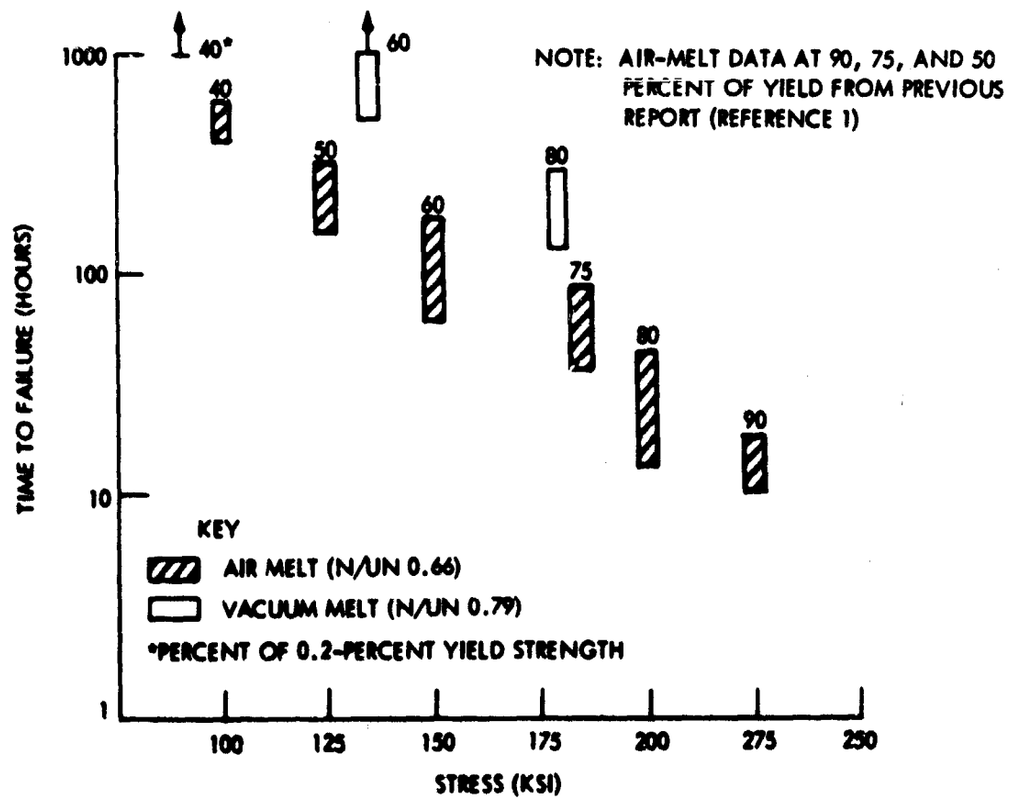

Figure 19 STRESS-CORROSION SUSCEPTIBILITIES OF AIR-MELT AND VACUUM-MELT H-11

V. DISCUSSION

This discussion is divided into three sections. The first is concerned with a comparison of the alloys and the various processes and the effect of each on stress-corrosion susceptibility. The second section describes the modes of fracture and their relation to various processing variables and methods of testing. The final section includes the supplementary discussion of the fractures obtained after cathodically or anodically charging stressed 4340 and 18-9-5 specimens.

A. THE EFFECT OF MATERIAL AND PROCESSING VARIABLES ON STRESS-CORROSION SUSCEPTIBILITY

Comparison of billets and plates of the same material showed, in general, the plate materials to be less susceptible to stress corrosion than billet materials. Evaluation of these materials in both the longitudinal and transverse grain directions showed this trend to prevail for all steels except H-11 and D6AC. There were no differences in the susceptibilities of H-11 billet and plate. The D6AC data were contradictory. In the transverse direction, D6AC plate was less susceptible than either transverse grain direction in a billet, while billet was superior to the plate when compared only in the longitudinal grain directions. Because of lack of information, it was not possible to determine the effects of various rolling and forging processes, but optical microscopic examination revealed the variation between plate and billet susceptibility to be partially due to changes in grain size. The less susceptible plate usually had a smaller grain size than the comparison billet. H-11 plate and billet grain sizes were the same, as indicated by their similar susceptibilities. The D6AC material indicated the operation of other unidentifiable factors since the plate and billet, with ASTM grain sizes 6 and 10 respectively, reversed their relative susceptibilities with changes in testing grain direction. The decrease in failure time with decreasing grain size revealed in this study has also been noted in 70-30 brass and 18-8 stainless steel by Robertson and Tetelman (Reference 5). One complicating factor in a comparison of this type in this study was the use of material from different heats. Though it is evident that the plate material is usually less susceptible, a more accurate determination of the degree of difference would depend on the evaluation of two alloy forms from the same heat.

The stress-corrosion tests of specimens taken from the various grain directions of the billets, plates, and sheets used in this program revealed that the transverse grain direction specimens were more susceptible than the longitudinal grain direction specimens. The relative susceptibility of the specimens from a given alloy may partially be related to the amount of grain elongation experienced during the mill processing of each form of material. Billet H of H-11 did not show any signs of grain elongation, which may be why this particular alloy did not reveal greater susceptibility for the transverse grain direction specimens.

The stress-corrosion susceptibility evaluation of the product shape using the U-bend specimen configuration requires an understanding of the relationship between the grain direction within a specimen and the direction of loading. For materials with completely equiaxed grains, this relationship is constant regardless of the direction from which a specimen is taken. For materials exhibiting grain elongation, this relationship is important in both the initiation and propagation of stress-corrosion cracks. From a purely geometrical point of view, the tendency for intergranular cracking (see Figure 20), which was the primary mode of failure in the alloys tested in this program, can be rated for a given alloy at constant stress level as shown in Table 22.

Table 22 RELATIVE SUSCEPTIBILITY FOR INTERGRANULAR CRACKING

Product Shape	Grain Direction	Relative Susceptibility
Billet	Transverse	Most Susceptible
Plate	Transverse	2nd Most Susceptible
Billet and Plate	Longitudinal	3rd Most Susceptible

Therefore, the comparison of product shapes with respect to stress-corrosion susceptibility of a given material using the U-bend specimen configuration can only be evaluated in this program from longitudinal grain direction specimens. Such a comparision (see Table 14) revealed that plate materials are less susceptible than billet materials. D6AC was an exception in which the longitudinal specimens from the billet were less susceptible than similar specimens from the plate. This contradiction for the D6AC alloy can be related to grain size and stress level. The average ASTM grain size for the plates and billets of 4335M, 4340, and H-11 was 8 and 9, while the billet material of D6AC had an ASTM grain size of 6 and the plate had 10. This smaller grain size of the plate material most likely had the greatest effect on increasing the initiation rate of intergranular cracking.

The relative susceptibilities of the materials after alternate-immersion testing were not always duplicated in the Seattle semi-industrial environment. This disparity appears to be partially traceable to variations in rainfall, in which the greatest number of failures occurred during the relatively dry summer months. These summer failures may be due to more severe testing conditions caused by alternate wet and warm dry periods. However, there were instances where these differences in semi-industrial failure tendencies were due to some unknown environmental factors. For example, significant variations in temperature or humidity over a 24-hour period could be encountered in the natural environment that would not be indicated in a consideration of average conditions. The alternate-immersion method of stress-corrosion testing does provide a laboratory test method of indicating highly stress-corrosion-susceptible materials and processes. Final comparative evaluation of any material would depend on judgment and experience with a material with a known service performance.

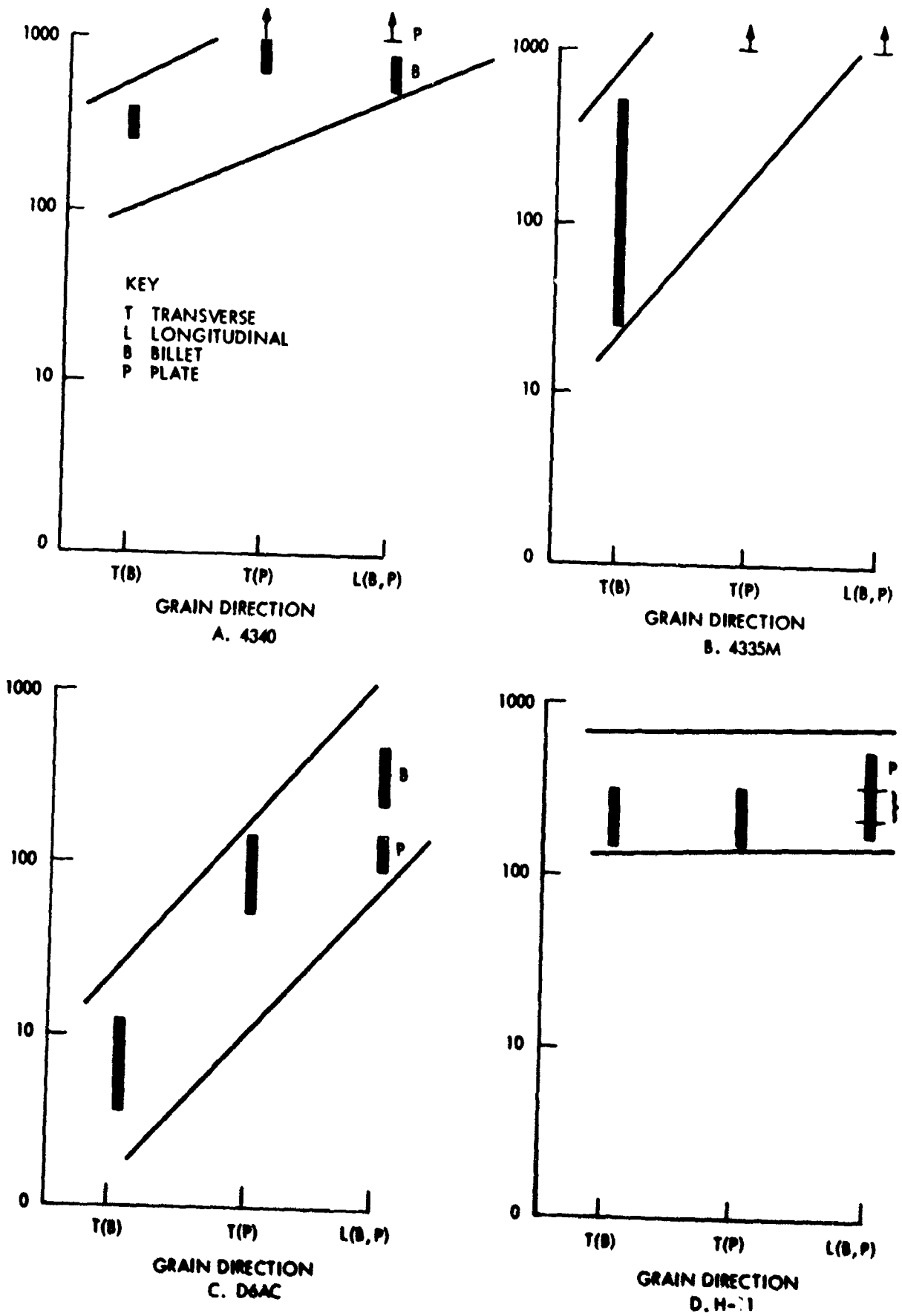

Figure 20 DEPENDENCE OF INTERGRANULAR CRACKING ON GRAIN DIRECTION

The increase in the stress-corrosion susceptibility with increasing heat-treat strength (Figure 10) has been demonstrated by testing the billet alloys of AFC 77, D6AC, 4335M, 4340, and H-11; the 18-7-5 billet alloy showed complete immunity to stress-corrosion cracking in the 3.5-percent NaCl solution.

A semilogarithmic plot of stress-corrosion susceptibility versus yield strength shows the relation to be somewhat linear for the AFC 77, 4335M, and H-11 alloys while the D6AC alloy revealed a significant but nonlinear change in the susceptibility over a small range in yield strength. The 4340 alloy revealed a maximum susceptibility at the 220- to 240-ksi ultimate strength range, which is in the "500-degree embrittlement" tempering temperature range. This embrittlement is related to formation of platelet cementite, which increases notch sensitivity and probably produces a stress-corrosion-sensitive path (Reference 6).

There appears to be some correlation between the change in susceptibility with yield strength and the change in yield strength with tempering temperature. For the AFC 77, 4335M, and H-11 alloys showing the near-linear change in susceptibility plotted in Figure 10, the curves of yield strength versus tempering temperature (Figures 11, 14, and 16, respectively) had negative increasing slopes. In the case of D6AC alloy, which did not show a linear change in susceptibility, the yield strength versus tempering temperature curve had a negative decreasing slope, as shown in Figure 13. The factors that control these curves have not been completely defined but are likely related to the change in the tempering products and their distribution with temperature.

There was a nearly direct correlation between the notch-to-unnotched ultimate strength ratios (N/UN) and the stress-corrosion susceptibilities for the D6AC, 4335M, and H-11 alloys. A low ratio (usually corresponding to high strength) indicated an increase in susceptibility. The 4340 N/UN ratios at the 272- and 242-ksi ultimate strengths were the same, whereas the 242-ksi-strength material was slightly more susceptible because of temper embrittlement. The AFC 77 alloy was an exception in which the ratio was nearly constant over the tempering range of 900 to 1300°F, while the stress-corrosion susceptibility decreased significantly with increasing tempering temperature. Previous stress-corrosion-susceptibility tests (Reference 1) on 4340, 4340M, 4330M, and H-11 revealed that these materials stressed to 90-percent of the yield strength were immune to failure in 1000 hours when the notch-to-unnotched ratios were greater than 1.20. The present results have shown the critical ratio is between 1.25 and 1.35 for 4340, 4335M, H-11, and D6AC alloys tested at 80 percent of their yield strength. Consequently, there appear to be critical ratios above which the low-alloy steels will exhibit immunity to stress-corrosion cracking in 1000 hours in a 3.5-percent NaCl solution at stress levels not exceeding 90 percent of the yield strength. The AFC 77 stainless steel at 80 percent of yield revealed a critical ratio of 0.73, while the 18-7-5 maraging steel had no failures above a ratio of approximately 0.90. The lower ratios of AFC 77 and 18-7-5, as compared to 4340, 4340M, 4330M, and H-11 alloys, may likely be associated with

small differences in chemistries and microstructures. These comparisons were made from notched data obtained when using the small billet notched tensile configuration shown in Appendix I. Since data from the small configuration are often complicated by net section yielding effects, a limited amount of data was obtained from 4340 billet using a larger notched specimen. An analysis of this latter configuration was presented in the previous report (Reference 1). These 4340 large notched tensile results also showed that an increase in the N/UN ratio from 0.34 to 0.78 corresponds to a decrease in stress-corrosion susceptibility. The latter ratios would always be lower than 1.0 since the large notched tensile ultimate strengths are less than the smooth tensile yield strength.

The stress-corrosion susceptibility as a function of the ultimate strength levels for AFC 77, D6AC, 4335M, 4340, and H-11 alloys was not directly related to the measured residual surface stresses shown in Table 8. Although the resultant surface stresses could be determined by adding the residual surface stresses and applied stresses, no correlation was found between these resultant stresses and susceptibility to failure. Comparison of the failure times with corrected stress levels for these alloys was inconclusive. Complicating such an attempted correlation are variations introduced by the small depth (<0.002 inch) to which the compressive residual surface stresses extend.

With the additional tempering treatments of AFC 77 at 800 and 1000°F, the stress-corrosion tests revealed that the susceptibility slightly increased from 800 to 900°F and then decreased from 900 to 1300°F (see Figure 11). This maximum susceptibility due to tempering at 900°F occurred where the alloy exhibited maximum yield strength. The N/UN ratios did not correlate with the susceptibilities over the entire tempering temperature range. The ratio was constant from 800 to 1000°F, and then showed a slight decrease at 1200°F followed by an increase at 1300°F. The total change of N/UN for the entire temperature range was only 0.1.

The evaluation of the alternate heat-treating processes designated as DADF and altered SCT 850 on AM 350 and AM 355 was only possible with the AM 355 alloy. The AM 350 alloy resisted stress-corrosion cracking with all heat-treating processes.

For the 0.060-inch AM 355, the standard SCT 850 condition was more susceptible than either the DADF or the altered SCT 850 condition, in which the controlling factor appears to be the carbide distribution. Volume percentages of the delta ferrite phase for each heat treatment of AM 350 and AM 355 were determined by lineal analysis and are shown in Table 23.

In the present study, the stress-corrosion failures of AM 355 were almost completely intergranular with a noticeable amount of carbides present on the grain faces. Carbides were also found adjacent to the delta ferrite regions, which were located primarily within the individual austenite grains (see Figure 21, Page 65).

Table 23 VOLUME PERCENT DELTA FERRITE IN AM 350 AND AM 355

Alloy	Sheet	Gage	Heat Treatment	Volume Percent Delta Ferrite
AM 350	A_1	0.042	SCT 850	11.3
	A_2	0.060	SCT 850	16.5
	A_2	0.060	DADF	18.2
	A_2	0.060	SCT 850*	17.5
	B	0.078	SCT 850	17.8
	F	0.020	SCT 850	7.1
AM 355	C	0.060	SCT 850	2.0
	C	0.060	DADF	3.0
	C	0.060	SCT 850*	2.0
	D	0.020	SCT 850	2.0

Because of the small percentages of delta ferrite present, the difficulty in optically determining the phases present, and the large differences in yield strength among the various treatments, the lower stress-corrosion susceptibility of the DADF and altered SCT 850 conditions on AM 355 compared to the standard SCT 850 cannot be completely explained. Indications were, however, that a greater amount of carbide precipitation occurred at the grain boundaries after the standard SCT 850 treatment and, hence, contributed to increased stress-corrosion susceptibility.

The decrease in the stress-corrosion susceptibility of the martempered specimens of 4335M and 4340 compared to oil-quenched specimens agrees with the conclusions reported by Bloom in a study of martempering 410- and 431-type stainless steels (Reference 7). Bloom predicts this decrease in susceptibility because of the reduction of residual stresses through martempering. However, previous results (Reference 1) from martempering 4340 at temperatures ranging from 450 to 800°F produced susceptibilities equal to or greater than the quench and tempered treatments. The notch-to-unnotched ultimate strength ratios for martempered specimens were higher, in both the present and prior studies, compared to oil-quenched specimens. The reversal in stress-corrosion results between the two programs may be due to differences in chemistry, since the previous martempering and oil-quenching studies involved different heats. Evaluation in the present study was based on data from one billet.

The ultimate strength of 200 ksi produced by austempering 4340 and 4335M at 600°F did not produce stress-corrosion-susceptible conditions. Similar strengths produced through oil quenching and tempering of these alloys were also stress-corrosion resistant; therefore, the lack of failures in both cases precludes the

* Altered SCT 850 condition.

possibility of evaluating the effect of a bainitic structure on stress-corrosion susceptibility. The lower notch-to-unnotched ratio for the bainitic structure indicates that it may be more susceptible than a tempered-martensite structure.

Since the simulated mill annealing treatments of 4340 and 4335M used in this program are additive to the actual treatments used in the processing of the billets at the steel companies, their effect on the stress-corrosion susceptibility cannot be truly evaluated. The failure times of these steels after mill annealing ranged over larger time periods than before mill annealing, which makes the evaluation of the relative susceptibilities difficult. The holding treatment was more detrimental than the cycling treatment for 4335M, while in 4340 both treatments had approximately the same range in failure times. The most significant effect observed from these treatments was the increase in the notch sensitivity from the holding treatment, which the smooth tensile specimens failed near the treads. X-ray diffraction analysis revealed approximately 4 volume percent retained austenite in the specimens that had been held at 1600°F, while there were no such indications from the 600 to 1200°F cycling heat treatment. Also, from electron microscopy studies, small regions near the prior austenite grain boundaries resembled retained austenite according to the work by Pelliessier (Reference 8). This retained austenite would increase the notch sensitivity of a material, which in turn would indicate increased stress-corrosion susceptibility. Although the present results are not conclusive, they do, however, point out that mill processing may be very influential on stress-corrosion susceptibility.

The variations in stress-corrosion susceptibility caused by ausforming, where susceptibility may be increased or decreased (see Table 16), apparently depends on material chemistry. The behavior of ausformed D6AC, 4335M, and 4340, compared to these materials in the nonausformed condition, indicates that prior mill processing may be of more significance than chemistry. The only means of determining which is of more importance would be to obtain billets of comparison materials that have received identical processing from the melt.

Cold deformation of heat-treated specimens by small amounts appears to have a slightly beneficial effect on the stress-corrosion susceptibility of AM 355, 4340, and H-11. There was a slight tendency for the susceptibility of 4340 and H-11 to decrease at 0.5-percent strain and then to increase at 1.0-percent strain. This was more evident in the AM 355 results in which 1.0-percent strain provided complete immunity to stress-corrosion cracking. AM 355 that was not deformed failed within 478 hours and after deforming 3.0 percent provided failures in two out of three specimens. The conclusions of Robertson and Tetelman (Reference 5) and Swann and Nutting (Reference 9) seem to provide an explanation for this behavior. It seems probable that in this situation the first effect of cold working was to increase the number of potential sites at the surface for the initiation of cracking. With the larger number of potential cracks forming, dissolution along any one of them would be slowed, which would decrease the susceptibility. As the amount of cold strain increases, the stress buildup due

to piled up dislocations at particular regions would be great enough to cause more selective potential crack sites and increase the likelihood of stress-corrosion cracking. Although these factors were not directly observed, this seems to be a reasonable explanation since there were no indications of the mode of cracking changing with deformation.

The variations of stress-corrosion susceptibility resulting from the mill annealing treatments, ausforming, and heat-treatment variations are shown in Figures 22, 23, and 24. These three graphs contain all the information so far mentioned and relate the alloy forms and strength level to stress-corrosion susceptibility. However, it must be kept in mind that the results reported for a particular steel are from only one heat and comparison to other steels may be complicated by mill history in addition to chemistry differences. These graphs show 18-7-5 steel to be the most satisfactory billet material at yield strengths ranging from 200 to 272 ksi. The most satisfactory low-alloy steels within the 200- to 240-ksi yield range were martempered 4335M and D6AC. At yield strengths below 200 ksi, the H-11, 4335M, and 4340 billets seemed to be equally resistant. AFC 77 was very susceptible to stress corrosion except at a low yield strength of 140 ksi.

Evaluation of the plate materials again shows 18-7-5 to be highly stress-corrosion resistant at the high yield strength of 240 ksi. This resistance to failure at a high yield strength was also exhibited by the hot/cold-worked 9Ni-4Co. The low-alloy steels D6AC, 4340, and H-11 were all susceptible but they could not be compared because of the widely varying yield strengths. At a yield strength near 210 ksi, 9Ni-4Co (0.26C) and 4335M were equally resistant, but the 9Ni-4Co (0.38C) that had received an unsatisfactory mill annealing treatment was very prone to failure. It was mentioned in an earlier portion of this discussion that lowering the billet N/UN ratio generally indicated increased stress-corrosion susceptibility. A similar relationship was revealed by comparing plate and billet fracture toughness properties with tendency to fail in a 3.5-percent NaCl solution. A plot of logarithmic times-to-failure versus fracture toughness is given in Figure 25. Those materials having the lower fracture toughness usually had the earliest failure times. One exception to this was shown by the 17-4PH alloy, which did not fail even though it had a relatively low fracture toughness. Comparison of the fracture toughness for the billets and plates of 4335M, 4340, and 18-7-5 revealed the plates to be slightly superior to the billets, which agrees with the stress-corrosion susceptibilities. More extensive fracture toughness testing is necessary to determine any critical toughness values for stress-corrosion-cracking immunity. Of particular interest is a comparison between the 18-7-5 and 18-9-5. The stress-corrosion resistance and fracture toughness of the former was much higher. No 18-7-5 stress-corrosion failures occurred, but the 18-9-5 material cracked very rapidly (in less than 1 hour). The 4340 billet large notched tensile specimen fracture toughness (K_{Ic}) values reported in Table 11 also show that an increase in fracture toughness corresponds to a decrease in stress-corrosion susceptibility.

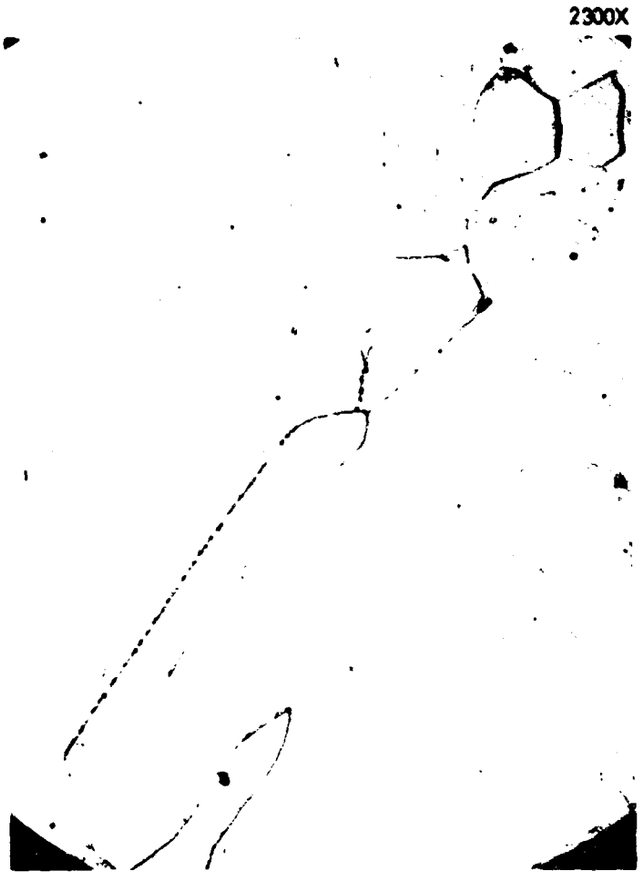

Figure 21 ELECTRON MICROGRAPH OF AM 355 IN THE DADF HEAT TREAT CONDITION
NOTE THE ISLANDS OF DELTA FERRITE OUTLINED BY CARBIDES

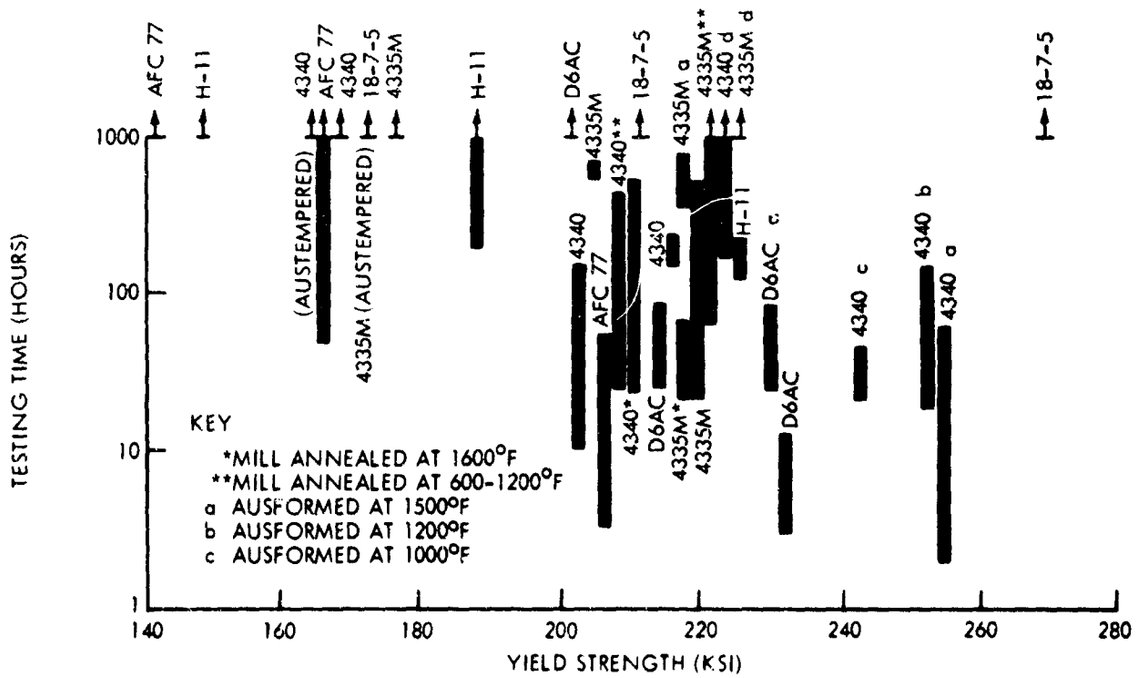

Figure 22 RELATIVE STRESS-CORROSION SUSCEPTIBILITY OF BILLET MATERIALS
ALL STEELS STRESSED TO 80% OF YIELD

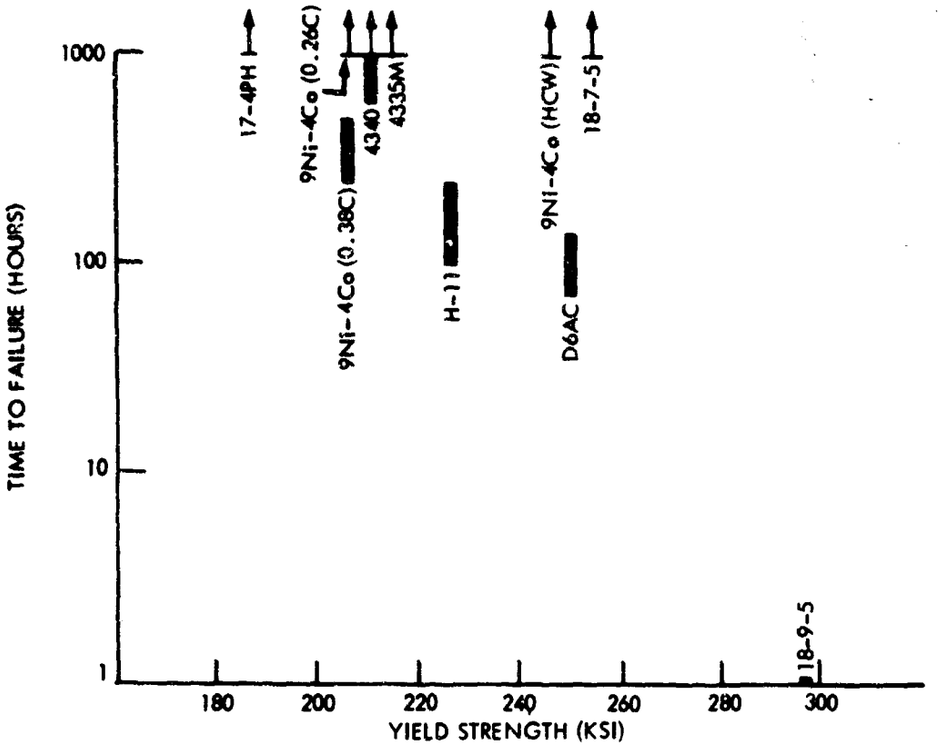

Figure 23 RELATIVE STRESS-CORROSION SUSCEPTIBILITY OF PLATE MATERIALS
ALL SPECIMENS STRESSED TO 80% OF YIELD

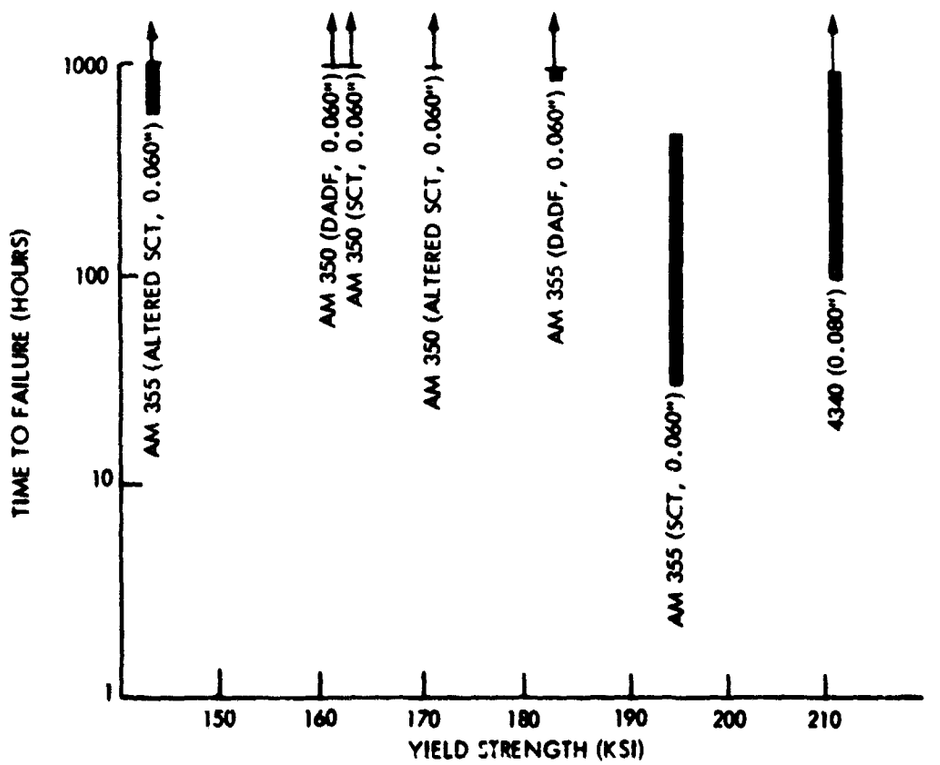

Figure 24 RELATIVE STRESS-CORROSION SUSCEPTIBILITY OF SHEET MATERIALS
ALL SPECIMENS STRESSED TO 80% OF YIELD

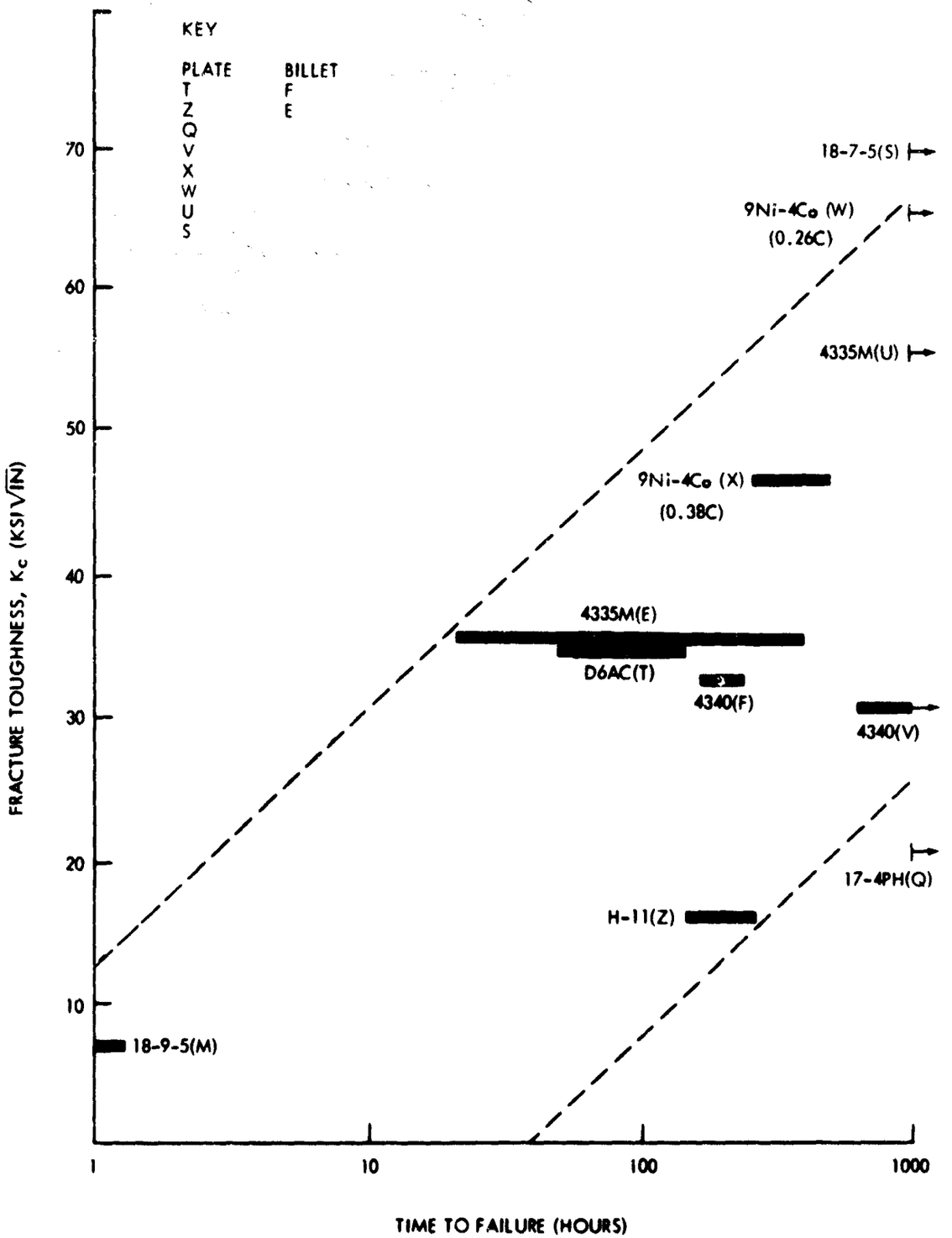

Figure 25 RELATIONSHIP BETWEEN STRESS-CORROSION SUSCEPTIBILITY AND FRACTURE TOUGHNESS

The fracture toughness, notch-to-unnotched ratios, and stress-corrosion susceptibility of AM 350 and AM 355 heat treated to the SCT 850 condition correlated in a similar manner as the low-alloy steels. However, the correlation was not very good when considering the variations in heat treatment and sheet thickness. It is well recognized that precipitation-hardening alloys experience a memory effect that shows up in the structure-sensitive properties of the material. These effects are not usually noticeable in the microstructure. Therefore, the evaluation of the stress-corrosion susceptibility and fracture toughness of precipitation-hardening alloys is somewhat meaningless without knowledge of mill-processing history.

The stress-corrosion susceptibility of the welded specimens was generally greater than the base materials, with the majority of plate failures occurring in the welds. The welded sheets failed in the heat-affected zones of the base metal. Internal porosity was present in a number of the welded plates and apparently acted as stress concentration points for the initiation of stress-corrosion cracks. (The minimum detectable flaw size is 2 percent of the thickness.) In a few instances, the satisfactorily welded specimens failed before the ones containing the porosity, indicating that internal porosity becomes significant only when it occurs at or near the surface of a specimen. Radiographic examination of the welds did not reveal the shapes of the individual internal voids. Comparison of the automatic and fusion welding methods did not reveal the superiority of either process and so both methods appear to produce welds equally susceptible to stress corrosion.

The effectiveness of the various protective coatings in retarding stress-corrosion cracking is shown in Table 20. Very few failures occurred with any of the alloys and those that did fail, failed only after several hundred hours of testing. Since only six specimens failed out of a total of 90 tested, it is not possible to draw conclusions regarding the degree of protection afforded by each of the five coatings studied. It is interesting to note that of the six failures, one was cadmium plated and painted, and three were cadmium-titanium plated. The other two specimens were only coated with the epoxy paint, but the failures occurred outside of the test area and the results were not considered typical. The low-embrittlement cadmium plating process used in this program was developed in the aerospace industry for aircraft and missile applications. This plating process produces a porous cadmium coating in which the sacrificial removal of the cadmium during the corrosion process may have caused hydrogen to be charged into the steel (Reference 10). For this reason, it is advisable to paint over cadmium plating for added protection.

The use of duplicate billets or sheets indicated the need to evaluate the stress-corrosion susceptibility of additional heats. Although the D6AC billets had comparable failure tendencies at the 80- and 60-percent stress levels, there was no correlation at 40 percent of yield. Reversing this, the comparison 4340, 4335M, and 4330M billets had widely varying failure times at 80 percent of yield but

were nearly the same at the 60- and 40-percent levels. The need for testing more than two heats is particularly evident when studying the H-11 air-melt and vacuum-melt results. Data so far indicate vacuum-melt H-11 is noticeably less susceptible to stress corrosion than air-melt H-11, but the difference may be due to trace alloy additions rather than the method of melting. No explanation can be given as to why the 0.20-gage AM 355 had such erratic failure times at all stress levels. Since the occurrence of the 0.060-gage AM 355 fracture was strongly dependent on stress levels, it appears that sheet thickness was less of a factor than mill-processing history in the stress-corrosion susceptibility of the thinner sheet. This indicated sensitivity to prior processing treatments again shows a need to know the complete background of a material when evaluating stress-corrosion results.

B. FRACTURE ANALYSIS OF STRESS-CORROSION CRACKING IN ALLOY STEELS

During the past few years, the study of fracture characteristics has been intensified with the utilization of the electron microscope. Replicas taken from selected fractures, produced by stress-corrosion and fracture toughness specimen failures, have been studied at magnifications ranging from 2000X to 10,000X. It is from these investigations that much of the information on fracture characteristics has been obtained. The main efforts in this program were directed toward determining the modes of fracture (whether transgranular or intergranular), the presence and distribution of precipitate particles, and the changes in fracture appearance with rate of crack growth.

A summary of the fracture face studies is contained in Table 24. Here it is shown that the majority of fractures originated by intergranular cracking. The only exceptions were the transgranular cracking of 4335M billet, which had been mill annealed at 1600°F, and the combination of intergranular and transgranular cracking in 18-9-5 plate. The grain sizes of the steels were determined from optical microscope studies. The new etchant that had been used to bring out the low-alloy-steel grain boundaries proved to be very satisfactory when used on 4340, 4335M, and D6AC. Although this reagent could be used on the H-11 steels, the uniformity of etching was not as complete and study of cracking at the fracture faces was limited.

The fracture surfaces of the stress-corrosion specimens included an origin area and a rapid fracture area. The stress-corrosion origins were characterized by semicircular corroded areas adjacent to the tension surface. (Examples are given in Figures 26 through 29.) Generally, the macro fracture appearances of all alloys were reminiscent of H-11 fracture surfaces shown in Figure 26. In all cases the origin area, regardless of its size, revealed a granular texture while the rapid fracture regions were typified by a fibrous texture with chevron markings radiating from the origin (see Figures 27 and 28). Product form did not seem to influence the fracture appearance of the stress-corrosion failures, except for the plate of 4340 which revealed definite grain orientation effects

Table 24 STRESS-CORROSION FRACTURE MODES

Alloy	Alloy Form	Heat Treatment	Strength		Fracture Mode (origin)	Grain Size (ASTM)
			Weight (ksi)	Yield (ksi)		
AFC 77	B	Standard	255	208	I	-
	B	Standard	220	168	I	-
AFC 77	B	Special 800°F Temper	241	197	I	-
	B	Special 1000°F Temper	257	200	I	-
Ladish D6AC	B	Standard	285	233	I	6
	B	Standard	242	216	I	6
	B	Special — Ausformed at 1500°F	301	261	I	6
	P	Standard	278	252	I	10
4335M	B	Standard	257	221	I	8
	B	Standard	234	205	I	8
	B	Special — Mill Annealed at 1600°F	270	-	T	8
	B	Special — Mill Annealed at 600-1200°F	260	220	I	8
	B	Special — Ausformed at 1500°F	266	230	I	8
	P	Standard	252	214	I	
4340	B	Standard	273	215	I	8
	B	Standard	242	205	I	8
	B	Special — Ausformed at 1500°F	308	259	I	8
	B	Special — Ausformed at 1200°F	298	251	I	8
	B	Special — Ausformed at 1000°F	287	242	I	8
	P	Standard	266	211	I	9
4330	B	Standard	229	197	I	-
H-11	B	Standard	279	224	I	9
	P	Standard	280	225	I	9
18-9-5	P	Standard	304	299	I+T	-
9Ni-4Co	P	Standard	~220	~205	I	-
AM 355	S	Standard	229	195	I	8
	S	Special — DADF	220	184		8
	S	Special — SCT'	197	143		4

B Billet
P Plate
S Sheet
I Intergranular
T Transgranular
M Martempered
DADF Double Age, Double Freeze
SCT' Altered SCT Process

5X

Figure 26 STRESS-CORROSION FRACTURE FACE OF H-11 PLATE MATERIAL AT 270 TO 300 KSI ULTIMATE STRENGTH. FAILURE TIME, 127 HOURS

5X

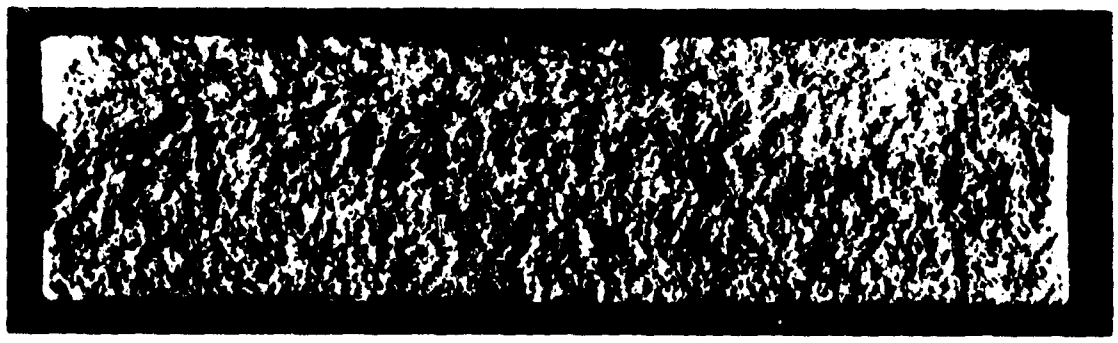

Figure 27 STRESS-CORROSION FRACTURE FACE OF 4340 BILLET MATERIAL AT 220 TO 240 KSI ULTIMATE STRENGTH. FAILURE TIME, 171 HOURS

4.5X

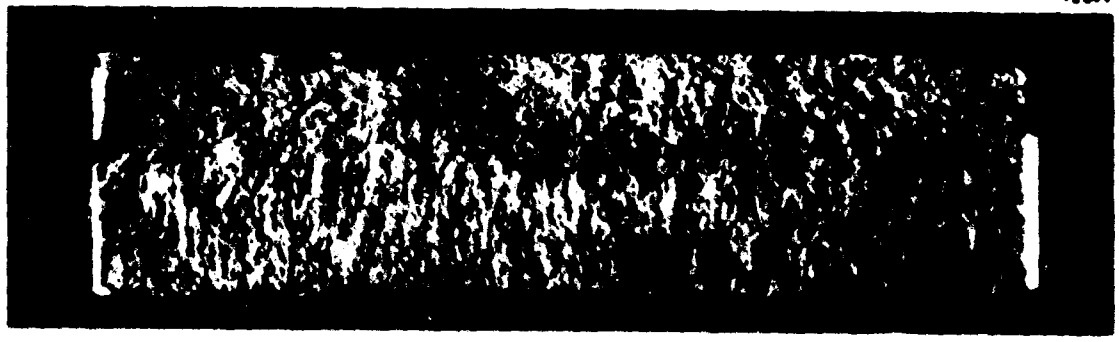

Figure 28 STRESS-CORROSION FRACTURE FACE OF D6AC BILLET MATERIAL AT 270 TO 300 KSI ULTIMATE STRENGTH. FAILURE TIME, 27 HOURS

4.5X

Figure 29 STRESS-CORROSION FRACTURE FACE OF 4340 PLATE MATERIAL AT 260 TO 280 KSI ULTIMATE STRENGTH. FAILURE TIME, 612 HOURS

(Figure 29). The only effect observed from the variations in heat treatment of a given alloy was an increase in the roughness of the rapid fracture regions with decreasing strength level. One exception was the billet specimens of 4340, which showed greater susceptibility at the 240-ksi strength.

The fracture faces from all alloys revealed shear lips along the tension surface away from the origin area. The size of the shear lips depended on the susceptibility of a material in which the more susceptible alloys such as AFC 77, D6AC, and 18-9-5 revealed very small shear lips. H-11, although not one of the more susceptible alloys, also revealed very small shear lips as well as small origin areas. The size of the origins was usually consistent for a given material with no indications of a relationship between susceptibility and origin size.

The stress-corrosion cracks propagated perpendicular to the direction of loading in every alloy except the ausformed materials in which the origin occurred at an angle of approximately 45 degrees to the tension axis. The reason for this change is not completely understood, but it is probably related to the rolling texture produced during the hot/cold working. Microstructure examination did show definite grain elongation in the direction of rolling.

Microfractographic examination of the stress-corrosion failures revealed that cracking occurred primarily along prior austenite grain boundaries as shown in Figures 30 through 34. The fracture surfaces revealed signs of corrosion that in some cases, especially in H-11 (see Figure 30), altered the surface to the extent of masking the mode of failure. The AFC 77 and D6AC alloys showed signs of secondary phase particles outlining the grain boundaries. These AFC 77 particles are shown in Figure 32. The particles were not identified in the AFC 77 alloy but X-ray diffraction revealed the carbides in D6AC to be Cr_2C_3.

The fractographs from the ausformed specimens produced an interesting observation for the process of cracking in the U-bend specimen configuration. The significant aspect of stress-corrosion cracking in the ausformed 4340 specimens is shown in Figures 35, 36, and 37. Figure 35 was taken from the origin area very near the tension surface. Notice the sharpness of the grain boundaries. Figure 36 was taken from the center portion of the origin area and shows that the intersection of the grain faces is becoming rounded. On the outer perimeter of the origin region the intergranular nature of the failure is less distinct because of the extreme rounding of the prior grain boundary areas, shown in Figure 37. The increasing amounts of material dissolution with crack extension indicate that the propagation rate of cracking decreases with increasing crack depth. The factors that govern the propagation rate of stress-corrosion cracks have not been established; consequently, no detailed explanation can be given at the present time.

The rapid fracture regions were characterized by some dimple formation, which is typical of ductile rupturing, and traces of intergranular cracking as shown in Figure 38. The amount of dimpling increased as the strength level decreased in all of the billet alloys except the 4340 alloy, which was heat treated in the 500°F

Figure 30 ELECTRON FRACTOGRAPH OF INTERGRANULAR CRACKING IN H-11 BILLET MATERIAL AT 270 TO 300 KSI HEAT TREAT STRENGTH RANGE
NOTE CORROSION PRODUCT ON FRACTURE SURFACE

Figure 31 ELECTRON FRACTOGRAPH OF INTERGRANULAR CRACKING IN D6AC BILLET MATERIAL AT 260 TO 280 KSI HEAT TREAT STRENGTH RANGE

1900X

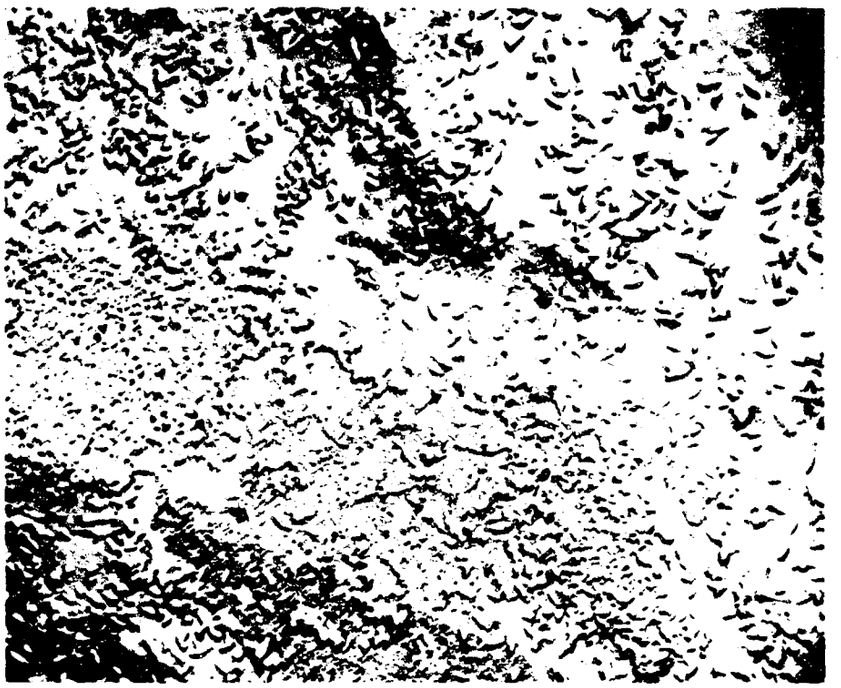

Figure 32 ELECTRON FRACTOGRAPH OF INTERGRANULAR CRACKING IN AFC 77 BILLET MATERIAL AT 250 TO 270 KSI HEAT TREAT STRENGTH RANGE
NOTE CARBIDE PARTICLES ON FRACTURE SURFACE IN ADDITION TO CORROSION PRODUCT

2100X

Figure 33 ELECTRON FRACTOGRAPH OF INTERGRANULAR CRACKING IN 4340 PLATE MATERIAL AT 260 TO 280 KSI HEAT TREAT STRENGTH RANGE
NOTE SMALL GRAIN SIZE

2550X

Figure 34 ELECTRON FRACTOGRAPH OF INTERGRANULAR CRACKING IN 9Ni-4Co PLATE MATERIAL AT 250 TO 270 KSI HEAT TREAT STRENGTH RANGE
NOTE CORROSION PRODUCT ON FRACTURE SURFACE

1900X

Figure 35 FRACTURE SURFACE AT ORIGIN NEAR TENSION SURFACE IN AUSFORMED 4340
NOTE SHARPNESS OF PRIOR AUSTENITE GRAIN BOUNDARIES

3500X

Figure 36 FRACTURE SURFACE AT ORIGIN CENTER IN AUSFORMED 4340

2150X

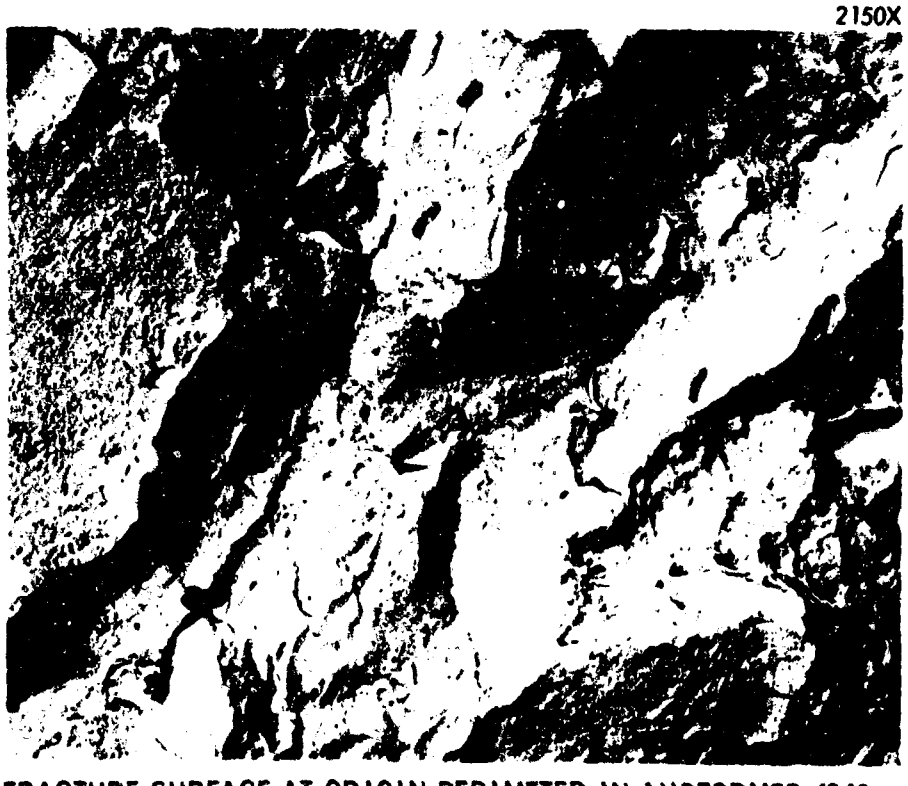

Figure 37 FRACTURE SURFACE AT ORIGIN PERIMETER IN AUSFORMED 4340

embrittlement range at the 240-ksi strength range. In the plate materials, the alloys that revealed the greatest ductility also revealed the greatest amount of dimple formation in the rapid fracture regions. This is shown in Figure 39 for the 9Ni-4Co alloy.

Optical microscopy studies were used primarily to determine grain size and mode of failure. Phase distribution determinations were not possible because of the microstructural complexities of alloy steels. However, some interesting aspects were noted in the stress-corrosion specimens. The optical microscope studies showed that cracking in the 4340, D6AC, and 4335M steels originated intergranularly, but that any transgranular cracking was difficult to identify. Examination of the 0.250-inch (thickness) dimension of the stress-corrosion specimens indicated that the grains in these steels were equiaxed, but bands of slightly smaller than average grains were noted in 4340 that were parallel to the original billet longitudinal grain direction. The grains in the 4340, 4335M, and D6AC ausformed steels were slightly elongated in the direction of rolling. The banding in 4340 and elongated grains in D6AC are shown in Figures 40 and 41, respectively.

Optical microscopy showed both the AM 355 and 4340 sheet stress-corrosion failures to be intergranular both in the origin and in the rapid-fracture regions. One surprising effect of altering heat treatments of AM 355 was the grain growth due to raising the SCT temperature by 50°F during the annealing process. This effect on stress-corrosion susceptibility could not be directly determined since this treatment had a much lower strength than that which had received the normal SCT treatment.

The macro fracture appearances of the fracture toughness specimens is shown in Figure 42, in which the total shear lip area of each specimen is related to the fracture toughness (see Appendix II). As previously noted, the stress-corrosion susceptibility of the materials decreased with increasing fracture toughness. The textures of the plane-strain areas (see Appendix II for description of terminology) varied between the various alloys and were not directly related to the texture from the stress-corrosion specimens.

The microfractography from the fatigue regions on the fracture toughness specimens revealed typical fatigue striations from all alloys. These striations were faint and difficult to observe in a number of cases. Typical examples are shown in Figures 43 and 44. The interface between the fatigue region and the plane-strain region was sharp and easily observed in the electron microscope (Figure 45). An interesting observation was noted in the fatigue regions of 4340 and 4335M specimens. In several areas, cracking followed prior austenite grain boundaries, resulting in localized intergranular failures (Figure 46). This type of failure is distinguished from intergranular stress-corrosion or hydrogen-embrittlement failures by the association of fatigue striations adjacent to the intergranular areas. The fatigue region from the 17-4PH specimens exhibited areas of crack propagation by cleavage (Reference 11) shown in Figure 47. The reason for the occurrence of cleavage during fatigue is not immediately obvious.

3500X

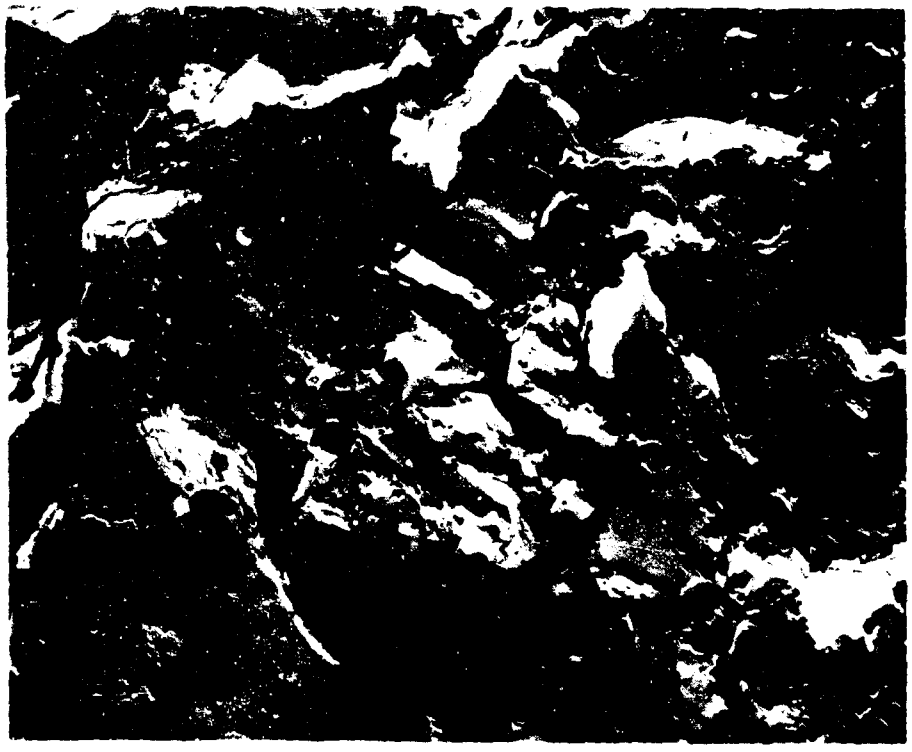

Figure 38 FRACTURE APPEARANCE OF THE RAPID CRACK REGION FROM A STRESS-CORROSION SPECIMEN OF D6AC
NOTE INTERGRANULAR TENDENCIES

3500X

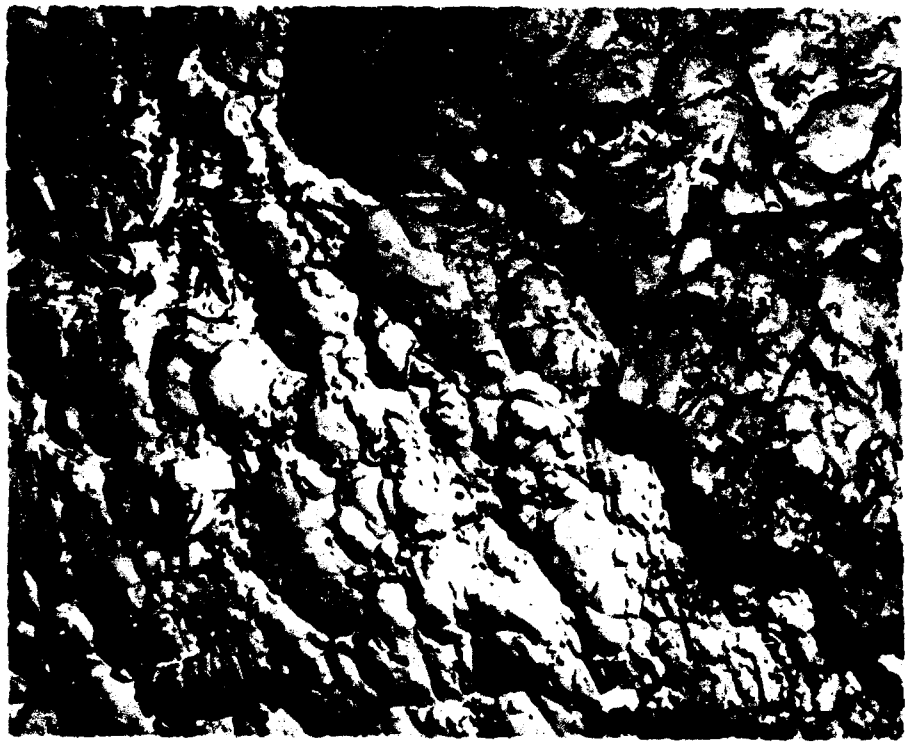

Figure 39 FRACTURE APPEARANCE OF THE RAPID CRACK REGION FROM A STRESS-CORROSION SPECIMEN OF 9Ni-4Co

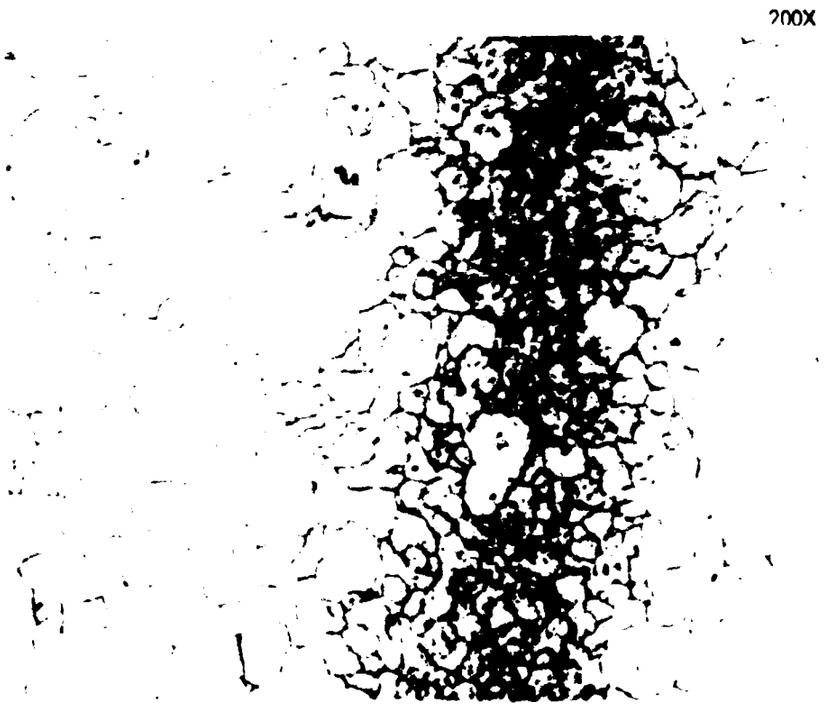

Figure 40 MICROGRAPH OF BANDING IN 4340 BILLET MATERIAL—ADS ETCH

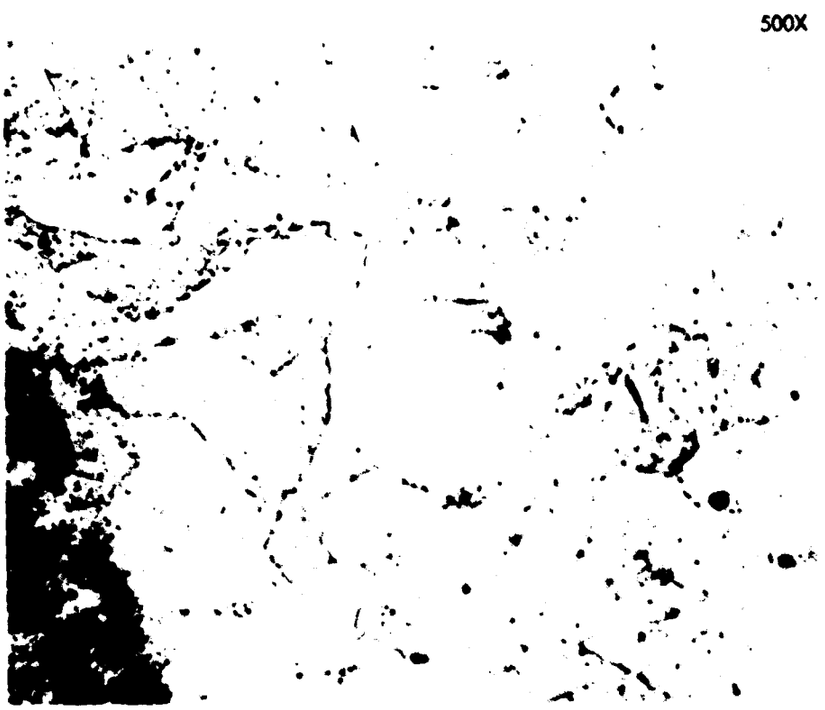

Figure 41 MICROGRAPH OF GRAIN ORIENTATION IN AUSFORMED D6AC—ADS ETCH

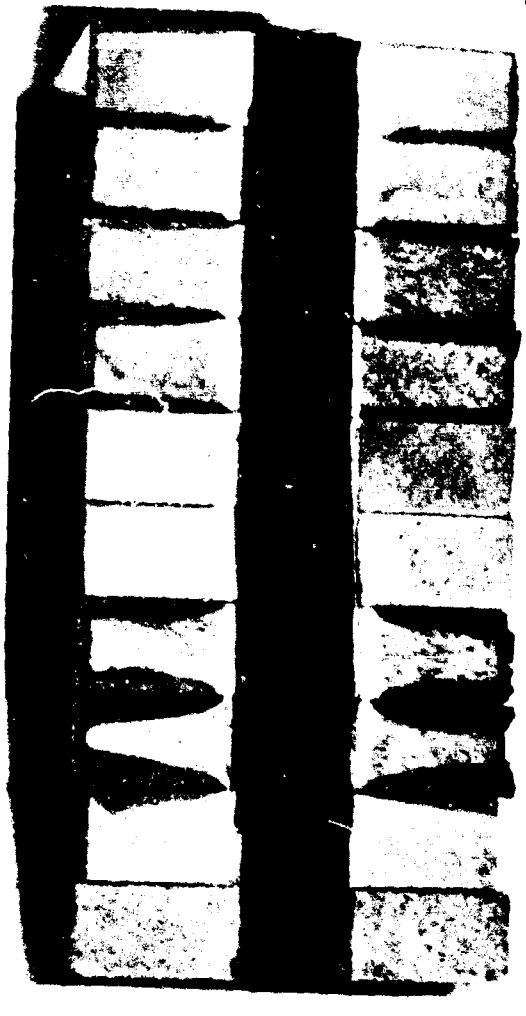

KEY

T TRANSVERSE GRAIN DIRECTION

L LONGITUDINAL GRAIN DIRECTION

Figure 42 FRACTURE FACES OF THE FRACTURE TOUGHNESS SPECIMENS FROM PLATE MATERIALS

3500X

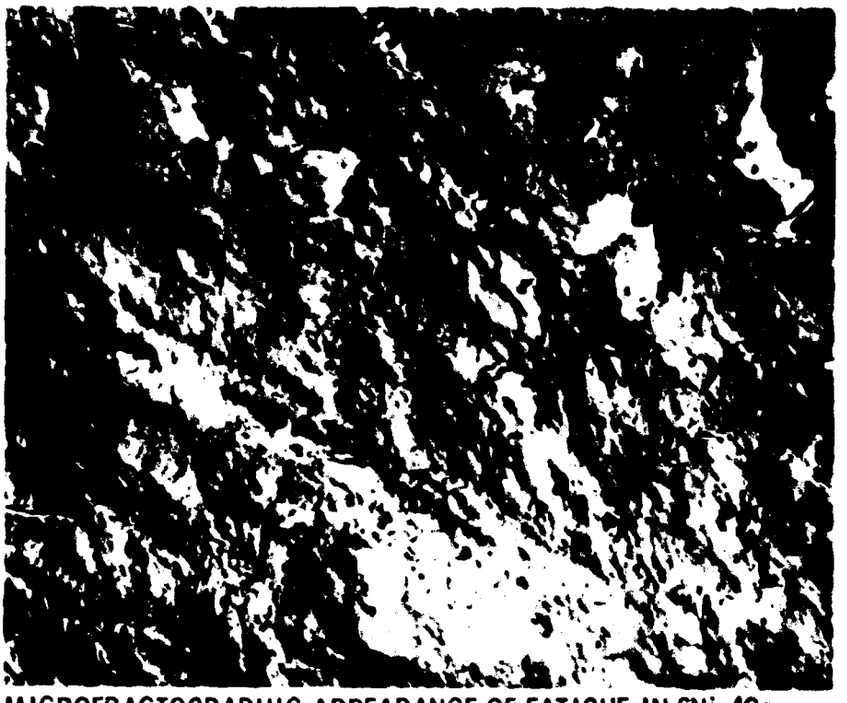

Figure 43 MICROFRACTOGRAPHIC APPEARANCE OF FATIGUE IN 9Ni-4Co

1900X

Figure 44 MICROFRACTOGRAPHIC APPEARANCE OF FATIGUE IN 18-7-5

1900X

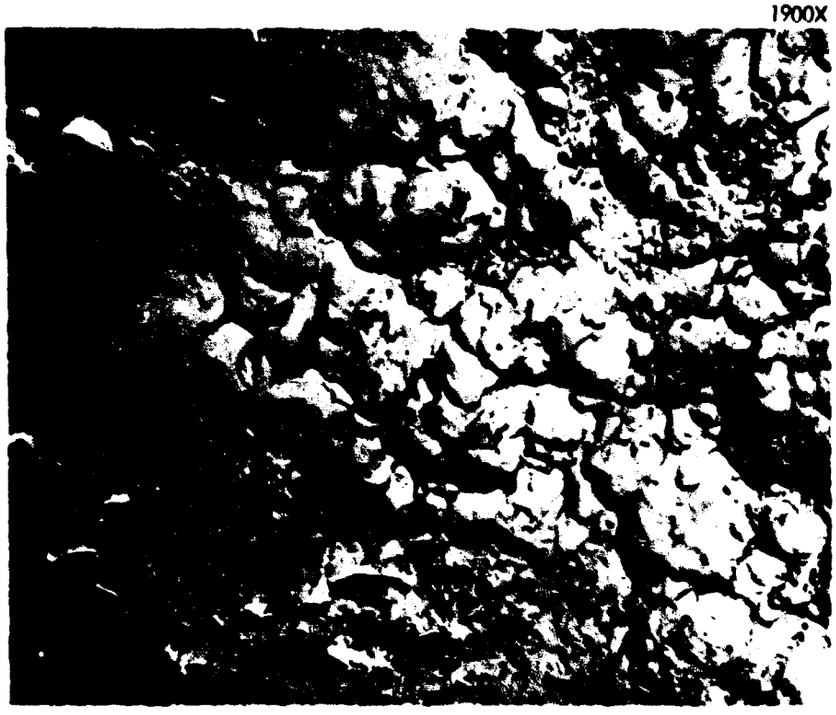

Figure 45 MICROFRACTOGRAPHIC APPEARANCE OF INTERFACE BETWEEN FATIGUE AND PLANE-STRAIN REGION IN 9Ni-4Co

NOTE THAT ELONGATION OF DIMPLES IS IN DIRECTION OF CRACK PROPAGATION, AS EXPECTED FROM STATE OF STRESS

1900X

Figure 46 MICROFRACTOGRAPHIC APPEARANCE OF FATIGUE IN 4335M

NOTE LOCAL INTERGRANULAR CRACKING

The fracture toughness plane-strain regions from all the alloys were characterized by dimpling (shown in Figures 48 through 51). The size of the dimples and the toughness of a specimen did not correlate; generally the dimple size was similar for all the low-alloy and high-nickel-alloy steels. The plane-strain fracture surface of the 18-9-5 maraging steel exhibited regions of crack propagation by decohesion along crystallographic planes (Reference 12). Although this alloy revealed a lower fracture toughness than 18-7-5, decohesion does not necessarily represent low energy absorption during crack propagation. Another interesting observation was encountered in the plane-strain regions of the H-11 specimens in which areas representing crack propagation by quasicleavage (Reference 11) were revealed (Figure 52). The various fracture surface appearances observed in the electron microscope from the fracture toughness specimens cannot be completely explained because of the large number of variables encountered in this program.

C. STRESS CORROSION AND HYDROGEN EMBRITTLEMENT

Although a great deal of work has been done by many investigators since the last report (Reference 1), there is not yet a precise distinction between hydrogen-embrittlement and stress-corrosion cracking in low-alloy steel. This is particularly evident since in many instances no separation can be made between hydrogen-embrittlement or stress-corrosion fractures. Previously it was mentioned that occasionally the differences in these modes of fracture can be ascertained from studies of crack shapes. Hydrogen embrittlement was characterized by narrow cracks with pointed tips and matching sides. Stress-corrosion cracks were relatively wide, the sides did not necessarily match, and the crack tips were rounded.

Subsequent work on the identification of hydrogen-embrittlement and stress-corrosion cracking has been done using 4340 heat treated to 276 ksi ultimate. U-bend specimens were stressed to 80, 60, or 40 percent of the yield strength and cathodically or anodically charged in 3.5-percent NaCl or 0.06 Na_2S solutions. Failures occurring when the specimens were the anode would supposedly be due to stress corrosion, while reversing the polarity would cause hydrogen embrittlement. From the failed specimens, two-stage germanium-carbon faxfilm replicas were taken of the origin areas. Comparison of these replicas revealed that the fracture origins were always intergranular. An example of this intergranular cracking at the origin is given in Figure 53. There was no apparent tendency for one fracture surface, caused by a particular type of charging, to have more corrosion products than another. This is not surprising since the presence of salt water on a fresh fracture face could easily cause pitting. At stress levels of 80 and 60 percent of yield, there were no differences in mode of fracture. There were no failures at 40 percent of yield. Failures in the Na_2S solution occurred only when the specimen was negatively charged. These hydrogen-embrittlement failures were also intergranular. A similar study was accomplished using 18-9-5 maraging steel at an ultimate strength of 310 ksi. Failures were obtained in 3.5-percent NaCl at 80, 60, and 40 percent of yield. In all instances, the fractures

were a combination of intergranular plus some transgranular cracking. An origin, typical of both negative and positive charging, is shown in Figure 54. These 4340 and 18-9-5 studies indicated that although the causes of stress-corrosion and hydrogen-embrittlement fractures may be different, the modes of fracture are the same.

2700X

Figure 47 MICROFRACTOGRAPHIC APPEARANCE OF FATIGUE IN 17-4PH
NOTE PRIMARY MODE OF FRACTURE IS BY CLEAVAGE

1850X

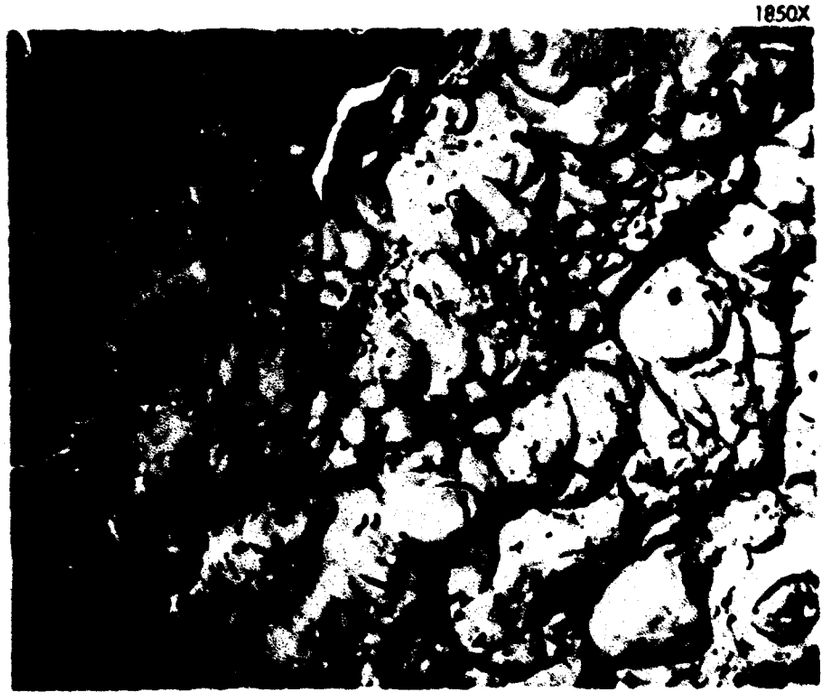

Figure 48 MICROFRACTOGRAPHIC APPEARANCE OF THE PLANE-STRAIN REGION IN 9Ni-4Co

Figure 49 MICROFRACTOGRAPHIC APPEARANCE OF THE PLANE-STRAIN REGION IN 18-7-5
NOTE THAT DIMPLES ARE SMALLER THAN IN 9Ni-4Co

Figure 50 MICROFRACTOGRAPHIC APPEARANCE OF THE PLANE-STRAIN REGION IN D6AC

Figure 53 FRACTURE ORIGIN PRODUCED BY ELECTROLYTICALLY CHARGING 4340

Figure 54 FRACTURE ORIGIN PRODUCED BY ELECTROLYTICALLY CHARGING 18-9-5

VI. CONCLUSIONS

1. For the alloys studied in both plate and billet form, plate is generally less susceptible to stress corrosion than billet material. Optical microscope studies showed that those differences in susceptibility between plate and billet could generally be explained on the basis of grain size — the smaller the grain size, the lower the susceptibility.

2. Alternate-immersion testing provides a laboratory means of evaluating highly stress-corrosion-susceptible materials and processes. Final evaluation of any material would depend on judgment and experience with a material with a known service performance.

3. The longitudinal grain directions in plate and billet have stress-corrosion susceptibility less than or equal to that of the transverse grain directions.

4. The lower the tensile strengths of AFC 77, D6AC, and 4335M, the higher the notched-to-unnotched ratio, and the less the stress-corrosion susceptibility.

5. The 4340 steel was less susceptible to stress corrosion at the 260- to 280-ksi strengths than at the 220- to 240-ksi strengths. There was no difference in notched-to-unnotched ratio between these strength levels.

6. AM 355 in the DADF and altered SCT 850 conditions was less susceptible to stress corrosion than when in the standard SCT condition.

7. Martempered 4340 and 4335M at 450°F was less susceptible than comparable oil-quenched material. The previous work (Reference 1) provided results that were exactly opposite, but the latter result may be due to the use of separate billets for the oil quenching and martempering evaluations.

8. Simulated mill annealing treatments carried out on the 4340 and 4335M low-alloy steels, coupled with the erratic results from the AM 355 thin sheet and the high-nickel steels, indicate that the history of melting and mill processing may have an influential effect on stress-corrosion susceptibility.

9. Ausforming, compared to material not ausformed, decreased the stress-corrosion susceptibility of D6AC and increased the susceptibility of 4340, but did not affect the susceptibility of 4335M. Ausforming at temperatures from 1000 to 1500°F did not alter the relative susceptibility of 4340.

10. Among the alloys tested, those least susceptible to stress corrosion at the indicated strengths are shown in Table 25.

Table 25 SUMMARY OF LEAST-SUSCEPTIBLE ALLOYS

Yield Strength (ksi)	Alloy	Alloy Form
270	18-7-5	Billet
210 to 230	18-7-5, martempered 4335M, and D6AC	Billet
170 to 190	H-11, 4335M, 4340	Billet
225	18-7-5	Plate
220	9Ni-4Co(0.26C) 4335M	Plate
180 to 200	17-4PH	Plate

11. Generally, increased fracture toughness along with an increase in the notched-to-unnotched ratio corresponds to a decrease in stress-corrosion susceptibility.

12. Optical- and electron-microscope studies of fractured stress-corrosion specimens showed the primary fracture mode was intergranular.

13. The final surface stress level could be determined by adding the residual surface stresses, determined by X-ray measurements, and the applied stresses. However, no correlation was noted between the magnitude of final stresses, obtained by adding residual and applied stresses, and stress-corrosion susceptibility.

14. Comparisons of 4340 and H-11 after various percentages of deformation indicated a decrease in susceptibility at 0.5-percent strain and an increase in susceptibility at 1.0-percent strain. AM 355 after 1.0-percent strain was less susceptible than before straining or after 3.0-percent strain.

15. Manual- and automatic-fusion-welded D6AC, 4335M, 4340, and H-11 plate, and AM 355 and 4340 sheet were more susceptible than these materials when not welded. No separation could be made between the two welding methods on the basis of relative susceptibility.

16. The five coatings studied — epoxy paint, cadmium plating, cadmium-titanium plating, flame-sprayed aluminum, and cadmium plating plus epoxy paint — all provided increased protection against stress-corrosion cracking. Cadmium and cadmium-titanium coatings appear to provide the least protection.

17. Tests were made to determine a threshold stress below which stress-corrosion failures would not occur. Comparisons of duplicate heats provided information on the range in failure times that could be expected from a given alloy. The comparative 4330M billets were failure resistant at 60 and 40 percent of yield and the 4335M and 4340 billets were failure resistant at 40 percent of yield during 1000 hours of alternate-immersion testing.

VII RECOMMENDATIONS

1. It is recommended that the 3.5-percent sodium-chloride alternate-immersion test be adopted as a standard laboratory test for the evaluation of steel alloys. In this way, future test data can be compared with that of the present study and also with that of the aluminum industry, where this method has been a standard test for many years.

2. It is recommended that the stress-corrosion test technique described here be used to supplement testing carried out in other government-sponsored programs. In this way, increased information regarding the effects of melting, mill processing, and fabrication variables on stress-corrosion susceptibility will be made available.

3. Continued support should be maintained on fundamental stress-corrosion studies of steel alloys to further the knowledge of stress-corrosion cracking.

4. Since elevated temperatures are known to be very influential in the environmental behavior of other alloy systems, consideration should be given to extension of this test technique to include temperature as a variable so that thick-section steel materials for supersonic flight applications can be evaluated.

REFERENCES

1. "Investigation of Susceptibility of High Strength Martensitic Steel Alloys to Stress Corrosion," Air Force Report ASD-TDR-62-876, September 1962.

2. "Measurement of Stress by X-Ray," Society of Automotive Engineers Report TR-182.

3. S. C. Lawrence, Jr., "Detection and Measurement of Sorbed Hydrogen," Hydrogen Embrittlement in Metal Finishing, Reinhold Publishing Co., New York, 1961.

4. C. H. Avery, "Screening Test Program for Evaluation of the Stress Corrosion Susceptibility of Alloys Under Consideration for Application as Skin Material," Douglas Aircraft Co., First Quarterly Progress Report, Report No. 30930, July 1962.

5. W. D. Robertson and A. S. Tetelman, "A Unified Structural Mechanism for Intergranular and Transgranular Cracking," ASM Symposium on Strengthening Mechanisms in Solids, Philadelphia, 1960.

6. L. J. Klingler, W. J. Barnett, R. P. Frohmberg, and A. R. Troiano, "The Embrittlement of Alloy Steel at High Strength Levels," WADC TR-53-205, July 1963.

7. F. K. Bloom, "Stress-Corrosion Cracking of Hardenable Stainless Steels," Corrosion, Volume 11, 1955, pp. 351t.

8. G. E. Pelliessier, Private Communication.

9. P. R. Swann and J. Nutting, "Stacking Faults and the Failure of Alloys in Corrosive Media," Journal of the Institute of Metals, Volume 88, 1959-60, pp. 478.

10. K. Bolton and L. L. Shreir, "Factors Affecting Hydrogen Absorption of High-Strength Steels During Cathodic Polarization," Corrosion Science, Volume 3, No. 1, January-March 1963, pp. 17.

11. C. D. Beachem, "An Electron Fractographic Study of the Mechanisms of Ductile Rupture in Metals," NRL Report 5871, December 31, 1962.

12. D. Crussard, F. Plateau, R. Tamhanker, G. Henry, and D. Lajeunesse, "A Comparison of Ductile and Fatigue Fractures," Fracture (Swampscott Conference, 1959), John Wiley and Sons, Inc., New York, 1959.

13. G. R. Irwin, "Fracture," Encyclopedia of Physics, n. VI, Springer, Berlin, 1958, p. 551.

14. G. R. Irwin, "Relation of Crack Toughness to Practical Applications," Welding J. Supplement, November 1962, p. 519S.

15. ASTM Committee Report, "Fracture Testing of High Strength Sheet Materials," ASTM Bulletin, January 1960, p. 29.

16. ASTM Committee Report, "Fracture Testing of High Strength Sheet Materials," ASTM Bulletin, February 1960, p. 18.

17. ASTM Committee Report, "Fracture Testing of High Strength Sheet Materials," Materials Research and Standards, November 1961, p. 877.

18. W. E. Anderson and P. C. Paris, "Evaluation of Aircraft Material by Fracture," Engineering Quarterly (ASM), Volume 1, No. 2, May 1961, p. 33.

19. M. Greenspan, "Axial Rigidity of Perforated Structural Members," J. of Research of the National Bureau of Standards, Volume 31, 1943, p. 305.

20. "Investigation of Stress-Corrosion Cracking of High-Strength Alloys," U.S. Army Ordnance Corps., Contract DA-04-495-ORD-3069, 1963.

21. P. Lilly and A. E. Nehrenburg, "Effect of Tempering Temperature on Stress Corrosion Cracking and Hydrogen Embrittlement of Martensitic Steels," ASM Transactions, Volume 48, 1956, p. 327.

22. F. L. Carr and F. R. Larson, "Fracture Surface Configurations of AISI 4340 Steel as Affected by Temperature and Geometry," presented before the American Society for Testing and Materials, Philadelphia, Pennsylvania, June 1962.

23. E. C. Roberts, "A Review of Stress Corrosion Cracking," Boeing Document D6-7502, Contract AF33(616)-7839, June 30, 1961.

24. D. Von Rooyen, "Qualitative Mechanism of Stress Corrosion Cracking of Austenitic Stainless Steels," Corrosion, Volume 16, 1960, pp. 421t.

25. W. C. Gallaugher, "Nature of Stress Corrosion Cracking," Boeing Document D6-4093, Appendix III, Contract No. AF33(616)-7839, AST-TDR-62-876, September 1962, pp. 178.

26. P. R. Swann, "Dislocation Substructure vs Transgranular Stress Corrosion Susceptibility of Single Phase Alloys," Corrosion, Volume 19, March 1963.

27. P. R. Swann and J. Nutting, "The Influence of Stacking Fault Energy on the Modes of Deformation of Polycrystalline Copper Alloys," Journal of the Institute of Metals, Volume 90, 1961-1962, p. 133.

28. D. L. Douglass, G. Thomas, and W. R. Roser, "Stacking Fault Energy Ordering and Transgranular Stress Corrosion Cracking in Austenitic Alloys," University of California, Lawrence Radiation Laboratory, Report No. UCRL-10712, Contract No. W-7405-eng-48, March 1963.

29. C. Edeleanu, "Conference on the Physical Metallurgy of Stress-Corrosion Fracture" (Pittsburgh, 1959), 1960, pp. 79.

30. J. G. Hines and T. P. Hoar, "The Stress-Corrosion Cracking of Austenitic Stainless Steels," Part II, "Fully Softened, Strain-Hardened and Refrigerated Material," Journal of the Iron and Steel Institute, Volume 184, 1956, pp. 166.

31. R. W. Staehle, F. H. Beck, and M. G. Fontana, "Mechanism of Stress Corrosion of Austenitic Stainless Steels in Chloride Waters," Technical Report No. 4 from Ohio State University RF Project 682, Contract No. NONr-495(11), July 1959.

32. C. J. Owen, "Stress Corrosion of High Strength Steels and Alloys: Artificial Environment," Mellon Institute Report No. 16, Contract No. DA-36-034-ORD-3277RD, April 30, 1962.

33. R. J. Uzdarwin, "Investigation of Stress-Corrosion Cracking of High Strength Alloys," Report No. 0414-01-6, Contract No. DA-04-495-ORD-3069, Aerojet-General Corp., March 1962.

34. W. I. Weibull, "Stress Corrosion Cracking in High Strength Steel or Hydrogen Embrittlement," presented at the 2nd International Congress, International Council of Aeronautical Sciences, Zurich, Switzerland, September 1960.

35. D. C. Briggs, J. U. MacEqan, and A. H. Yates, "The Corrosion Behavior of Welded Low Alloy Steel," Corrosion, Volume 16, April 1960, pp. 205t.

36. W. L. Williams, "Chloride and Caustic Stress Corrosion of Austenitic Stainless Steel in Hot Water and Steam," presented as Symposium on Basic and Applied Science in the Navy, March 19-20, 1957.

37. H. L. Logan, M. J. McBee, and M. Romanoff, "Stress-Corrosion Cracking of Type 304 Stainless Steel at 455 to 615°F," Materials Research and Standards (ASTM), Volume 3, No. 3, August 1963, pp. 635.

38. J. J. Harwood, "The Mechanism Stress Corrosion Cracking of Austenitic Stainless Steels," ASTM Special Technical Publication No. 264, Stress-Corrosion Cracking of Austenitic Chromium-Nickel Stainless Steels, published by ASTM, Philadelphia, Pennsylvania, March 1960, pp. 22.

39. R. J. Favor, O. L. Deel, and W. P. Achbach, "Design Information on AM 350 Stainless Steel for Aircraft and Missiles," DMIC Report 156, Battelle Memorial Institute, July 26, 1961.

40. R. Banning and S. Wilson, "Stress Corrosion Cracking Investigation on AM 350 CRT and AM 355 CRT," Boeing Document T2-1876, 1960.

41. M. Watanabe and Y. Mukai, "Study of Stress Corrosion Cracking of Austenitic Stainless Steels," Technology Reports of Osaka University, Volume 10, No. 392-413, March 1960, pp. 439.

Appendix I

SPECIMEN CONFIGURATIONS

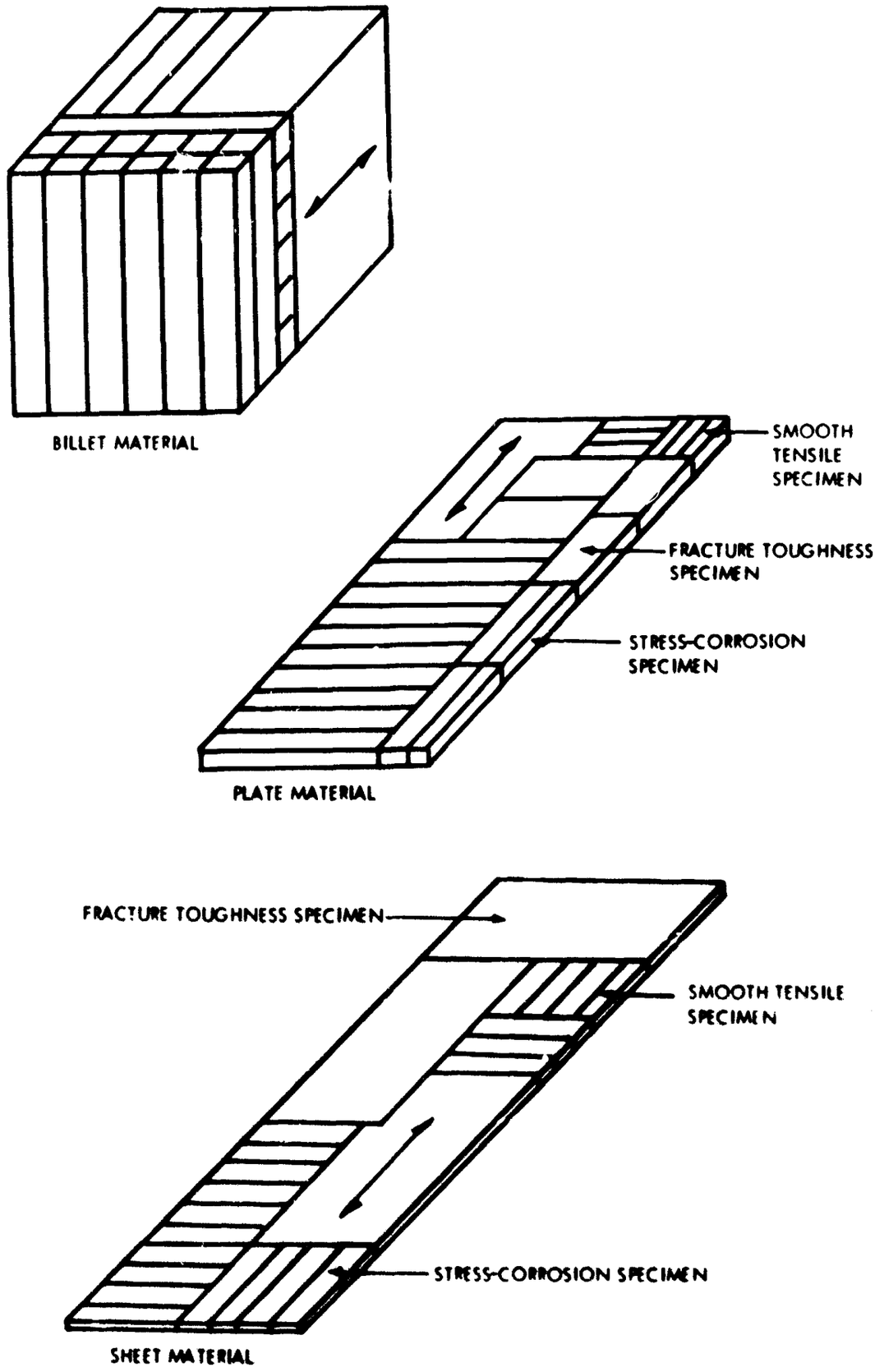

Figure 55 SCHEMATIC ILLUSTRATION OF SPECIMEN LOCATIONS FROM EACH MATERIAL FORM

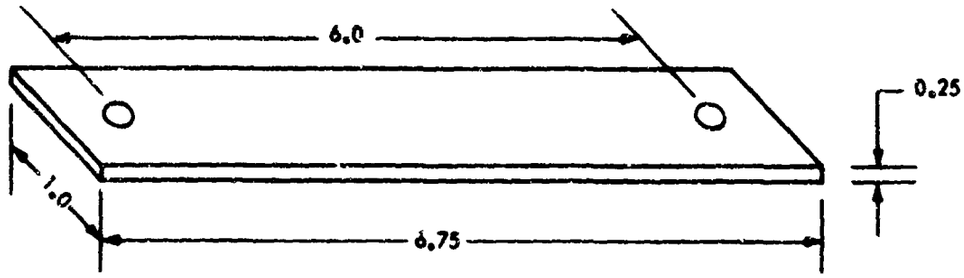

BILLET AND PLATE MATERIAL

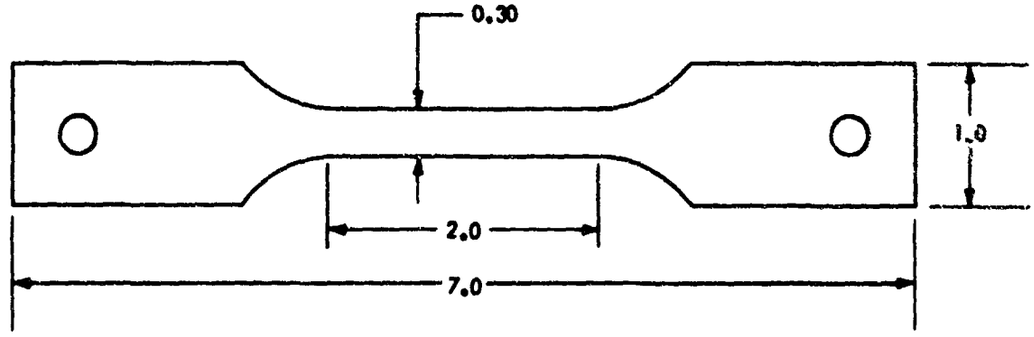

SHEET MATERIAL

DIMENSIONS ARE IN INCHES

Figure 56 STRESS-CORROSION SPECIMEN CONFIGURATIONS

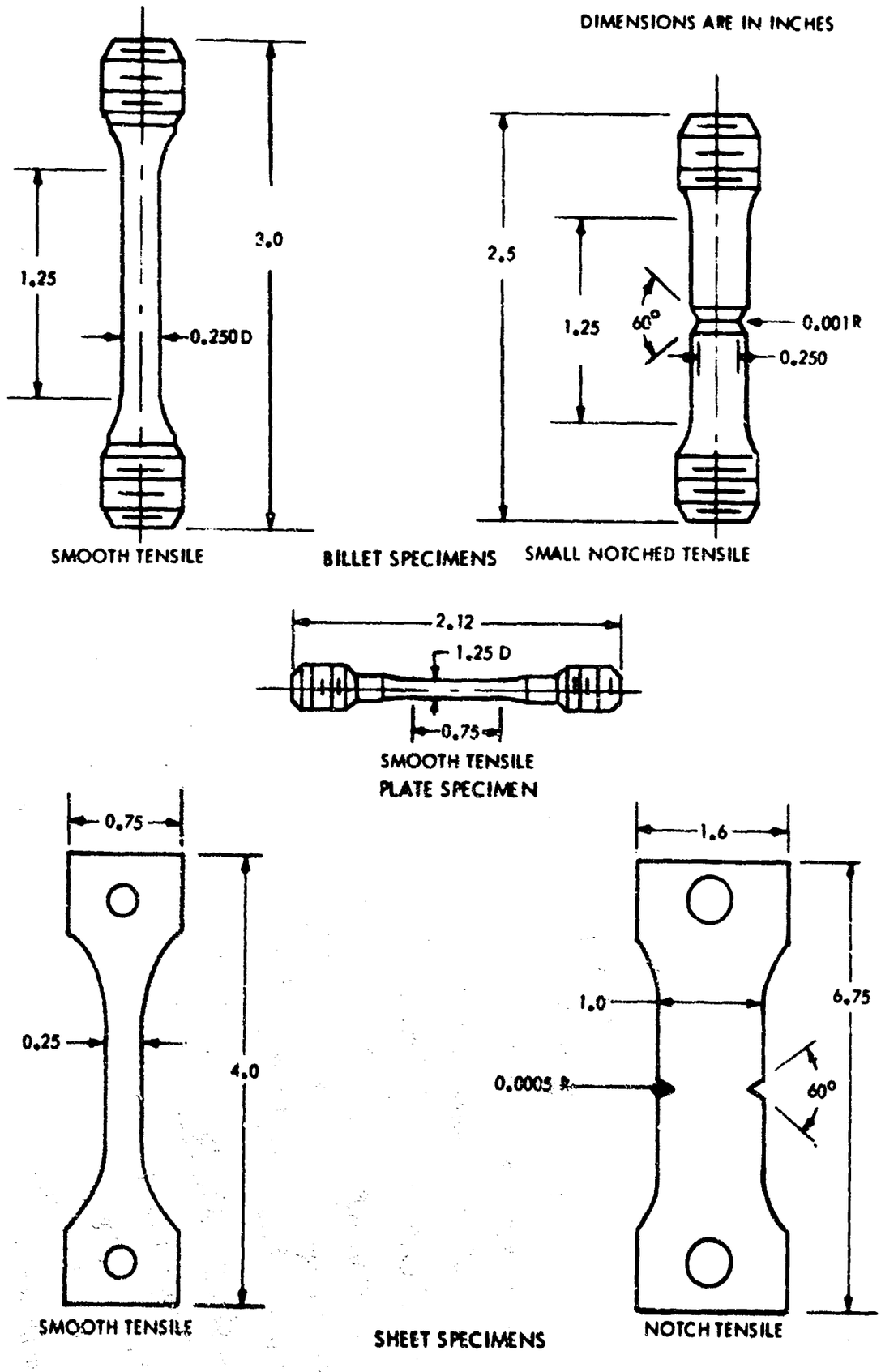

Figure 37 SMOOTH AND NOTCHED TENSILE SPECIMEN CONFIGURATIONS

DIMENSIONS ARE IN INCHES

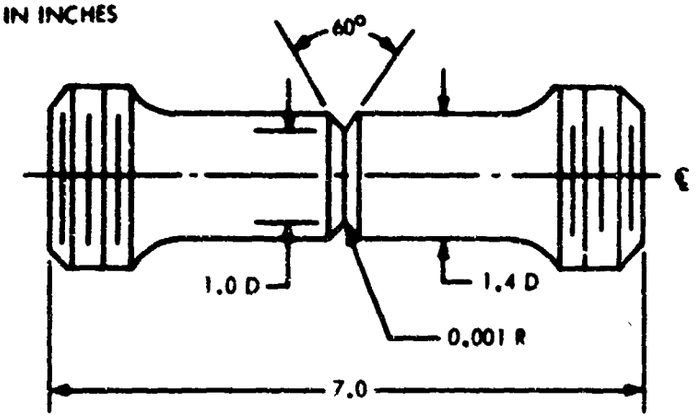

LARGE ROUND NOTCHED BILLET

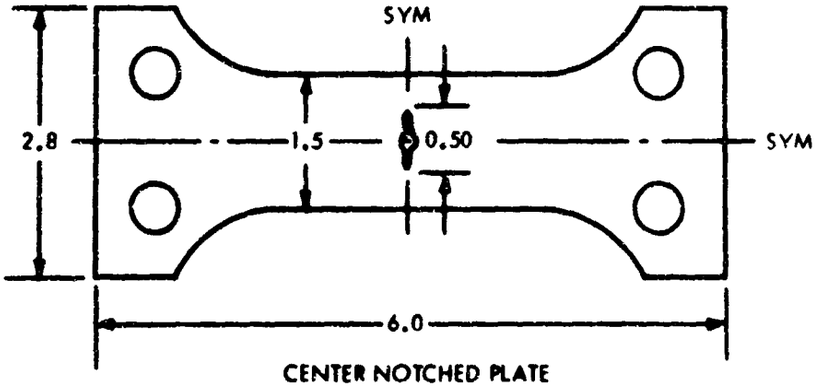

CENTER NOTCHED PLATE
(CENTER CRACKS PRODUCED BY FATIGUING)

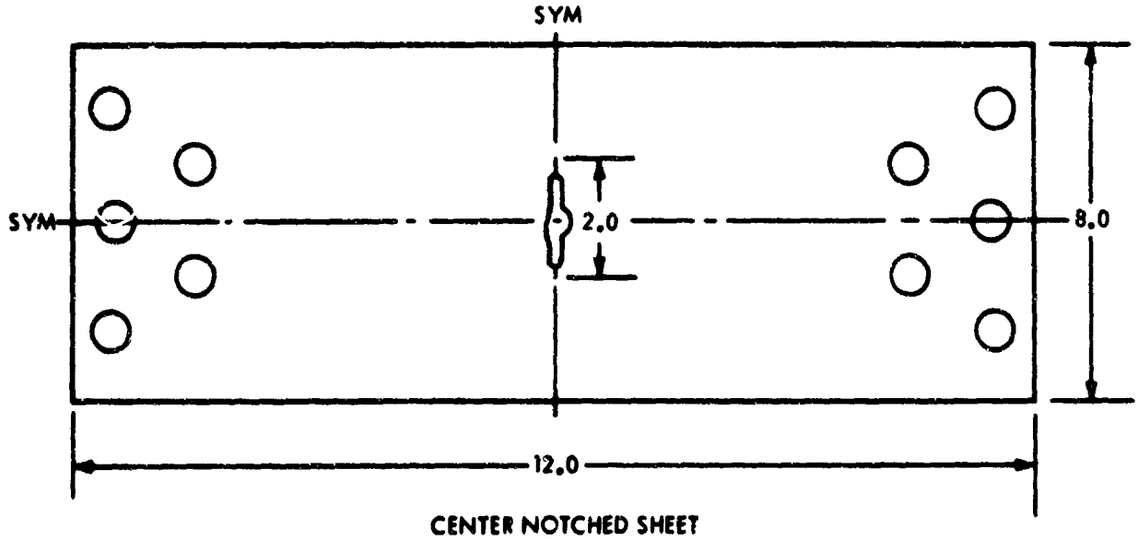

CENTER NOTCHED SHEET
(CENTER CRACKS PRODUCED BY FATIGUING)

Figure 58 FRACTURE TOUGHNESS SPECIMEN CONFIGURATIONS

Appendix II

FRACTURE TOUGHNESS EVALUATION

A. DEFINITION OF FRACTURE TOUGHNESS PARAMETERS

The concept of fracture mechanics has developed from the theory of elasticity and the testing of materials to evaluate their resistance to brittle fracture. Irwin (References 13 and 14) has provided descriptions of both the analytical and practical approaches to fracture mechanics. The American Society for Testing Materials (References 15, 16, and 17) has attempted to provide some degree of standardization for fracture toughness testing of high-strength sheet materials.

One fracture mechanics approach is based on assessing the intensity of stress at the crack tip of a centrally fatigue-cracked panel. The stress intensity factor, designated as either block K or script k may be regarded as a measure of the elastic transmission of external load into the region surrounding the crack tip (Reference 18). These are related as follows:

$$k = \sigma_G \sqrt{a}\ \alpha \quad (\text{psi}\sqrt{\text{in.}})$$

$$K = \sqrt{\pi}\ k = \sigma_G \sqrt{\pi a}\ \alpha \quad (\text{psi}\sqrt{\text{in.}})$$

Here 2a is the total fatigue crack length, σ_G is the gross area stress, and α is a geometry correction factor. This factor is required to correct for the finite size of specimen geometry since elasticity theory is generally based on an infinite sheet analysis. Two forms of this correction factor are in use today. One is based on a tangent function (Reference 13) and the other is based on a polynomial expression described by Greenspan (Reference 19). This latter factor is approximately 3 percent higher than the tangent correction factor at a crack-length-to-panel-width ratio of 0.4. This difference decreases at lower ratios and the two factors may be considered equivalent for most computations.

The polynomial expression for α is as follows:

$$\alpha = \frac{\sqrt{4 + 2\left(\frac{a}{b}\right)^4}}{2 - \left(\frac{a}{b}\right)^2 - \left(\frac{a}{b}\right)^4}$$

Here, 2b is the total panel width.

The critical stress intensity factor is calculated for the condition where the crack runs catastrophically with no increase in load. At this condition the values of the stress intensity factor are denoted as K_c or k_c. When panels are statically tested in standard tensile testing equipment at loading rates of 2500 psi per second, estimates of the amount of slow crack extension are often made in order to calculate K_c or k_c.

With the steel alloys evaluated in this program, fracture toughness panel tests were made at loading rates of approximately 500,000 psi per second. This high loading rate was used to approximate the loading rates encountered in service. In this way slow crack extension during testing is eliminated or minimized. Also, with the high-strength steel alloys, conservative critical stress intensity factors result with the high loading rates.

The criterion for valid fracture toughness tests with centrally cracked panels is that the net section stress σ_N must be less than 80 percent of the 0.2-percent yield strength. If σ_N is greater than 80 percent of the yield strength, the measured value of K_c or k_c is conservative.

The critical value of K_c or k_c can be measured for either plane stress or plane strain conditions. In the latter case, the critical value is denoted as K_{Ic} or k_{Ic}. With the center-cracked panels tested in this program, the low shear fraction in the rapid fracture area of most of the specimens indicates that conditions of plane strain have been reached or closely approached (see Table 11). Interpretation of whether the value is plane stress or plane strain should be based on the percent shear fracture.

Two large round notch specimens designed to yield a plane strain K_{Ic} value were tested for two strength levels of 4340. In this case K_{Ic} is calculated from the following expression and the criterion for a valid test is that σ_N should not exceed 110 percent of the 0.2-percent yield strength.

$$K_{Ic} = 0.233\ \sigma_N \sqrt{\pi D}$$

B. TESTING PROCEDURE

The small panel specimens were cyclically loaded to produce a fatigue crack tip. The maximum to minimum loads (β) were maintained at a ratio of 20 to 1 during fatigue cracking. The specimens were failed in tension at a rapid load rate in a horizontal jig. The load rates were greater than suggested by the ASTM fracture committee (Reference 16) because the higher load rates were more representative of actual loading in thick-section aircraft components. The loads were measured with an SR-4 strain-gaged dynamometer bar and recorded with a time-based oscillograph.

The large round notched specimens were not fatigue cracked. They were tested at a load rate of 2500 psi per second. Loads were recorded with the same instrumentation used for the panel tests.

Appendix III

SUPPLEMENTAL WORK— PREVIOUS STRESS-CORROSION STUDY

A. ENVIRONMENT

During the first stress-corrosion study at The Boeing Company (Seattle, Washington), which was supported by an Air Force contract, a similar investigation (Reference 20) was in progress at the Aerojet-General Corporation (Azusa, California). To correlate the Aerojet and Boeing data, three 4340 specimens (275-ksi ultimate strength) were stressed to 75 percent of yield at Boeing and sent to Aerojet. These specimens were continuously immersed in the 3.0-percent aqueous NaCl solution at Aerojet until failure. Failure times were then compared to those obtained from specimens of the same billet at Boeing after alternate immersion in 3.5-percent aqueous NaCl.

Continuous-immersion failure times were much longer than those after alternate-immersion testing. Whereas Aerojet failures were between 50 and 105 hours, comparable Boeing failures occurred between 1 and 26 hours. Heat treatment and test data are contained in Table 26.

Table 26 HEAT TREATMENT, CONTINUOUS-IMMERSION, AND ALTERNATE-IMMERSION TESTING OF 4340

Investigator	Test Method	Time to Failure (hr)
Aerojet-General Corporation	Continuous immersion in 3.0-percent NaCl solution	50, 82, 105
The Boeing Company	Alternate immersion in 3.5-percent NaCl solution	1, 3, 26

Heat Treatment:

Austenitize at 1500 to 1550°F for 45 minutes, oil quenched.
Double temper at 400°F for 3 + 3 hours.
Ultimate Strength: 275 ksi.
Yield Strength: 230 ksi.
Stress Level: 75-percent yield (175 ksi).

B. IMPACT TESTING

Evaluation of previous notched-to-unnotched ultimate strength ratios showed that a decrease in this ratio corresponded to an increase in stress-corrosion susceptibility. Comparison of impact values from the literature also revealed a decrease in impact properties correlated with increased susceptibility. To determine if this latter relationship actually existed, Izod impact specimens were cut from the previously stress-corrosion-tested billets of 4340, 4340M, 4330M,

and H-11. All impact specimens were cut from the same billet transverse grain directions and given the same heat treatments as the stress-corrosion specimens. The heat treatments are given in Table 27. Following heat treatment and final machining, all Izod specimens were tested at room temperature.

Plotting of the impact energy and stress-corrosion failure times with tempering temperature results showed the dip in the impact curves of all steels to correspond with the most stress-corrosion-susceptible conditions. Impact values and tensile properties are given in Tables 27 and 28. These stress-corrosion and impact relationships are shown in Figures 59 through 62.

This data reveals a definite correlation between microstructure and stress-corrosion cracking sensitivity. However, the extreme complexity of these alloys did not permit the identification of the predominant stages operating during the different tempering treatments. Similar work was done by Lilly and Nehrenburg (Reference 21) on 410 stainless steel. They found a correlation between impact properties and hydrogen embrittlement. These results suggest similarities between the mechanisms causing stress-corrosion cracking and hydrogen embrittlement.

Evaluation of the Izod impact fracture faces was based on the criteria used by Carr and Larson (Reference 22) in a study of fracture face appearance as a function of testing temperature. These investigators adopted the following terms to denote three characteristic fractographic zones:

1) Fibrous — discontinuous circumferential ridges;

2) Radial shear — radial markings that appear to be shear elements;

3) Shear lip — terminal part of the fracture consisting of a smooth shear element (macroshear) bordering the free surface or surfaces of the specimen.

In the present study, there was no evidence of a fibrous structure. All fracture faces contained the radial shear markings and shear lips along the free surfaces. Generally, the most noticeable effects of altering tempering temperatures were coarsening of the radial markings and changes in the size of the shear lips.

With an increase in tempering temperature there was a gradual coarsening and darkening of the radial structures. The temperatures at which this coarsening became most noticeable depended on the material. This behavior was least evident when examining 4330M. Here, the difference between the 400 and 1000°F structures was slight. However, 4340 and 4340M showed a definite demarcation as the result of tempering temperature, where coarsening was first noted at the 600 and 800°F temperatures, respectively. This change in the H-11 structure occurred at 1100°F. There was no apparent change in the size of the 4330M shear lips normal to the specimen notch. These same shear lips on the 4340 600°F temper and 4340M 800°F temper specimens were noticeably reduced in size compared to specimens of these steels tempered at the other temperatures.

Table 27 HEAT TREATMENTS AND IZOD IMPACT PROPERTIES OF 4340, 4340M, 4330M, and H-11

Material	Austenitizing Treatment	Tempering Temperature (°F)	Tempering Time (hr)	Impact Energy (ft-lb)
4340 Billet K	1525°F ±25°F for 45 minutes Oil quenched	400	3 + 3	9.50, 8.75, 8.50
		600	2.5 + 2.5	5.50, 5.00, 3.25
		800	1.5 + 1.5	12.75, 9.75, 7.25
		1000	1.5 + 1.5	13.50, 13.25, 12.50
4340M Billet P	1600°F ±25°F for 45 minutes Oil quenched	400	3 + 3	12.50, 11.75, 8.50
		600	3 + 3	9.00, 8.75, 7.25
		800	2.5 + 2.5	12.00, 8.50, 7.00
		1000	1.5 + 1.5	12.00, 10.00, 9.25
4330M Billet R	1575°F ±25°F for 45 minutes Oil quenched	400	3 + 3	11.25, 11.00, 10.50
		600	2.5 + 2.5	10.25, 9.00, 7.50
		800	1.5 + 1.5	12.25, 11.00, 10.50
		1000	1.5 + 1.5	16.75, 16.25, 13.75
H-11 Billet V	1850°F ±25°F for 45 minutes Oil quenched	600	3 + 3 + 3	10.00, 9.25, 8.25
		800	3 + 3 + 3	6.75, 6.50, 6.00
		1000	3 + 3 + 3	8.75, 7.50, 6.75
		1100	3 + 3 + 3	14.50, 14.00, 12.25

Table 28 SMOOTH TENSILE PROPERTIES OF 4340, 4340M, 4330M, and H-11

Material	Tempering Temperature (°F)	Ultimate Strength (ksi)	Yield Strength (ksi) (0.2% Offset)	Red in Area (%)	Percent Elongation/Inch
4340	400	275	230	12	5
	600	240	210	12	4
	800	205	187	18	6
	1000	175	158	26	9
4340M	400	296	240	26	8
	600	290	245	28	8
	800	250	206	28	9
	1000	224	204	28	10
4330M	400	250	205	14	7
	600	227	196	14	7
	800	202	185	25	8
	1000	188	174	18	9
H-11	600	302	~ 254	~ 16	6
	800	295	~ 264	~ 4	3
	1000	303	260	11	5
	1100	235	201	30	8

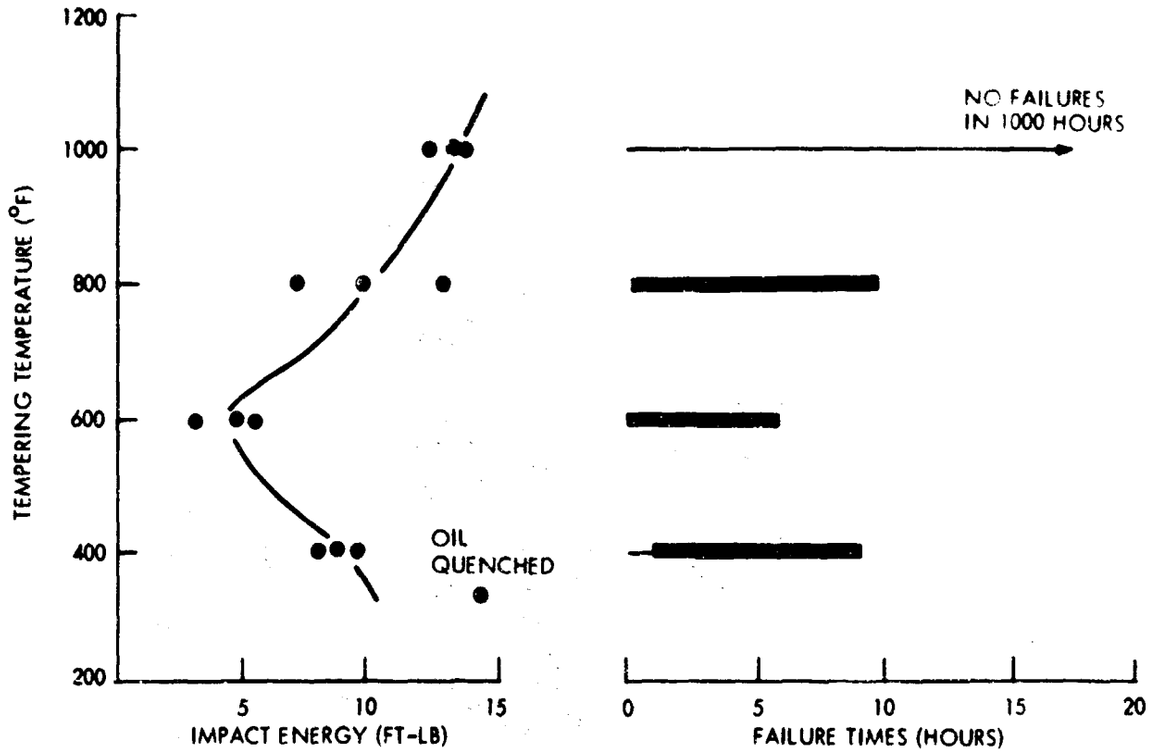

Figure 59 IMPACT PROPERTIES AND STRESS-CORROSION FAILURE TIMES OF 4340

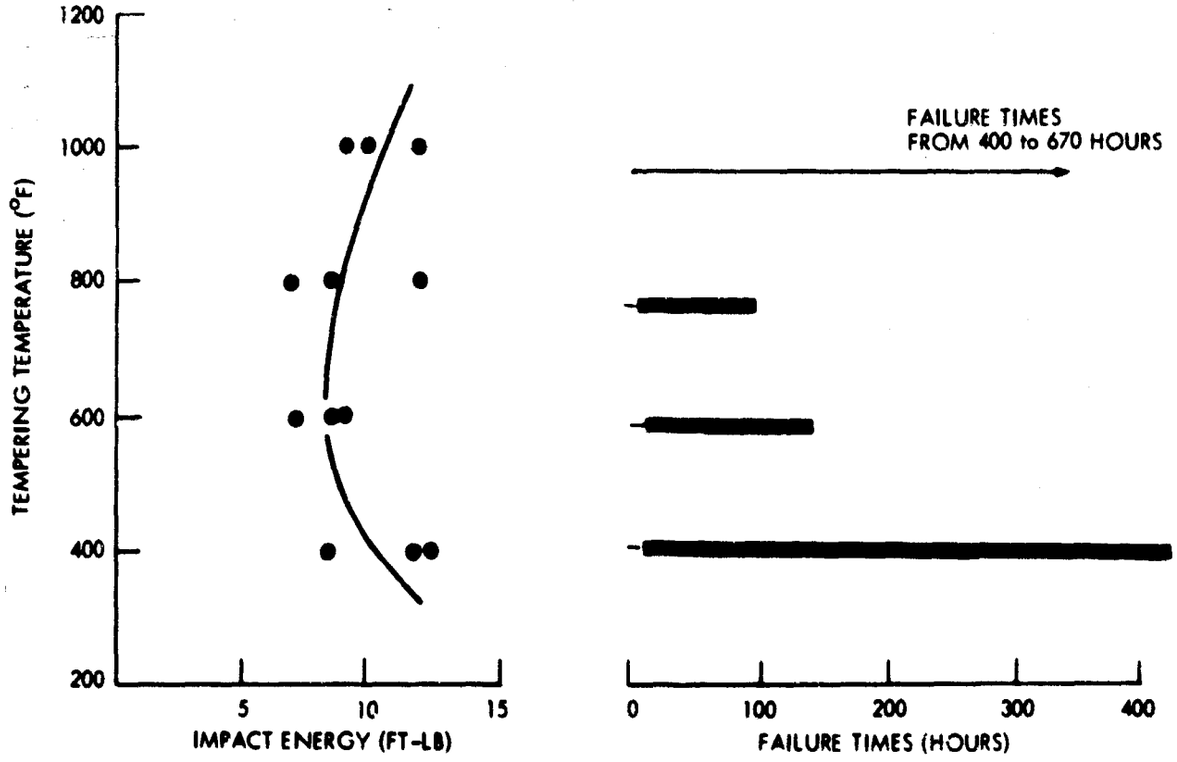

Figure 60 IMPACT PROPERTIES AND STRESS-CORROSION FAILURE TIMES OF 4340M

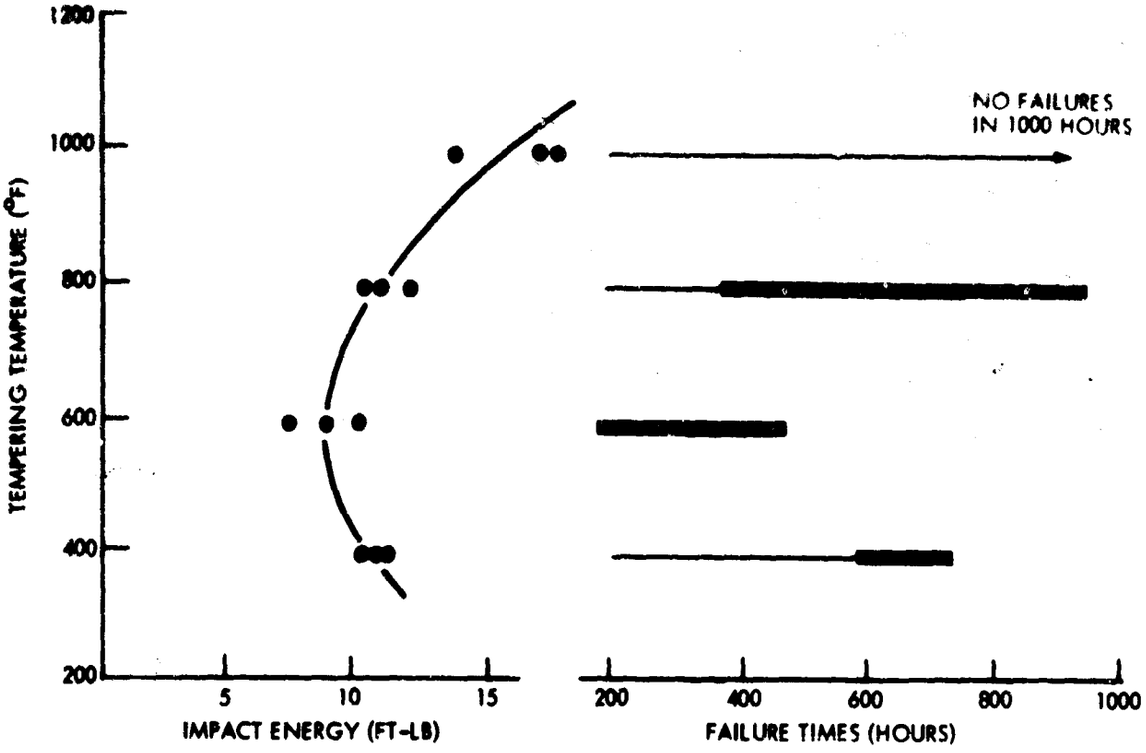

Figure 61 IMPACT PROPERTIES AND STRESS-CORROSION FAILURE TIMES OF 4330M

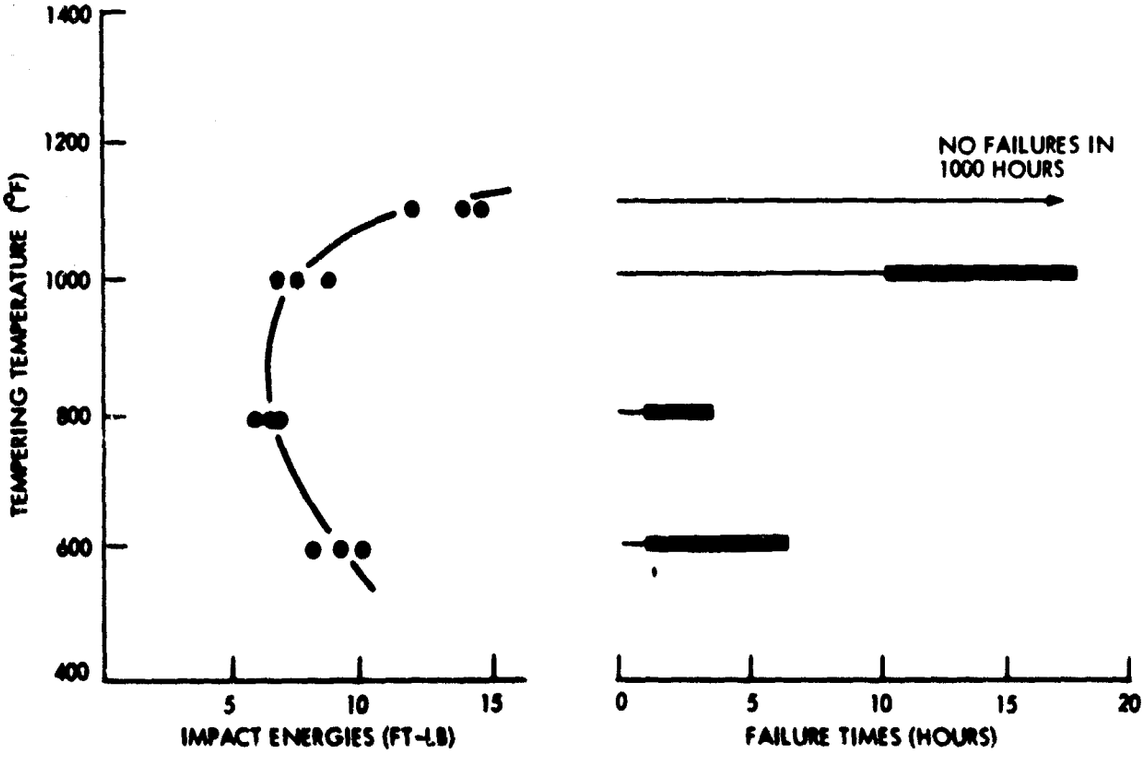

Figure 62 IMPACT PROPERTIES AND STRESS-CORROSION FAILURE TIMES OF H-11

The H-11 600, 800, and 1000°F temper specimens had very small shear lips compared to those obtained after tempering at 1100°F.

A number of correlations appeared to exist between the 4330M, 4340, and 4340M steels. The tempering temperatures at which these similarities were present are shown in Table 29.

Table 29 TEMPERING TEMPERATURES THAT PRODUCED SIMILARITIES IN FRACTURE FACE APPEARANCES

Material	Tempering Temperature (°F)		
	1*	2	3
4330M			400, 600 800, 1000
4340	400	600	800, 1000
4340M	400, 600	800	1000

*Definition of numbers given on Page 110

Of particular interest is the close correlation between the 4340 and 4340M fracture faces, where the fracture faces from the former steel were reproduced by the 4340M at tempering temperatures 200°F higher. The 4330M fracture faces produced at all tempering temperatures were similar to the higher-tempering-temperature 4340 and 4340M fracture faces.

One characteristic of the H-11 fracture faces that was not noted on the 4340, 4340M, or 4330M fracture faces was a ridge about one-fourth the specimen thickness in from the edge opposite the specimen notch. This ridge, which was parallel to the notch, became very pronounced at the 1000 and 1100°F tempering temperatures. There was no correlation between the size of this ridge and stress-corrosion susceptibility. Examples of the 4340, 4340M, 4330M, and H-11 impact fracture faces are shown in Figures 63 through 66.

Examination of the impact curves shows that the dip in the 4340 and 4340M impact curves at 600 and 800°F, respectively, corresponds to a noticeable change in the appearance of these fracture faces when compared to the lower-tempering-temperature fracture faces. It is these 600 and 800°F temper specimens which have the small shear lips and also first show a noticeable coarsening of the radial structure.

Although the 4330M 400, 600, and 800°F tempering-temperature impact energies were only slightly higher than comparable 4340 and H-11 values, the 4330M stress-corrosion susceptibility was noticeably less. However, all the 4330M impact fracture faces were similar to high-tempering-temperature (low-stress-corrosion-susceptibility) 4340, 4340M, and H-11 impact fracture faces.

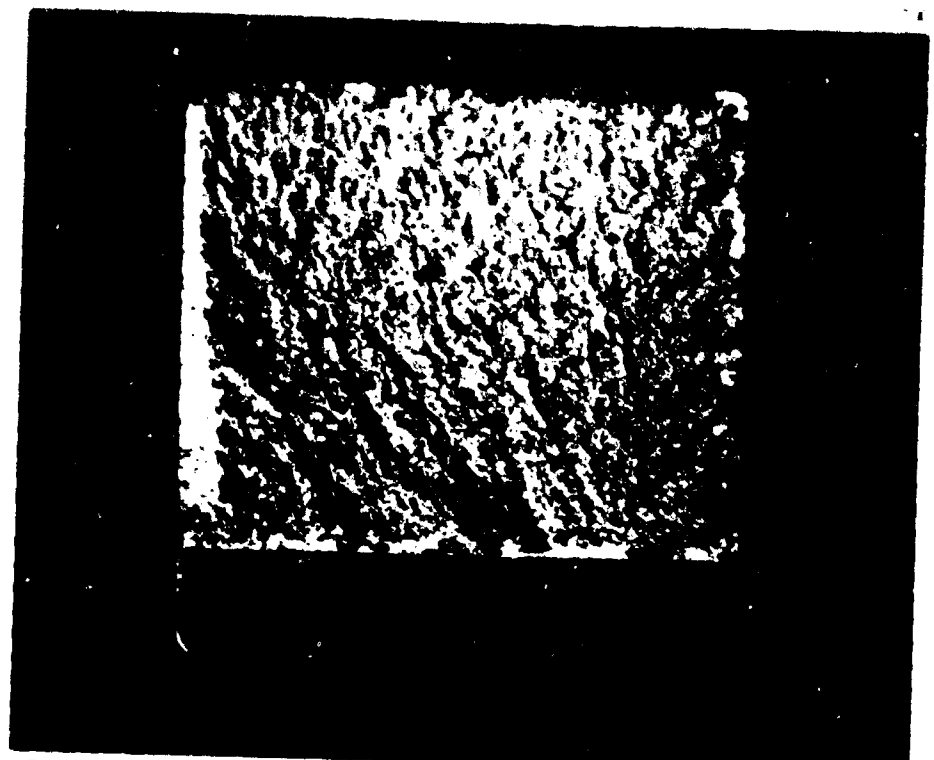

Figure 63 IZOD IMPACT FRACTURE FACE OF 4340 AFTER 400°F TEMPER

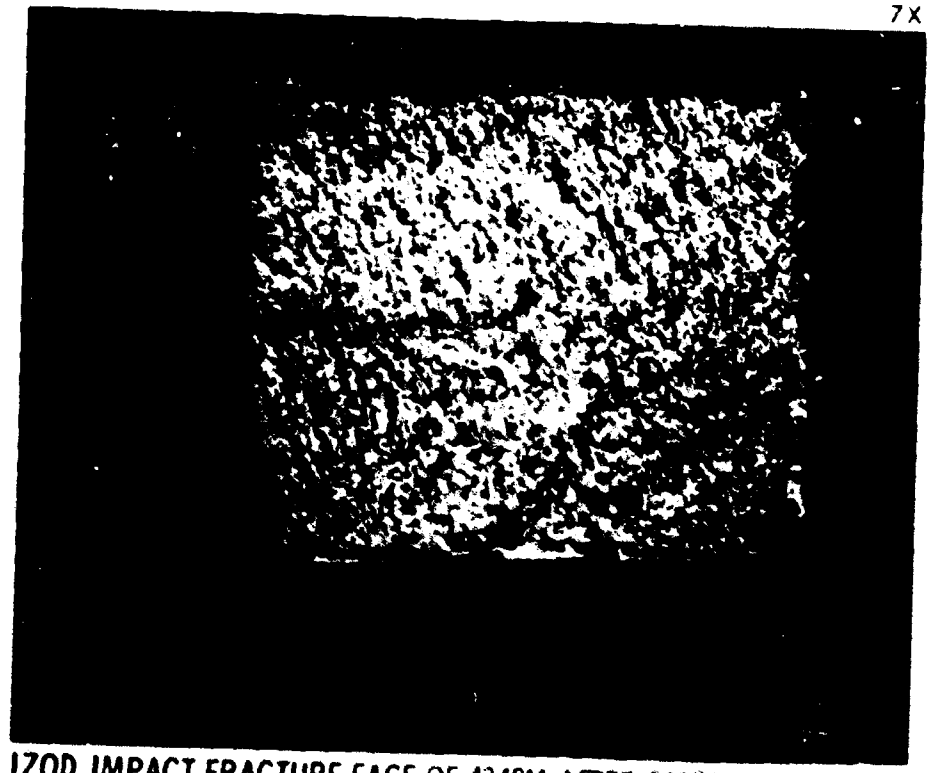

Figure 64 IZOD IMPACT FRACTURE FACE OF 4340M1 AFTER 800°F TEMPER

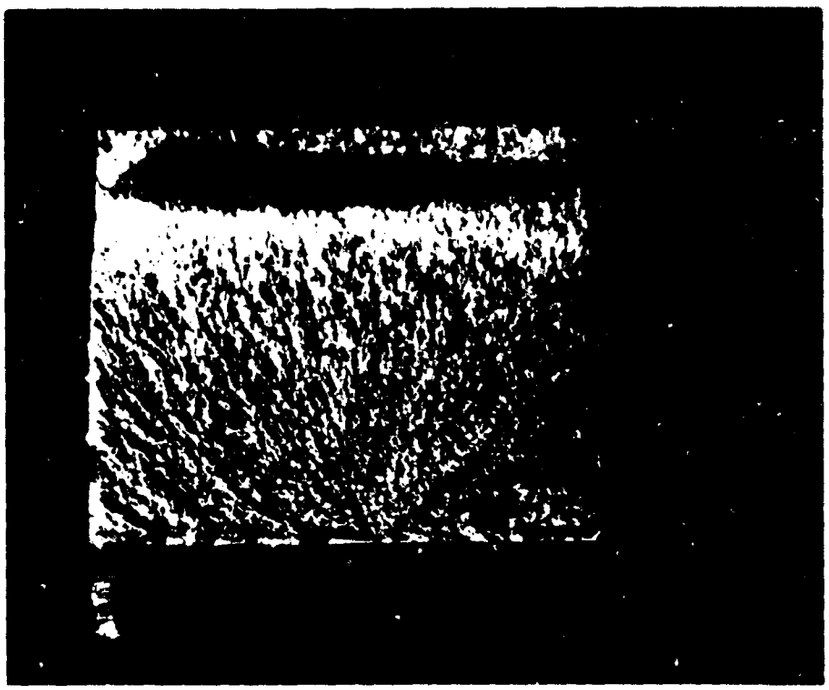

Figure 65 IZOD IMPACT FRACTURE FACE OF 4330M AFTER 600°F TEMPER

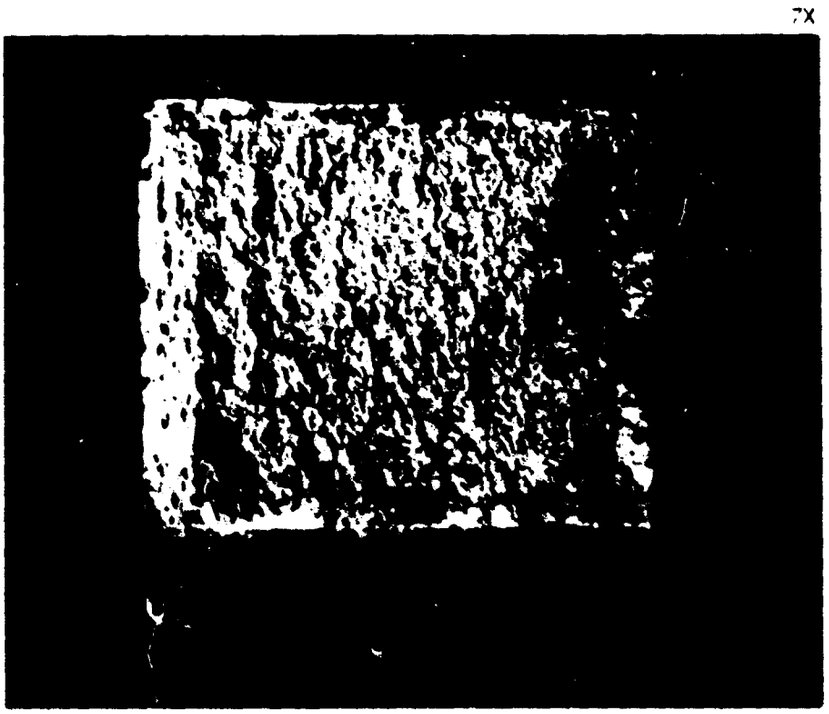

Figure 66 IZOD IMPACT FRACTURE OF H-11 AFTER 1000 F TEMPER

The H-11 impact fracture faces produced by tempering (600, 800, 1000°F) to the most stress-corrosion-susceptible conditions had very small shear lips. These H-11 Izod specimens, representing the lowest impact energies, had noticeably less coarse radial markings than those produced by tempering at 1100°F. H-11 tempered at 1100°F had very low stress-corrosion susceptibility.

Briefly, the study of the 4340, 4340M, 4330M, and H-11 impact specimens indicated the following correlations with stress-corrosion susceptibility.

1) An inverse relationship was noted between impact energies of the 4340, 4340M, 4330M, and H-11 steels and stress-corrosion susceptibility. Comparisons of different heat-treat conditions of a particular steel show that a decrease in impact properties corresponds to a more stress-corrosion-susceptible condition.

2) The most stress-corrosion-susceptible condition is represented by a slightly coarsened radial structure on the impact fracture faces with relatively small shear lips along the free surfaces.

3) The least stress-corrosion-susceptible condition is represented by a more heavily coarsened radial structure with relatively large shear lips along the free surfaces.

Appendix IV

REVIEW OF RECENTLY PUBLISHED LITERATURE ON STRESS-CORROSION CRACKING

A. INTRODUCTION

The stress-corrosion-cracking susceptibility of materials is essentially a measure of the interplay between stresses, corrosion, and crack-sensitive paths with each metal or alloy having its own particular corrosive environment that initiates cracking through primarily an electrochemical mechanism (Reference 23). There is no known case of stress-corrosion cracking in an aqueous medium that cannot be arrested by stopping the corrosion reaction (Reference 24). Stress-corrosion failures usually occur catastrophically after a time delay.

This literature survey is an extension of the previous survey (Reference 25) with emphasis on recent publications. The majority of investigations have been related to the study of modes of stress-corrosion failures and related factors such as the effect of grain size, alloying elements, plastic deformation, corrosive media, heat treatment, microstructures, stress, welding, and surface conditions.

B. MECHANISMS OF STRESS-CORROSION CRACKING

All proposed theories of stress-corrosion cracking have involved some type of electrochemical mechanism. These theories have been designated as the electrochemical theory, mechanical theory, strain accelerated decomposition theory, anodic shift theory, and the film theory and are described in the previous survey (Reference 25). At least one of these theories has found application in the description of stress-corrosion failures from the large variety of published data, but attempts for unification of these theories have met with failure at the present time.

C. MODE OF CRACKING

The mode of stress-corrosion cracking can be either transgranular or intergranular depending on the metallurgical nature of the material. Intergranular cracking has been related to potential differences between the grain boundary regions and the grain material. Robertson and Tetelman (Reference 5, Chapter 8) have studied intergranular stress-corrosion failures from a theoretical approach and have concluded that intergranular cracking is initiated by the concentration of stresses from piled up dislocations across a grain boundary plane. The result is a preferential and rapid attack along these planes that significantly reduces the fracture stress of the boundary. These boundaries, which block the passage of dislocations, can be other than grain boundaries, such as twin boundaries.

Their model for intergranular failure requires a grain size dependence in which they show the stress-corrosion failure time of 70/30 brass and 18-8 stainless steel to increase linearly with the square root of the inverse of the grain size. In face-centered cubic materials the evaluation of the grain size must include annealing twins since their presence will reduce the number of dislocations piled up at a grain boundary. If it is assumed that a coherent twin boundary has half

the energy of a stacking fault, the density of annealing twins would be greater in a material of low stacking fault energy (Reference 5). By increasing the silicon content in Cu-Si alloys, the stacking fault energy decreased and the susceptibility to intergranular failure decreased. This change in susceptibility was related to the smaller distance between barriers produced by the annealing twins.

Robertson and Tetelman have also concluded that nucleation of transgranular cracking is related to the stress concentration produced by dislocation pile-ups at Cottrell-Lomer locks. The barrier strength is related to the number of dislocations the Cottrell-Lomer lock can withstand, which is inversely proportional to the stacking fault energy of a system. Therefore, if a material has a high stacking fault energy, the barrier strength is low and the probability for nucleation of transgranular cracks is decreased.

Swann (Reference 26) has studied the stress-corrosion susceptibility and mode of cracking in deformed single-phase alloys. He has also found that the mode of cracking is dependent on stacking fault energy, but that the relative magnitude of stacking fault energies (SFE) produces basically two types of dislocation distributions. Low SFE allows extension of the partial dislocations and hinders cross slip. As a result, the dislocations remain in their slip planes producing a coplanar dislocation array. On the other hand, a high SFE will allow the dislocations to climb out of their slip planes and form a cellular distribution. Swann has shown that the coplanar distributions have a greater transgranular stress-corrosion susceptibility than the cellular distributions. Therefore, the addition of solute atoms, which decreases the SFE, will cause an increase in the stress-corrosion susceptibility. This has been observed for the addition of Zn, Al, Ge, and Si to copper (Reference 27) and Cr, Mo, Nb, and Ti to austenitic steels (Reference 28). The increase in the nickel content in the 18-8 type stainless steel decreases the SFE, which explains the stress-corrosion resistance of high-nickel-content stainless steels (References 26 and 28).

Douglass, Thomas, and Roser (Reference 28) have shown that the SFE is not the only criterion for determining the stress-corrosion susceptibility of a material. Short-range order (SRO) affects both stress-corrosion susceptibility and SFE as shown by the susceptibility of ordered Cu_3Au, which has a high SFE. Consequently, both SRO and SFE must be considered for evaluation of transgranular cracking.

D. CRACK INITIATION

Swann and Nutting (Reference 9) have reported preferential etching of thin foils in the region of stacking faults for Cu-Zn and Cu-Al. Although the conditions prevailing during electropolishing may not be the same as those encountered in stress-corrosion tests, there are many similarities which point toward a correlation. This preferential etching of stacking faults gives support to Edeleanu's (Reference 29) theory of alternate slow and rapid movement of stress-corrosion cracks. "The slow movement is associated with the dissolution of the stacking

faults, producing a crack which propagates in a brittle manner until intersection with another fault."

During deformation, the number of stacking faults intersecting a surface is increased, causing slower dissolution of any one fault. Therefore, in a work-hardened material, cracking should be widespread. This phenomenon of branching cracks has been observed by Hines and Hoar (Reference 30).

All theories proposed for the initiation of stress-corrosion cracking are related to physical areas on a surface concerned with stress concentration or chemical potential differences. Swann and Nutting's (Reference 9) preferential etching of stacking faults is related to solute segregation. Robertson and Tetelman's (Reference 5) crack initiation is related to stress concentration at Cottrell-Lomer locks.

E. CRACK PROPAGATION

There has not been any new significant data on crack propagation rates especially in relation to transgranular versus intergranular failures. The generally accepted net rate of stress-corrosion failures is 0.1 to 5.0 mm/hour (Reference 30). However, Staehle, et al. (Reference 31) observed that the cracking of 347 stainless steel occurs initially by short bursts and then in the latter stage of cracking the bursts extend over 2 to 10 grains.

F. EXPERIMENTAL OBSERVATIONS

The following is a brief resume of the experimental observations reported in the literature.

1. Observations of Stress-Corrosion Cracking in High-Strength Steels

Experimental investigations of stress-corrosion susceptibility on high-strength steel alloys have been mainly concerned with materials and environments associated with rocket motor cases. Owen (Reference 32) has reported that the effect of environment on the susceptibility of Vascojet 1000, in decreasing order, was phosphate, chloride, sulfate, nitrate, and sulfide solutions. With the first three exhibiting the same order of detrimental effect. The H-11 specimens shattered in a number of pieces especially in phosphate, chloride, and sometimes sulfate solutions. Multifractures did not occur, however, in nitrate solutions. The high-strength D6AC alloy was most resistant to stress-corrosion failures in comparison with H-11, 4137Co, and 300M.

Uzdarwin (Reference 33) has shown that the D6AC, 300M, and H-11 alloys are generally most susceptible in distilled water and 3.5-percent NaCl solution in comparison with tap water, $Na_2Cr_2O_2$ solution (0.25-percent), 1-percent marquenching salt solution, trichloroethylene, cosmoline, and a 4-percent soluble oil solution. The susceptibility of these alloys also decreased with decreasing yield strengths.

Stress-corrosion tests on bolts torsionally stressed have shown HY-Tuf to be less susceptible than 1366 (Swedish alloy similar to 4340) in a humidity cabinet (Reference 34).

The increased resistance to corrosion adjacent to welds in SAE steel have been associated with change in chromium distribution during cooling (Reference 35). As the cooling rate from the austenitic temperature is decreased, the corrosion resistance increases because of the greater retention of chromium in ferrite. At very slow cooling rates, secondary effects of carbide shape and size appear to counteract the chromium effect. However, the relative change in susceptibility is not significant with cooling rate.

2. Observations of Stress-Corrosion Cracking in Stainless Steels

The metallurgical factors influencing intergranular cracking of austenitic stainless steels have been fairly well established and are reported in a number of published papers. The factors affecting transgranular cracking have been previously discussed.

Staehle, et al. (Reference 31) have reported that the stress-corrosion susceptibility of 347 stainless steel depends on a balance of oxygen and NaCl concentration. As the oxygen increases, less chloride is required for cracking. Similar conditions have been reported by Eckel and Williams (Reference 36) for intermittent wetting and drying in alkaline-phosphate-treated chloride waters. Staehle, et al., observed stress-corrosion cracks at stresses as low as 2000 psi at 50 ppm NaCl. Also, at this low NaCl concentration the tendency for cracking did not change as the stress increased.

Staehle, et al., have also noted that a smooth surface presented a more resistant condition for nucleation of stress-corrosion cracks. The cracks occurred in the region of highest stress for a smooth surface while an abraded surface resulted in cracks occurring in regions of low stress. The crack distribution was related to residual surface stresses induced by abrading.

Logan, et al. (Reference 37) investigated the effect of temperature on the stress-corrosion susceptibility of 304 stainless steel. At 570°F, failures occurred at chloride concentrations as low as 5 ppm at 20,000 psi. The presence of oxygen was necessary for crack initiation. There was no correlation between temperature (within range of 455 to 615°F) and susceptibility to stress-corrosion cracking at constant chloride concentration and stress.

Harwood (Reference 38) emphasizes the importance of chlorides in the stress-corrosion susceptibility of austenitic stainless steels in which, in the absence of chlorides or caustics cracking, will not occur in high purity water or steam. Oxygen is also necessary for pitting in austenitic stainless steels in NaCl solutions. However, in concentrated metal chloride solutions (i.e., $MgCl_2$) stress-corrosion and pitting can occur to deoxygenated solutions.

Harwood has stated that, in general, an increase in temperature shortens the time to failure because of increased crack initiation, but some influence is exerted on the rate of cracking.

Favor, et al. (Reference 39) reported that the double aging treatment of AM 350 was more susceptible to intergranular corrosion than the SCT treatment. The significant factor was the precipitation of chromium carbides during the former treatment. Banning and Wilson (Reference 40) reported that the SO_2 environment causes both AM 355 CRT and AM 350 CRT to be stress-corrosion susceptible while alternate immersion in 3.5-percent NaCl, cyclic humidity, and alkaline soil environments did not produce susceptible conditions.

Watanabe and Mukai (Reference 41) have shown that the tensile strength of austenitic stainless steels diminishes suddenly after a specimen has been immersed for three-fourths of the failure time. Also, the number of stress-corrosion cracks increased as the stress increased, with the critical stress for crack initiation being higher than the critical stress for crack propagation.

Numerous other investigations have shown similar results for the various factors affecting the stress-corrosion susceptibility of high-strength and stainless steels. The conclusions from all stress-corrosion test results are:

1) Stress-corrosion cracking is primarily an electrochemical phenomena;

2) Specific environments are required for each alloy and metal;

3) Tensile stresses, applied or internal, are required for the promotion of stress-corrosion cracking.